Electrochemical CO_2 Capture from Seawater: Design and Assessment of Bipolar Membrane pH-Swing Process

Zur Erlangung des akademischen Grades eines
DOKTORS DER INGENIEURWISSENSCHAFTEN (Dr.-Ing.)

von der KIT-Fakultät für Chemieingenieurwesen und Verfahrenstechnik des
Karlsruher Instituts für Technologie (KIT)
genehmigte

DISSERTATION

von

M.Sc. Mehran Aliaskari
aus Esfahan, IRAN

Tag der mündlichen Prüfung: 26.06.2026
Erstgutachter: Prof. Dr. Harald Horn
Zweitgutachter: Prof. Dr. Mathias Ernst

Acknowledgements

This work would not have been possible without the help and support of my colleagues, family and friends throughout the past few years. I would like to thank a few here. I would like to express my sincere gratitude to **Prof. Harald Horn**. Thank you for your guidance, support and unwavering trust. Your trust has boosted my confidence over the years.
For taking on the role of second examiner on my thesis, I would like to thank **Prof. Mathias Ernst**.
I would also like to thank my direct supervisor, **Dr.-Ing. Florencia Saravia** for her invaluable support and feedback. Thank you for all your time during our many weekly Monday meetings at 10:00. Anytime there was a problem I could not handle, I knew I could share it with you and we would find a way to solve it, I have learned a lot in the process.
I thank all of the colleagues in the water chemistry and technology department of Engler-Bunte-Institut, this is an amazing place to do a PhD and I am proud for being a member. I would like to thank my fellow PhDs and colleagues for their support and friendship: **Andreas, Yair, Xiao, Ben, Suheyla, Jonas, Stephan, Amelie, Prantik, Ali, Max** (both of them)**, Nurul, Sophie, Alina, Melanie, Giorgio, Jan, Mina and Willow**. It was great to spend the last few years doing so many things together, from our yearly retreats in Bad Herrenalb, to the Aquameister football event, and running as EBI-team in the Badische Meile. I consider myself lucky to have been able to work with you. I am also grateful to the students whom I had the pleasure to supervise during this time: **Jochen, Lukas, Simin and Jiyoon**, I have learned a lot from working with you and wish you utmost success in your next steps.
EBI would not function without a lot of work behind the scene, for that I want to thank **Gudrun Abbt-Braun** for her unmatched effort and work ethic. For their support in all the administrative tasks, a big thanks to **Ursula Schäfer** and **Sylvia Heck**. I also acknowledge the support of our laboratory technicians, **Axel, Uli, Mathias, Raphi and Maya** for the many samples they have analyzed for this work and **the workshop team,** especially **Freddy & Erwin**, for their practical help and assistance with the production of the flowcell.
Many people were there with me during both happy and sad times. Above all, I am deeply grateful to my beloved wife, **Anis**, for her unconditional love and friendship throughout the past years. I am also grateful to **my parents** and sisters, **Sima, Simin and Sara**, for their constant encouragement and support, despite the long distances between all of us. Finally, I thank all my friends for their kindness and support. In particular, **Shabnam, Christopher** for being the best friends we could have imagined and **S.Mohammad, Behrooz, Lee and all other friends** for being there in celebrations and making the hard days bearable.

Abstract

In order to achieve net-zero greenhouse gas emissions by mid-century, deep emission reductions and the removal of several gigatonnes of carbon dioxide (CO_2) per year are required. In this context, the ocean is used as the source for electrochemical pH-swing CO_2 capture by bipolar membrane electrodialysis (BPMED), since seawater contains (on a volumetric basis) around 120 times more inorganic carbon as dissolved inorganic carbon (DIC) than the atmosphere contains CO_2. This thesis defines and experimentally validates BPMED operating windows and process configurations for CO_2 capture from seawater and desalination brines that reduce specific electrochemical energy consumption, mitigate inorganic scaling on the alkaline side driven by Mg^{2+} and Ca^{2+} precipitation, and maintain stable operation.

A brief introduction in Chapter 1 explains how electrochemical systems are used for carbon capture from seawater. Chapter 2 quantifies how current density, flow velocity, electrolyte composition and feed salinity govern dissolved inorganic carbon removal, specific energy consumption (SEC) and current efficiency in BPMED-based CO_2 capture. A 10-cell BPMED stack is operated with synthetic seawater (DIC 180 mg/L) over 4–12 mA/cm^2, solution velocities of 1–3 cm/s and conductivities of ∼8–50 mS/cm. A narrow energy-optimal regime is identified at intermediate conditions: around 7–8 mA/cm^2, SEC reaches ∼2.3 kWh/kg CO_2 (1.7 kWh/kg CO_2 with $K_3/K_4[Fe(CN)_6]$ electrolyte) with up to 80 % DIC removal. At high conductivities (e.g. concentrated desalination brines, ≥50 mS/cm), further ohmic gains are offset by increased co-ion leakage and hindered water transport in the bipolar membrane, so the SEC increases and H^+/OH^- utilization decreases.

Chapter 3 addresses scaling on the alkaline side of the bipolar membrane, a primary operational bottleneck previously inferred mainly from stack voltage rise and pressure drop. A dedicated flow cell with optical access to the BPM surface is integrated into an electrodialysis system, enabling in-situ, real-time optical coherence tomography (OCT) imaging of scaling while current (0.3–0.8 A) and flow (3–7 L/h, 0.5–2 cm/s), DIC content and ion composition (Mg^{2+}, Ca^{2+}, SO_4^{2-}) are systematically varied. Scaling is shown to be dominated by heterogeneous $Mg(OH)_2$ formation, with thick deposits (up to 100 μm) forming in low-shear regions between spacer filaments. Only thin, patchy layers (up to 30 μm) form at lower currents and higher velocities. Seawater-level DIC buffering suppresses extreme local pH shifts and reduces scaling, whereas near-zero DIC feeds produce severe deposits. Variations in the concentration of divalent ions (Mg^{2+}, Ca^{2+} and SO_4^{2-}) in the feed and SEM images, confirm Mg^{2+} as the main scaling agent. Alkaline-side scaling in BPMED is thus established as a locally structured $Mg(OH)_2$ process governed by the interplay of current density, hydrodynamics and buffering at the BPM interface, providing mechanistic guidance for operating windows, spacer design and process configurations that limit scaling while maintaining the required pH swing.

Chapter 4 tests and validates a BPMED-based process configuration in which CO_2 is captured from seawater while NaOH is co-produced. Conventional in-situ concepts feed seawater directly through the BPMED stack, evolving CO_2 on the acidic side and returning the decarbonized stream to the alkaline side for neutralization, exposing the bipolar membrane to Mg^{2+} and Ca^{2+} and causing rapid scaling due to the high local pH, whereas ex-situ concepts first generate acid and base from softened brines and then use them outside the stack for acidification or alkalinisation, reducing scaling at the expense of higher complexity, energy demand and also more membrane area due to the needed process configuration. In this chapter, a closed-loop alkaline BPMED configuration is implemented in which an NaCl solution is continuously recycled in the alkaline cell; the produced alkaline solution is used both to soften seawater or desalination brines for use in the loop and to neutralize the acidic CO_2-free seawater before discharge. The closed-loop system is operated with model seawater over 6–32 mA/cm^2, 1–3 cm/s and 35–70 mS/cm and achieves >80 % DIC removal at SEC <3 kWh/kg CO_2 while producing up to ∼0.1 mol/L NaOH (2 L) at 1.8–2.2 kWh/kg NaOH with 60–85 % current efficiency. In a benchmark ex-situ mode, NaOH is produced at ∼1.8 kWh/kg NaOH with current efficiencies up to 90 %. The energy consumption of the closed-loop configuration remains comparable while no macroscopic scaling is observed over the tested operating window and time scales. Demonstrating that CO_2 capture from seawater and electrochemical NaOH production are jointly realised at energy intensities similar to dedicated ex-situ (for NaOH) and in-situ operation (for CO_2) with strongly mitigated alkaline-side scaling.

Overall, this work has shown that BPMED-based CO_2 extraction from seawater can only be optimally achieved within a narrowly defined but controllable operating window. This work contributes to the further development of BPMED from a proof-of-concept to a quantitatively investigated and mechanistically understood technology with realistic scaling potential in combination with desalination plants.

Kurzfassung

Die Erreichung des "Netto Null Emissionen" Ziels bis Mitte des Jahrhunderts erfordert weitreichende Emissionsminderungen, sowie die permanente Entfernung mehrerer Gigatonnen Kohlenstoffdioxid (CO_2) aus der Atmosphäre pro Jahr. Als globale CO_2 Senke enthält Meerwasser rund 120-mal mehr gelösten anorganischen Kohlenstoff (DIC) pro Volumeneinheit als CO_2 in der Luft vorhanden ist. Vor diesem Hintergrund stellt der Ozean eine vielversprechende Quelle für eine elektrochemische pH-Wechsel Abscheidung von CO_2 mittels Bipolare Membranelektrodialyse (BPMED) dar.
Eine kurze Einleitung in Kapitel 1 erklärt, wie elektrochemische Systeme zur Kohlenstoffabscheidung aus Meerwasser eingesetzt werden. Kapitel 2 beschreibt die Untersuchungen zum Einfluss der Stromdichte, des Volumenstroms, der Elektrolytzusammensetzung und des Salzgehalts des Feedstroms auf den spezifischen Energieverbrauch (SEC) und die Stromausbeute in einem BPMED-basierten CO_2-Extraktionsprozess. Die Untersuchungen erfolgten in einem BPMED-Stake bestehend aus zehn Zellen mit synthetischem Meerwasser (DIC = 180 mg/L) und deckten einen Bereich der Betriebsparameter ab mit einer Stromdichte von 4–12 mA/cm^2, einer mittleren Strömungsgeschwindigkeit von 1-3 cm/s und einer elektrischen Leitfähigkeit des Feeds von 8-50 mS/cm ab. Ein schmales energetisches Optimum wurde bei einer Stromdichte von 7-8 mA/cm^2 gefunden, mit einem resultierenden SEC von ca. 2,3 kWh/kg CO_2 bei einer Entfernung von bis zu 80% des DIC. Bei einer Erhöhung der elektrischen Leitfähigkeit auf $\geq$50 mS/cm wurden ohmsche Gewinne durch verstärkte Leckage von Ko-Ionen sowie verminderten Wassertransport durch die bipolare Membrane abgeschwächt. Diese hatte einen erhöhten SEC zu Folge, wobei die H^+/OH^--Nutzung abnahm.
Kapitel 3 befasst sich mit dem anorganischen Scaling auf der alkalischen Seite der bipolaren Membran. Dieses stellt einen zentralen betrieblichen Nachteil dar, der bislang primär indirekt aus einem Spannungsanstieg und Druckverlust im Membran-Stake abgeleitet wurde. Eine individuell konstruierte Fließzelle mit integriertem optischem Fenster ermöglichte in-situ eine orts- und zeitaufgelöste Beobachtung des Scalings auf der alkalischen Seite der BPM-Oberfläche in einem Elektrodialysesystem mittel optischer Kohärenztomographie (OCT). Die Scaling-Entwicklung wurde bei der systematischen Variation der Prozessparameter beobachtet: Strom (0,3–0,8 A), Durchfluss (0,5–2 cm/s), DIC-Konzentration und Ionenzusammensetzung der Lösung (Mg^{2+}, Ca^{2+}, SO_4^{2-}). Es zeigte sich, dass die Deckschicht von einer heterogenen $Mg(OH)_2$-Ausfällung dominiert wurde, wobei sich Scalingdicken von bis zu 100 µm in den schwach überströmten Bereichen zwischen den Spacer-Filamenten bildeten. Angelegte Niedrige Ströme sowie hohe Strömungsgeschwindigkeiten führten dagegen lediglich zu dünnem lokal begrenztem Scaling ($\leq$30µm). Die vorhandene Pufferkapazität des DICs im Meerwasser unterdrückt eine extreme lokale pH-Verschiebung und reduziert folglich die Bildung von Scaling. Im Gegensatz dazu zeigten sich bei DIC-freien Feedströmen ausgeprägte anorganische Ablagerungen. Die Variation der Konzentration von bivalenten Ionen (Mg^{2+}, Ca^{2+}, SO_4^{2-})

im Feed, sowie Aufnahmen der Scalingschicht mittels Rasterelektronenmikroskopie bestätigten Mg^{2+} als primären Scalingverursacher. Die Belagbildung auf der alkalischen Seite in der BPMED konnte damit als lokal strukturierter $Mg(OH)_2$-Prozess etabliert werden, der durch das Zusammenspiel von Stromdichte, Hydrodynamik und Pufferung an der BPM-Grenzfläche bestimmt wird. Die mechanistischen Leitplanken zur Begrenzung der Deckschichtbildung bei gleichzeitiger Erhaltung des erforderlichen pH-Schwungs werden durch die untersuchten Betriebsparameter, die Spacer-Konstruktion sowie die Prozesskonfiguration definiert.

In Kapitel 4 wurde eine BPMED-basierte Prozesskonfiguration untersucht und validiert, in der CO_2 aus Meerwasser bei gleichzeitiger NaOH-Produktion extrahiert wurde. In einer konventionellen in-situ Prozessführung wird Meerwasser direkt durch den BPMED-Stack geführt, wobei auf der sauren Seite CO_2 entsteht und der entkarbonisierte Strom zur Neutralisierung der alkalischen Seite zugeführt wird. Mg^{2+} und Ca^{2+} werden dabei der bipolaren Membran ausgesetzt und es kommt zu einer schnellen Deckschichtbildung induziert durch einen hohen lokalen pH-Wert. Im Gegensatz dazu werden in einer ex-situ Prozessführung Säure und Base aus enthärteten Solen gewonnen und diese außerhalb des BPMED-Stacks zur Ansäuerung bzw. Alkalisierung eingesetzt. Damit kann das Scalingrisiko vermindert werden, wobei sich jedoch der benötigte Energiebedarf und die Komplexität des Systems aufgrund der erforderlichen Prozessführung erhöht. In diesem Kapitel wurde eine geschlossene alkalische BPMED-Kreisführung implementiert, in der eine NaCl-Lösung kontinuierlich in der alkalischen Zelle rezirkuliert wurde. Die erzeugte alkalische Lösung wurde einmal zur Enthärtung von Meerwasser oder Sole aus Entsalzungsanlagen für den Einsatz im Kreislaufprozess und zum anderen auch zur Neutralisation des sauren, CO_2-freien Meerwassers vor dessen Rückführung in den Ozean verwendet. Das geschlossene System wurde mit Modellmeerwasser bei Stromdichten von 6–32 mA/cm^2, Strömungsgeschwindigkeiten von 1–3 cm/s sowie einer elektrischen Leitfähigkeit des Meerwassers von 35–70 mS/cm betrieben. Die maximal erzielte DIC-Entfernung lag bei $\geq$ 80% mit einem SEC $\leq$3 kWh/kg CO_2, während bis zu 0.1 mol/L NaOH (Volumen = 2 L) produziert wurde. Dies entsprach einer SEC von 1,8–2,2 kWh/kg NaOH mit 60–85 % Stromausbeute. Zum Vergleich konnten in einem Benchmark ex-situ Prozess NaOH mit einer SEC von 1,8 kWh/kg NaOH bei einer Stromausbeute von bis zu 90% produziert werden. Dies zeigt, dass die CO_2-Extraktion aus Meerwasser mit gekoppelter elektrochemischer NaOH-Produktion bei einem spezifischen Energieverbrauch vergleichbar zu einer dedizierten ex-situ-Betriebsweise (für NaOH) bzw. in-situ-Betriebsweise (für CO_2) realisiert werden kann. Gleichzeitig wird das Scaling Risiko auf der alkalischen Seite der BPMED in der gekoppelten Prozessführung stark verringert.

Zusammenfassend konnte in dieser Arbeit gezeigt werden, dass BPMED-basierte CO_2-Extraktion aus Meerwasser nur innerhalb eines eng begrenzten, aber kontrollierbaren Betriebsfensters optimal realisiert werden kann. Diese Arbeit trägt dazu bei, um BPMED von einem Proof-of-Concept hin zu einer quantitativ untersuchten und mechanistisch verstandenen Technologie mit einem realistischem Skalierungspotential in Koppelung mit Entsalzungsanlagen weiterentwickeln zu können.

List of Figures

List of Tables

List of Abbreviations

AEL	Anion exchange layer
AEM	Anion exchange membrane
BECCS	Bioenergy with carbon capture and storage
BPM	Bipolar membrane
BPMED	Bipolar membrane electrodialysis
CCUS	Carbon capture and storage
CDI	Capacitive deionization
CEL	Cation exchange layer
CEM	cation exchange membrane
DAC	Direct air capture
DACS	Direct air capture and storage
DIC	Dissolved inorganic carbon
EC	Electrical conductivity
ED	Electrodialysis
EDX	Energy dispersive X-ray
EV	Electric vehicles
IEA	International energy agency
IEM	Ion exchange membrane
IL	Interfacial layer
MCDI	Membrane capacitive deionization
MD	Membrane distillation
MRV	Monitoring, reporting and verification
NZE	Net zero emissions
OCT	Optical coherence tomography
PAA	Polyacrylic acid
PCET	proton-coupled electron transfer
PMA	Polymaleic acid
PV	Photovoltaic
RO	Reverse osmosis
SEC	Specific energy consumption
SEM	Scanning electron microscope
WD	Water dissociation
WDR	Water dissocation reaction

Contents

Chapter 1

Introduction

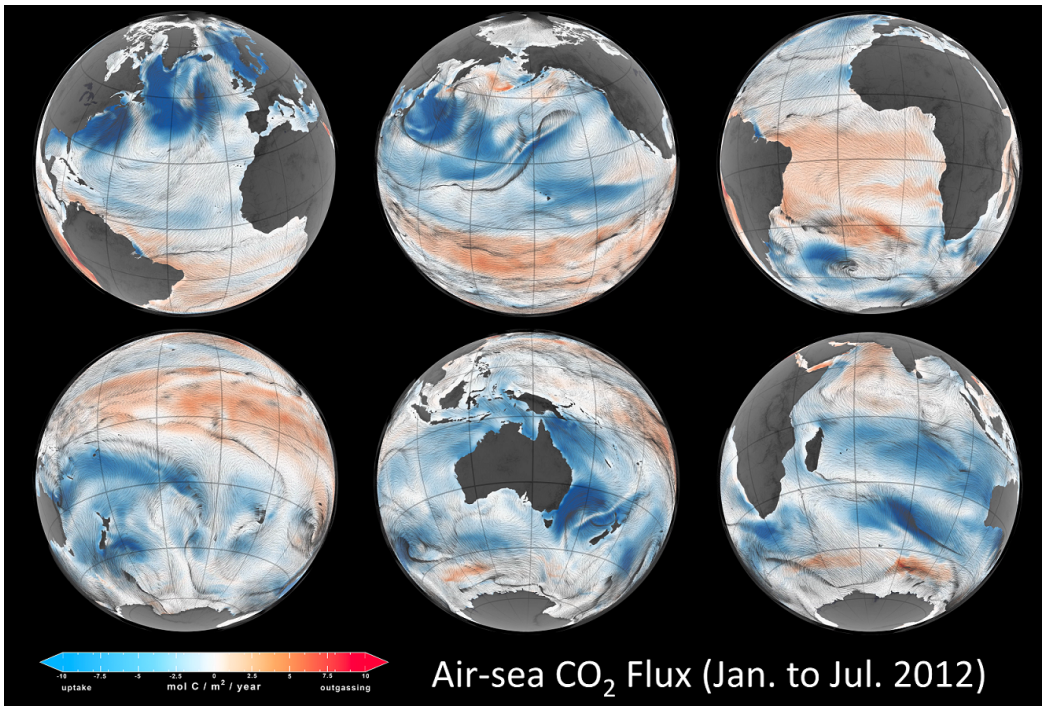

1.1 The Need for Carbon Capture

The global effort to combat climate change is focused on achieving net zero emissions to limit average global warming to 1.5 °C by 2050 [8]. However, this pathway has narrowed significantly, as global energy-related carbon dioxide (CO_2) emissions reached a new record high of 37.7 gigatonnes (Gt) in 2024 [9]. Although the energy sector has undergone major shifts since 2021, progress has been highly varied across technologies. There have been extremely positive developments, most notably the rapid progress of key clean energy technologies like solar photovoltaic (PV) panels and electric vehicles (EV), which are seeing accelerated deployment and capacity expansion in line with

image adapted from [7]

(or even ahead of) the net zero emission (NZE) scenario milestones. However, the transition has also faced significant headwinds in technologies requiring long lead times. The 2023 update of the "Net Zero Roadmap" report by the International Energy Agency (IEA) [1] reveals slower technological and market development progress for options like hydrogen and Carbon Capture, Utilisation, and Storage (CCUS) than initially anticipated. CCUS, in particular, has a history largely defined by underperformance, with slow deployment and limited progress in scaling up project pipelines and related infrastructure, leading to a downward revision of its near-term role in the NZE Scenario by IEA ([1]). The total projected CO_2 capture capacity required by CCUS in the NZE Scenario was reduced by 0.8 Gt for 2030 (falling from 1.8 Gt to 1.0 Gt) and by 1.6 Gt for 2050 (falling from 7.7 Gt to 6.1 Gt) in the 2023 update compared to the 2021 version (See the green section under the x-axis in Figure 1.1, representing the negative emissions from CO_2 capture from the atmosphere).

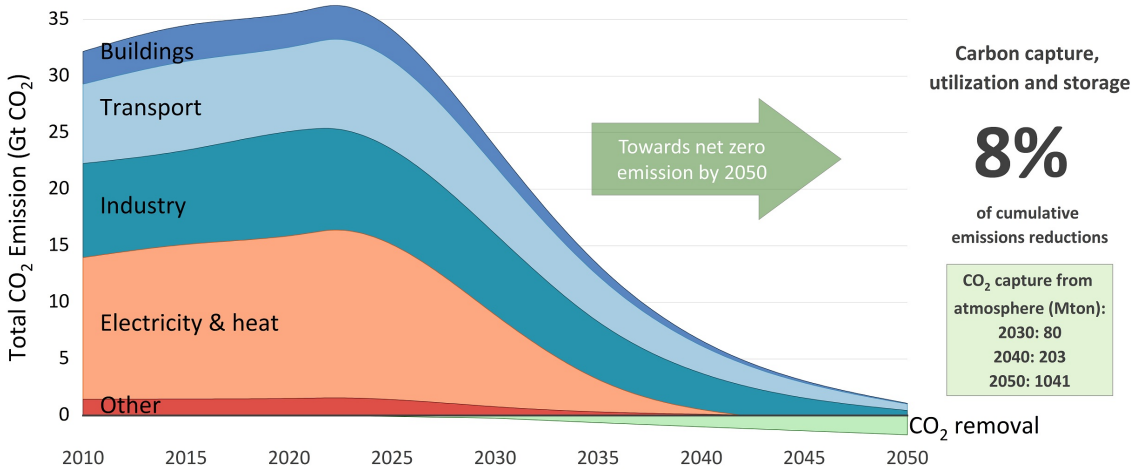

Figure 1.1: Key global emission milestones over time to achieve net-zero emissions by 2050. Projected global CO_2 capture capacity: If all announced projects materialize and current growth trends persist, capacity could reach net-zero levels by 2030. Accelerating project lead times (especially for CO_2 storage development) remains critical. information adapted from [1].

Despite the sluggish development of long-lead-time options, technologies focused on carbon management remain an essential component of the mitigation portfolio required for achieving net zero CO_2 emissions by 2050. CCUS is critical because it offers substantial emissions reductions primarily between 2030 and 2050, enabling the decarbonisation of sectors where emissions reductions through electrification are technically challenging. Even in the ambitious updated NZE Scenario, which accounts for accelerated electrification, residual CO_2 emissions from fuel combustion persist concentrated in hard-to-abate sectors such as industry and transport. In an optimistic transition pathway (NZE Scenario), technologies like CCUS, Direct Air Capture and Storage (DACS), and Bioenergy with Carbon Capture and Storage (BECCS) are vital for balancing these final residual emissions, necessitating a total CO_2 removal of 1.7 Gt in 2050 (amounting to 0.7 Gt CO_2 removal from the atmosphere by 2050). Conversely, a pessimistic scenario, involving further delays to ambitious policy action, would make the path to 1.5 °C much steeper and require a massive, costly reliance on

carbon removal technologies (scaling DACS and BECCS to over 5 Gt CO_2 removed annually later this century). Therefore, regardless of the pace of global climate action, carbon capture technologies are indispensable tools for mitigating persistent, hard-to-abate emissions originating predominantly from industry and transport sectors [1].

Each year, ca. 38 Gt of CO_2 are released into the atmosphere. Of this total, at least 35% comes from decentralized sources that cannot be mitigated locally [10]. Any emissions that remain uncaptured accumulate in the atmosphere, where they eventually reach equilibrium with dissolved CO_2 in the ocean through the carbonate system (see Chapter 2), causing ocean acidification and an increase of dissolved inorganic carbon (DIC) concentration in oceans around the globe over the last decades [11]. Although atmospheric carbon concentration is relatively low (around 400 ppm), the amount of dissolved inorganic carbon in seawater, when expressed as CO_2 gas, is over 140 times higher by volume than CO_2 in air [12]. Moreover, the ocean's vast surface area enables rapid air–sea carbon exchange, making it possible to indirectly capture atmospheric carbon through ocean-based removal strategies [13, 14].

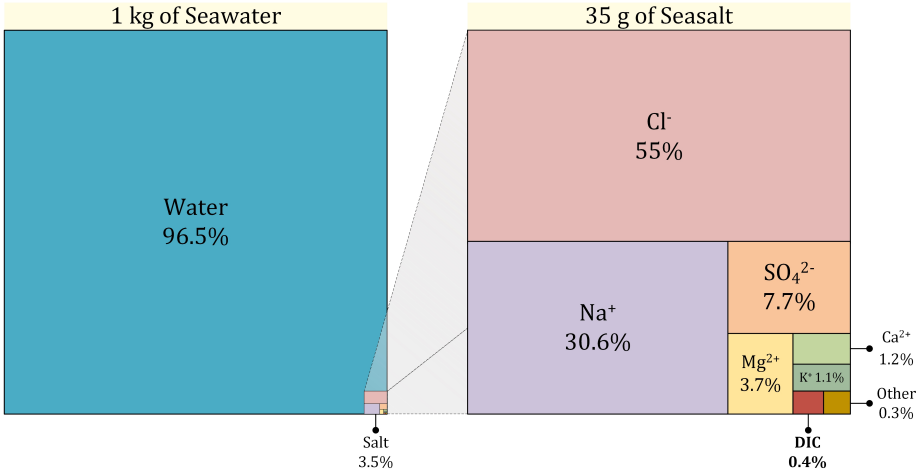

Figure 1.2: The relative proportions of each major ion in seawater, adapted from [2].

1.2 Electrochemical Approaches to CO_2 Capture

Electrochemical carbon capture uses electricity to drive the chemical reactions needed for CO_2 removal, offering a fully electrified pathway that aligns with renewable energy systems. Unlike conventional carbon capture (which often relies on heat-driven processes or chemical solvents), electrochemical methods can be powered directly by intermittent renewable electricity and adjusted on demand [15, 16]. This means CO_2 can be captured without combustion or thermal regeneration steps, making the process more flexible and potentially more energy-efficient. In addition, electrochemical systems can be modular and tunable: capture rates can be controlled by adjusting the electrical current or voltage, and units can be scaled up by stacking or numbering up of cells. These traits make electrochemical approaches attractive for a future decarbonized industry that seeks to harness clean electricity for emissions control [15, 16]. If CO_2 can be efficiently extracted from seawater, the surrounding ocean and atmosphere will equilibrate, and more atmospheric CO_2 will

passively dissolve into the ocean to replace what was removed [17]. This approach could thus help achieve net-negative emissions by enhancing the ocean's natural uptake of CO_2.

The pH-swing concept: Virtually all electrochemical CO_2 removal methods rely on manipulating the pH of a solution to control the form and fate of the dissolved inorganic carbon [15]. When CO_2 dissolves in water, it forms bicarbonate and carbonate ions (collectively "DIC"). By raising the pH (making the solution more alkaline), DIC is converted into bicarbonate/carbonate, allowing the water to absorb additional CO_2 from air. Conversely, by lowering the pH (making the solution acidic), bicarbonate/carbonate ions are converted back into CO_2, which can then be collected as a concentrated stream [18]. Electrochemical systems achieve this "pH swing" without adding chemical reagents: instead, an electric current is used to generate acid and base internally or externally (see Chapter 4) to alter the chemical equilibrium. After the CO_2 is stripped out in the acid step, the now slightly alkaline water can be returned to the ocean, where it will uptake more CO_2 from the atmosphere over time [17, 19]. In essence, the ocean acts as an intermediary "CO_2 sponge" – electrochemical reactors periodically wring out the sponge by acidifying the water to release CO_2, then send the CO_2 depleted water back to absorb more CO_2 from the air. A variety of reactor designs have been developed to carry out this pH-swing based carbon capture:

Redox-mediated CO_2 capture: These systems use redox-active chemical agents to alternately bind and release CO_2. In these systems, an electrochemical cell drives a reversible reaction in a chemical sorbent. For example, certain organic molecules (such as quinones) or metal complexes can capture CO_2 when reduced and release it upon oxidation (or vice versa) [20]. By applying a voltage, the sorbent's affinity for CO_2 is switched on and off in an "electro-swing" cycle (see Figure 1.3a). One advantage of redox-mediated approaches is that they can operate in a single liquid phase and do not necessarily require large pH changes. They can often run in aqueous solutions (avoiding flammable organic solvents) and can leverage fast electrochemical switching of the sorbent [16]. Researchers have demonstrated such systems for direct air capture, using organic mediators that capture CO_2 at one electrode and release it at the opposite electrode when the polarity is reversed [21]. While much of the redox-mediated CO_2 capture research has focused on capturing from gaseous streams, the same principles could be applied to CO_2 in water. The challenge is finding redox couples that are highly selective, stable over many cycles, and capable of carrying sufficient CO_2 per cycle to be practical. This is an active area of research bridging electrochemistry and chemical absorption techniques. Inorganic redox electrodes can modulate pH without soluble mediators by driving proton-coupled electron transfer (PCET) at the electrode interface, creating reversible local acid/base swings in seawater (Figure 1.3b) [17]. Membrane-free chloride-based systems (e.g., Ag/AgCl paired with Bi forming oxychloride species) enable cyclic pH modulation and DIC release. More broadly, metal oxides achieve pH swings via reversible proton uptake/release under applied potential (e.g., $MnO_2 \leftrightarrow MnOOH$), while hydrous transition-metal oxides ($Ni(OH)_2$, FeOOH, WO_3, $RuO_2{\cdot}xH_2O$) leverage hydrated surface layers and functional groups to buffer protons; their behavior is tunable through hydration, redox state, and structure. In particular, hydrated WO_3 can act as a reversible proton reservoir with kinetics governed by electrolyte and operating conditions, potentially aiding pH-asymmetric electrochemical systems [3, 22].

Electrolysis and "water-splitting" cells: Water-splitting cells can be repurposed as carbon-capture devices by using the electrochemically generated pH swing to manipulate seawater carbonate chemistry rather than solely producing H_2. Under applied current, the anode generates an acidic stream that can shift dissolved inorganic carbon toward CO_2 for release, while the cathode produces

OH^- that increases alkalinity, converting dissolved CO_2 to bicarbonate/carbonate and enabling electrochemically driven ocean alkalinity enhancement (OAE); in the presence of Mg^{2+} or Ca^{2+}, this alkaline environment can further promote carbonate mineralization, offering a pathway that can reduce reliance on separate gas–liquid contactors. This concept is also used for alkali absorbent (re)generation [23], with hydrogen as a co-product that may improve process value. Because the strongest pH shifts occur near electrode surfaces, recent designs aim to improve practical capture performance and stability by decoupling direct electrolysis from extreme local pH (e.g., using soluble redox couples to shuttle H^+ or OH^- between electrodes [16]) or by employing bipolar membranes to maintain separated acidic/alkaline environments while enabling direct seawater operation. The main operational barriers to carbon-capture deployment in seawater remain [24]: scaling and fouling can block transport and degrade electrodes, and chloride oxidation at the anode can generate chlorine and downstream byproducts, motivating strategies that suppress or re-purpose chlorine within integrated capture architectures (Figure 1.3c).

Bipolar membrane electrodialysis (BPMED) is one of the leading designs for electrochemical CO_2 capture from water. A bipolar membrane is a special ion-exchange membrane that, under an electric bias, splits water into H^+ and OH^- ions. In a BPMED stack, alternating layers of ion-selective membranes are used to create acidified and alkalinized streams from a saltwater feed [25]. In BPMED carbon capture, the acidic stream (rich in H^+) converts dissolved bicarbonate in seawater into CO_2 gas, which can be extracted (often by applying a vacuum or sparging) [18] (see Figure 1.3d). Meanwhile, the adjacent basic stream (rich in OH^-) becomes strongly alkaline and can be recombined with the CO_2-depleted water to make an alkaline effluent that is returned to the ocean. Researchers have demonstrated prototype BPMED systems that extract CO_2 from real seawater in this way (see Chapter 2). BPMED approaches have the advantage of using well-understood membrane technology (often adapted from electrodialysis or desalination) to generate the pH swing. However, they rely on expensive ion-exchange membranes and typically require additional measures (or sacrificial electrodes) to balance charges at the electrodes, which can add complexity and cost [26].

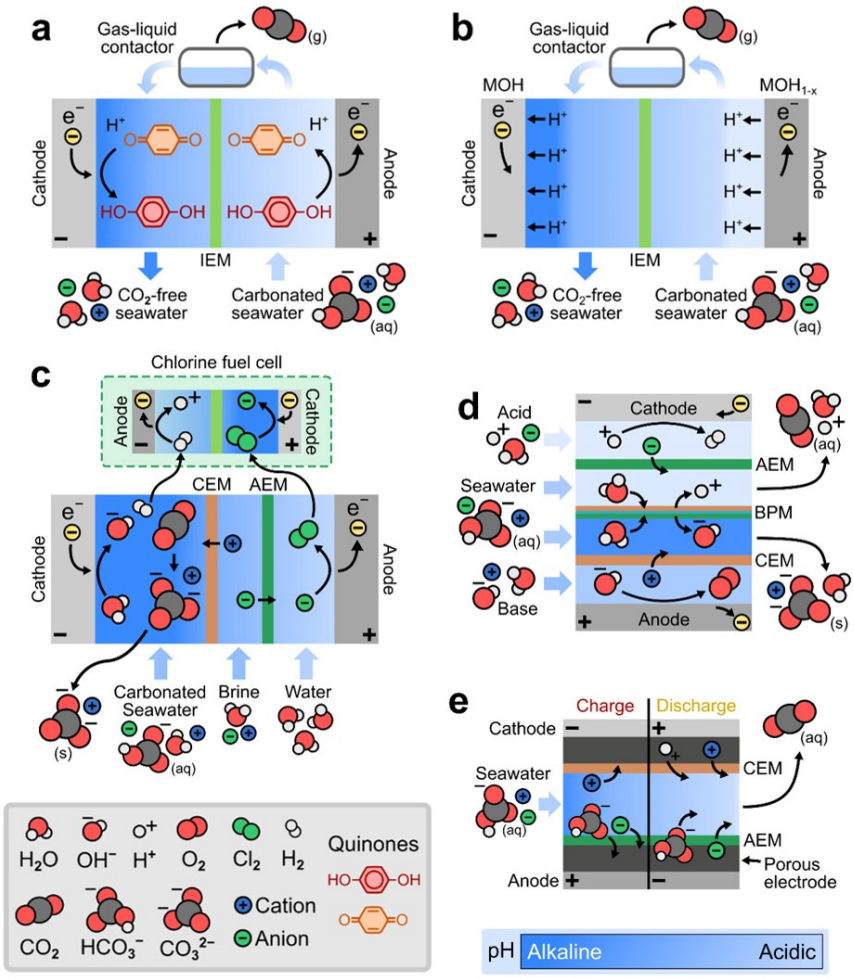

Figure 1.3: pH-swing electrochemical methods for CO_2 capture from seawater. Key approaches include: (a) molecular redox mediators, (b) inorganic redox-active electrodes, (c) seawater electrolysis coupled with Cl_2 fuel cells, (d) bipolar membrane electrodialysis, and (e) membrane capacitive deionization (MCDI), taken with permission from [3].

Capacitive deionization (CDI): Capacitive approaches use electrically charged surfaces (capacitor electrodes) to remove ions from solution. In a membrane capacitive deionization (MCDI) cell, for instance, applying a voltage causes cations and anions in the seawater to migrate into porous electrodes or behind ion-exchange membranes, effectively removing those ions from the bulk solution [27]. If designed correctly, this can remove more cations (e.g., Ca^{2+}, Na^{+}) than anions, leaving the bulk solution slightly acidic, thereby releasing CO_2. Reversing the voltage releases the ions, making the solution alkaline and enabling it to take up CO_2 again. In essence, CDI can create a swing between a CO_2-rich (acidic) and a CO_2-lean (alkaline) solution without the traditional water splitting process (Figure 1.3e). The appeal of CDI is that it avoids chemical reactions at the electrodes and instead relies on physical ion adsorption/desorption, which can be energy-efficient. A proof-of-concept study showed that MCDI could capture CO_2 from air-equilibrated water purely by electrical charging, forming bicarbonate ions during the capture step and releasing CO_2 gas upon discharge

[28]. However, the CO_2 capacity of CDI systems is limited by the surface area of electrodes and the ion-selectivity of the process, and efficiency can drop at very low concentrations. Still, this approach underscores the diversity of electrochemical means to induce a pH swing or otherwise isolate CO_2 and takes advantage of the inexpensive carbon based electrodes.

Emerging membrane-less systems: Given the cost and fragility of membranes in many designs, new approaches aim to eliminate ion-exchange membranes entirely. A recent example is a system developed by Rahimi *et al.*, which uses membrane-free electrochemical cells operating in a cyclic manner [29]. The proposed system presents a membraneless electrochemically mediated amine regeneration system by fundamentally redesigning the process configuration and using gas diffusion electrodes as both the anode and cathode. Eliminating the membrane and the need for additional equipment such as the absorption column, flash tank, and pumps, significantly reduces the process footprint and simplifies the flow diagram. The developers report energy consumption on the order of 0.5 kWh per kg CO_2 for their prototype system. The broader point is that membrane-less or hybrid designs (such as using reactive electrodes or soluble redox shuttles) could simplify the system and reduce costs [29]. By avoiding expensive membranes and chemical additives at the electrodes, these designs aim to tackle two common pain points of earlier systems. While still in early development, such innovations show the creativity in the field to improve robustness and economic viability.

Key advantages of electrochemical CO_2 capture, especially for ocean-based systems, include their integration with renewable energy and co-production of valuable outputs. These processes run on electricity, so as renewable power becomes cheaper and more abundant, electrochemical methods become more attractive for large-scale deployment. In contrast to thermal processes, an electrochemical reactor can be swiftly turned on or off or modulated, which is ideal for matching the variable supply of solar or wind power. Some designs also inherently produce useful co-products: for example, hydrogen gas from water-splitting or even chlorine byproducts in certain systems, which could potentially be sold or utilized. Moreover, the modularity of electrochemical cells means systems can be distributed or scaled up in a piecemeal fashion – for instance, a direct ocean capture unit might be installed at an existing desalination plant [19], or numerous small units could be placed on ships or offshore platforms to collectively remove CO_2 while in transit. This opens the door to capturing diffuse emissions (like those from shipping or coastal industries) that would be hard to tackle with centralized plants.

Current limitations and challenges: Despite their promise, electrochemical CO_2 capture technologies are still in their infancy and face several hurdles before they can contribute meaningfully to climate mitigation. Most prototypes to date have only been tested at laboratory or bench scale, with a few start-ups in Europe and USA going to pilot plant phase and handling relatively larger volumes of water and CO_2 [30]. A pilot plant, run by company Captura, is operational since early 2025 and has a capacity of 1000 tons of CO_2 per year.

A major issue is the sheer amount of throughput required: one study estimated that to remove around 0.1 Gt of CO_2 per year using ocean electrochemical methods, a volume of water equal to 1.3 Gt per year would need to be treated (or about 3 million m^3/day), which is up to 5–10 times greater than the production of the world's largest reverse osmosis desalination plants, and would require the supply of around 2,000 TWh of electricity annually [30]. This highlights the massive infrastructure that would be needed for electrochemical removal at climate-relevant scales (including large arrays of electrodes and membranes, and pumps to move these vast quantities of seawater). Crucially, for these methods to achieve net-negative emissions, the electricity must be sourced from carbon-free or renewable energy; if the energy source is carbon-intensive, the CO_2 generated during power production could significantly offset, or even exceed, the CO_2 removed from the ocean.

Energy use is a central concern: there is a theoretical minimum energy required to separate CO_2 (on the order of 20 kJ per mole for CO_2 at atmospheric concentrations), and real systems inevitably use several times that amount due to inefficiencies. Early electrochemical systems have reported energies around 100–200+ kJ per mole CO_2 (i.e. 0.6 to more than 1.3 kWh per kg) [17, 26], though rapid improvements are being made. For instance, a recent redox-mediated approach operated stably for over 200 hours and achieved 50 kJ per mole CO_2 at 10 mA/cm^2 current density[16]. Continued research aims to drive this energy number closer to the thermodynamic limit by reducing resistive losses, overpotentials, and auxiliary loads (such as pumping power).

Another major challenge, particularly for seawater-based capture, is dealing with ***fouling and scaling***. Seawater contains not only dissolved CO_2 but also significant levels of calcium, magnesium, and other ions (Figure 1.2). When the local pH is raised in an electrochemical cell (either to create a strongly alkaline environment to mineralize CO_2 [6], or for neutralizing the acidic CO_2-free seawater (see Chapter 2)), the dissolved minerals tend to form solid carbonates and hydroxides. This inorganic scaling can clog membranes and drastically reduce performance over time. Practically all reported ocean capture systems note this issue: for example, scaling by calcium/magnesium carbonates on the alkaline side of a BPMED or electrolysis cell is an "inherent issue" that reduces efficiency if not managed [19]. Proposed solutions include pre-treating the seawater to remove hardness (which adds cost and complexity), periodically acid-washing or reversing the system to dissolve precipitates, or operating the electrochemical cells in regimes that minimize pH extremes.

Another concern is the high capital costs. Electrochemical cells require specialized materials (electrode, ion-exchange membranes, power electronics) that can be expensive, and can deteriorate faster in contact with corrosive saltwater environments. Bipolar membranes, for instance, are currently far more costly than the commodity amines used in conventional scrubbing. Moreover, building offshore or coastal facilities to house these systems (or retrofitting ships and platforms) will require substantial investment. Early cost analyses have accordingly put electrochemical direct ocean capture on the high end of carbon removal options – several hundred dollars per tonne of CO_2 at minimum [26]. There is optimism that with technology learning curves and the use of cheaper materials, costs could fall dramatically (some start-ups claim future costs below $100 per ton for improved designs) [31]. Still, closing that gap will require significant engineering advances, economies of scale, and likely reductions in renewable energy prices.

Finally, as with any large-scale climate intervention, there are practical and environmental consider-

ations. Electrochemical CO_2 removal from seawater will necessitate handling enormous water flows – intakes and outfalls must be designed to avoid harming marine life (similar to concerns at desalination plants) [30]. The local alteration of water chemistry (making it commonly more alkaline) could impact marine ecosystems if not carefully managed, though proponents note that returning slightly alkaline water to the ocean could help counteract ongoing ocean acidification [19].
Verifying the net carbon removal is also non-trivial; it requires confirming that the treated water indeed absorbs additional CO_2 from the air and that the captured CO_2 is securely stored away. In this regards, Isometric has recently certified a monitoring, reporting and verification (MRV) protocol for CO_2 equivalent removal from atmosphere by CO_2 capture from seawater [31].
Despite the named challenges, research and pilot efforts are accelerating, driven by the clear need for durable carbon removal solutions. Electrochemical CO_2 capture, especially using the ocean as a vast interface, remains an essential candidate technology, one that, if matured, could address emissions from hard-to-decarbonize sectors and complement other carbon management strategies in the push for net-zero emissions by 2050. The following sections will delve deeper into specific components (such as the ion exchange membranes used in these systems), the fate of the captured CO_2, and the overall objectives and scope of this thesis.

1.3 Ion Exchange Membranes

The BPMED stack is composed of charged, dense ion-exchange membranes (IEMs, figure 1.4). These include cation-exchange membranes (CEMs, negatively charged), anion-exchange membranes (AEMs, positively charged), and bipolar membranes (BPMs). A BPM consists of a cation- and anion-exchange layer (CEL and AEL) laminated together, with a water dissociation catalyst positioned between them [32]. The type of IEM used determines the dominant ion carrier within the system [33]. For industrial use, key considerations include IEM cost, lifetime, permselectivity, and electrical resistance [34, 35]. In pH-swing capture using BPMs, reducing the voltage required for the water dissociation reaction toward its thermodynamic limit, rather than the current high value of approximately 0.83 V [36, 37], could lower process energy consumption by up to threefold. While IEMs operate under an electric field, microporous gas-liquid membrane contactors used for carbon capture work under partial pressure gradients of CO_2 [38].

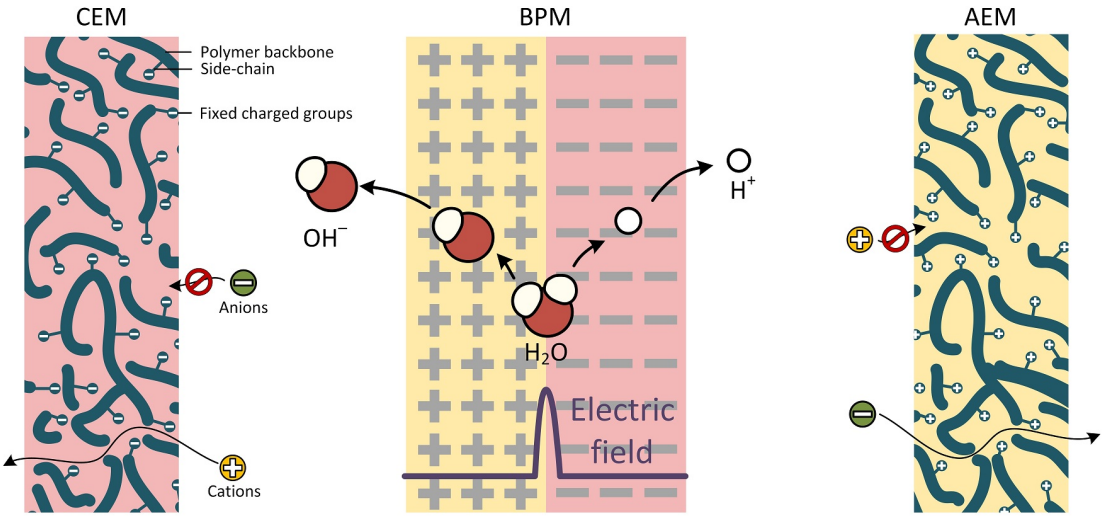

Figure 1.4: From right to left, the three types of ion-exchange membranes (IEMs): Anion-exchange membrane (AEM), which selectively transports negatively charged species, Bipolar membrane (BPM), designed to facilitate rapid water dissociation under an applied electric field, and Cation-exchange membrane (CEM), which selectively transports positively charged ions.

1.4 Fate of the Captured CO_2

Once separated as a concentrated stream, CO_2 can follow several pathways (Figure 1.5). First, it may be injected (typically in supercritical form) into deep geological formations such as saline aquifers, depleted oil and gas reservoirs, or unmineable coal seams, where it is trapped structurally, residually, solubly, and eventually by mineralisation over timescales of centuries to millennia. Second, CO_2 can be mineralised more directly by reaction with suitable mineral-rich rocks (for example basalts or ultramafic formations), forming stable magnesium and calcium carbonates that provide effectively permanent storage. Together, these geological and mineral pathways are currently regarded as the main options for durable CO_2 storage. A third route is to utilise CO_2 as a feedstock for products and energy carriers, for example in the electro-synthesis of fuels and chemicals (carbon capture and utilisation, CCU) [39]. Another emerging CCU pathway is the production of polymers and bioplastics, where captured CO_2 is incorporated into polymer backbones either directly or via CO_2-derived intermediates. Use of CO_2 in fuels or other short-lived products does not by itself achieve net carbon removal, because the carbon is ultimately re-emitted. However, when combined with renewable hydrogen and low-carbon energy, such pathways can enable the production of so-called net-zero or low-carbon fuels, in which the CO_2 released during combustion is approximately balanced by prior uptake in the capture step, rather than originating from fossil resources. In addition, revenues from CO_2-derived products can help offset the cost of capital-intensive capture and storage infrastructure, potentially accelerating early deployment of capture technologies in industry [39].

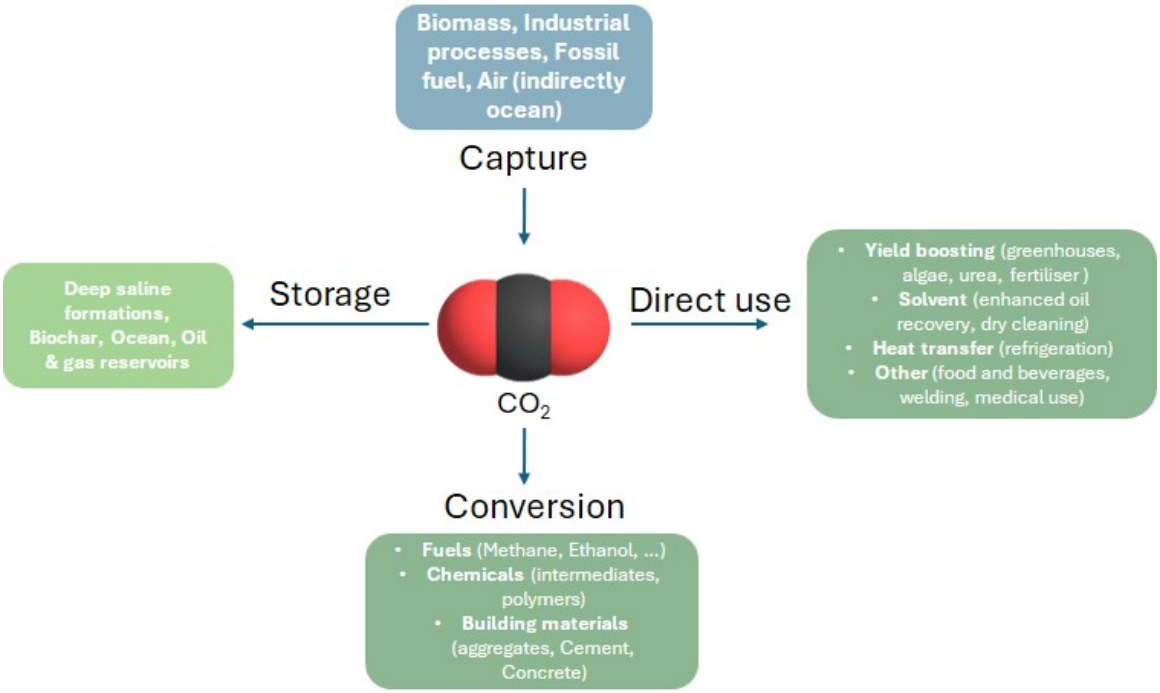

Figure 1.5: Simplified classification of CO_2 capture, utilization, and storage (CCUS) pathways (adapted from [4]) Globally, about 230 $MtCO_2$ per year are utilized.

1.5 Research Objectives and Outline of the Thesis

Electrochemical CO_2 capture offers several advantages over conventional thermal processes, including direct use of renewable electricity, modular implementation, and the ability to treat dilute CO_2 streams such as seawater. However, current concepts suffer from high specific electricity demand and operational challenges such as inorganic scaling, particularly in alkaline environment. These issues are especially relevant for BPMED, a promising yet emerging pH-swing technology for CO_2 capture from seawater.

This thesis therefore focuses on oceanic CO_2 capture using BPMED. Through a series of complementary experimental studies, it aims to quantify the impact of key operating parameters and electrolyte composition, elucidate the mechanisms of inorganic scaling on the alkaline side of bipolar membranes, and evaluate advanced BPMED configurations that integrate CO_2 capture with alkaline product generation. The overarching research question is to understand and improve the performance and robustness of BPMED under relevant conditions, with particular emphasis on energy consumption and inorganic scaling:

> How can BPMED be designed, operated, and integrated with other available streams (e.g. desalination brine) in order to enable energy-efficient, scalable and environmentally sustainable electrochemical CO_2 capture from seawater, while managing scaling on the alkaline side?

To address this question, the thesis focuses on three specific research questions, each described

extensively in separate chapters:

RQ1 – Process performance and operating window (Chapter 2): How do feed salinity, flow rate, applied voltage/current density, and electrolyte composition affect DIC removal, specific electrical energy consumption, and current efficiency in BPMED-based CO_2 capture from water, and to what extent can tailored electrolyte solutions reduce the energy demand?

RQ2 – Scaling mechanisms and controlling factors (Chapter 3): What are the dominant mechanisms and controlling parameters of inorganic scaling on the alkaline side of bipolar membranes under seawater-like conditions, and how do current density, hydrodynamics (flow rate and spacer configuration), ion composition (in particular Mg^{2+}, Ca^{2+} and $SO_4{}^{2-}$), and DIC content influence scaling volume, coverage, and morphology?

RQ3 – Closed-loop integration and NaOH co-production (Chapter 4): Can a closed-loop alkaline BPMED configuration, integrated with a gas–liquid membrane contactor, be operated to simultaneously capture CO_2 from seawater and produce NaOH, while limiting scaling and achieving competitive specific energy consumption and high current efficiency compared with conventional BPMED operation?

A final, cross-cutting objective of the thesis is to synthesize the insights from these studies into practical guidelines for the design and operation of BPMED-based CO_2 capture processes, including recommended operating windows and scaling-mitigation strategies. Throughout the thesis, performance and energy metrics are consistently reported to enable a transparent comparison of different configurations and operating conditions.

Chapter 2

A Systematic Analysis Of Operating Parameters For CO_2 Capture From Seawater By Bipolar Membrane Electrodialysis (BPMED)

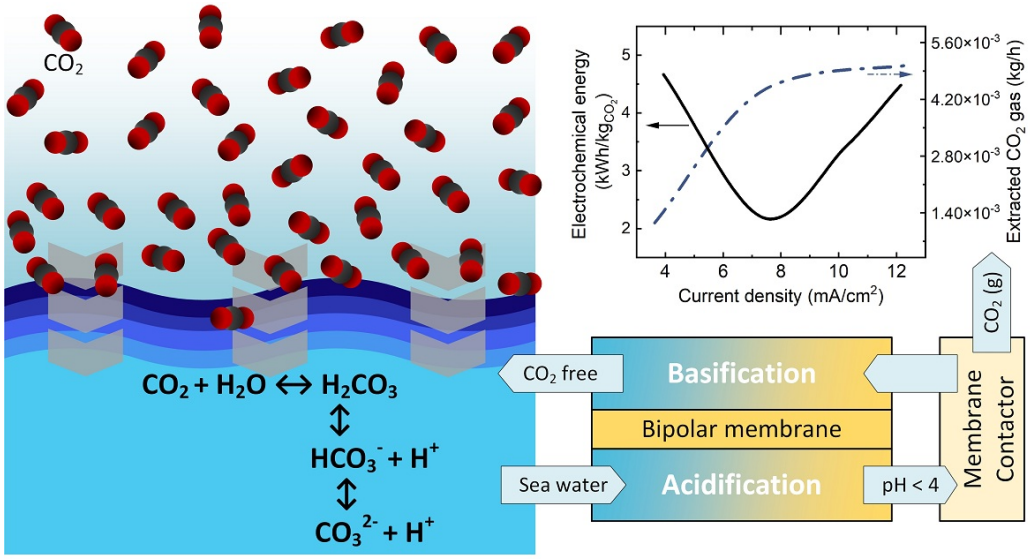

This chapter is published as:
Aliaskari, M., Wezstein, J., Saravia, F., & Horn, H. (2024). A systematic analysis of operating parameters for CO_2 capture from seawater by Bipolar Membrane Electrodialysis (BPMED). Separation and Purification Technology, 339, 126679.
doi: https://doi.org/10.1016/j.seppur.2024.126679

2. A Systematic Analysis Of Operating Parameters For CO_2 Capture From Seawater By Bipolar Membrane Electrodialysis (BPMED)

Abstract

With the escalating environmental impact of carbon dioxide (CO_2) emissions, effective CO_2 capture is of paramount importance. Fully electrochemical processes can play a key role in this endeavor. In particular, bipolar membranes can induce the necessary ΔpH to convert the bicarbonate present in water into dissolved CO_2, which can later be extracted. The primary goal of this study is to better understand the working mechanisms of the BPMED pH swing carbon capture process. Factors such as flow rate, voltage, current density, feed water salinity and alternative electrolytes are investigated to optimize carbon capture from water. Here, a pilot scale BPMED membrane stack and a membrane contactor were used with model water similar to seawater. The extent of bicarbonate removal, mass flow of CO_2 gas and energy intensity were measured. By using a new electrolyte solution (0.1 M $K_3/K_4[Fe(CN)_6]$), a 20% reduction in energy consumption was observed (by avoiding the water dissociation reaction in cathode and anode). While at low salinities (about 2 mS/cm) CO_2 production was limited and resulted in high energy consumption, at salinities ¿9 mS/cm an increasing energy demand was observed due to increased ohmic losses and limited bicarbonate concentration. Increasing the flow rate in the membrane stack allowed more bicarbonate and consequently more CO_2 gas to be extracted. Changing the velocity from 1 to 3 cm/s resulted in a reduction in energy consumption from 3.7 to 2.5 kWh/kg CO_2. The study concludes that further research is needed to increase the efficiency of the BPMED process, particularly in long-term operation and to mitigate scaling/fouling effects on the bipolar membrane. Despite its current limitations, BPMED provides a fully electrified alternative for CO_2 capture from water.

Keywords:

Bipolar-Membrane, Carbon Capture, Direct Ocean Capture, Electrodialysis

2.1 Introduction

Damaging impact of carbon dioxide (CO_2) increases the need for emission control and carbon capture (from both air and ocean waters) where possible [40]. To achieve the Paris agreement's target of limiting the global temperature increase to 1.5 °C above pre-industrial levels, a net zero greenhouse gasses emission by year 2100 is necessary [8, 41]. Negative emission technologies (NET) can remove CO_2 from carbon sinks (atmosphere and ocean) [42]. And offset emissions that are difficult to eliminate, such as those from aviation, agriculture, and industrial processes [43]. On the other hand, the collected CO_2 from these technologies can be used to produce carbon-based fuels in power-to-x processes [44]. To avoid further CO_2 emissions, integrating renewable energy in the overall process and following the minimum qualifications for zero emission is necessary [42, 45].

Electrochemical processes have proven to be more efficient since they do not use chemicals and target the molecules directly rather than the medium, and they can be easily integrated with renewable energy sources [15, 46]. These processes have been used to capture CO_2 from both air [47, 48] and seawater [26, 49, 50]. Direct air capture (DAC) is used to extract CO_2 from the ambient air. It has been the focus of many research works in the past years and is considered the state-of-the-art technology for CO_2 capture [51–54]. In DAC processes, CO_2 is first absorbed by an absorbent, and is extracted later.

In CO_2 capture from seawater however, the absorption process is removed (since the large surface of seawater has already made that happen) and CO_2 is extracted indirectly from seawater. Seawater contains between 80 and 120 mg/L CO_2 at all depths [55]. This is around 120 times more than the concentration of CO_2 in air (750 mg/m^3) [15] This makes seawater an alternative to the ambient air as a source for CO_2 capture.
An initial study by Willauer *et al.* [56] demonstrated the ability of ion exchange resins to remove bicarbonate from seawater. However, the large amounts of demineralized water, acid and base solutions required to regenerate the resins make these processes inappropriate. The electrochemical regeneration of the resins are also investigated in a later study to reduce the cost and also avoid the use of chemicals [49]. More recent studies have focused on different approaches of carbon capture from seawater by using bipolar membranes. These include acidifying the seawater to extract gaseous CO_2 [57], or in situ carbonate mineralization by increasing the pH of the sea water [6]. Moreover, by using acid and base generation from seawater with BPMED, ocean alkalinity can be enhanced and CO_2 from atmosphere is safely stored in oceans in form of bicarbonates [14].

2.1.1 Direct air capture (DAC)

In DAC processes, CO_2 is captured from ambient air and produce a more concentrated stream of CO_2 [58]. There are different methods of DAC, however, the two furthest developed techniques are liquid solvent and solid sorbent DAC [59].
In liquid solvent processes, CO_2 in the air is absorbed by the solvent, once in solution, it diffuses through the bulk until it reacts with a solvent specie and is therefore "captured" [59]. Various solvents are used for this purpose, from alkaline solutions of NaOH and KOH to amines and peptides [60]. For the extraction of CO_2 from the solvent, several thermal and chemical methods can be employed, namely the more traditional method of thermal swing and newly investigated methods such as carbonate crystallization or electrochemical processes [35]. With solid sorbents, materials with affinity to CO_2 are favored. Solid-based sorption is divided to physisorption and chemisorption, which are again divided into inorganic and organic types [61]. After the sorbent is saturated with CO_2, the filter (which contains the sorbent) is heated and the CO_2 is released [62].
The specific electrical energy consumption for the most advanced methods of DAC ranges from 0.2 to 1.2 kWh/kg CO_2 (global average of more than 0.4 kWh/kg CO_2). The required thermal energy consumption of the same systems ranges from 1.1 to 1.9 kWh/kg CO_2 (global average of ca. 1.7 kWh/kg_{CO2}) [51, 63]. Low concentration of air forces huge amounts of air to be processed for CO_2 extraction, e.g. in a 1 Mt-CO_2/year plant, processing of at least 46000 m^3/s of air is necessary [34]. No single technology can reduce global emissions alone, and the development of other technologies will also be necessary [64, 65].

2.1.2 Dissolved inorganic carbon (DIC) in water

Around 23% of all emitted CO_2 is adsorbed by the oceans through a series of chemical reactions (see equation (2.1)). The higher concentration of CO_2 in air has resulted in an increased levels of the dissolved inorganic carbon (DIC), which in part has acidified the oceans [40, 66].

$$CO_2(g) \rightleftharpoons CO_2(aq) + H_2O \rightleftharpoons H_2CO_3 \rightleftharpoons H^+ + HCO_3^- \rightleftharpoons 2\,H^+ + CO_3^{2-} \tag{2.1}$$

The solubility of CO_2 in water decreases slightly with increasing salinity. At a constant temperature of 20 °C, the solubility constant coefficient (K_0) of CO_2 with zero salinity is $3.910 \cdot 10^{-2}$ mol/L·atm. At the normal sea water salinity of 3.6%, K_0 is reduced to $3.245 \cdot 10^{-2}$ mol/L·atm [67]. The CO_2 solubility is also dependent on the pH, temperature and pressure of the studied systems. At higher CO_2 partial pressures solubility increases, while increased temperatures result in lower solubility of CO_2 in water. Under basic conditions (for example, when hydroxide is added and alkalinity is increased), reaction (2.1) is shifted to the right, allowing higher levels of DIC at slightly higher equilibrium pH values once equilibrated, thereby increasing the total DIC concentration in the water [68]. Depending on the pH of the water, DIC can take different forms. Figure 2.1 shows the speciation of DIC in seawater composition in a pH range of 2 to 12. As it is seen, at neutral pH, most of the DIC is available in the bicarbonate form.

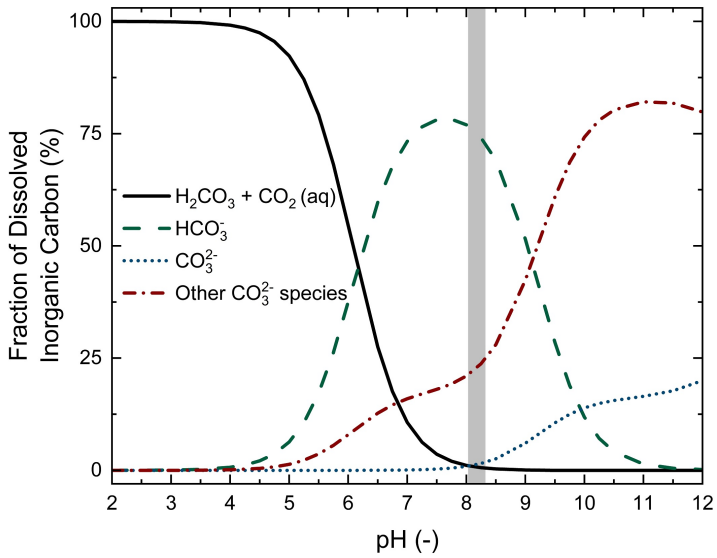

Figure 2.1: DIC speciation over pH 2-12, grey bar shows the pH range of seawater. Modelled with Visual MinteQ 3.1 by fixing pH at different values, the ionic strength was calculated based on the concentrations of ions present in solution (North Sea water composition, EC: 50 mS/cm, 20 °C, atmospheric CO_2 pressure: 0.00038 atm)

The total DIC can be described by the sum of all carbonic fractions:

$$\mathrm{DIC} = [\mathrm{H_2CO_3}] + [\mathrm{CO_{2(aq)}}] + [\mathrm{HCO_3}-] + [{\mathrm{CO_3}}^{2-}] \tag{2.2}$$

In presence of other ions, additional carbonate species (for example $NaCO_3^-$, $NaHCO_3$(aq)) must be added to equation 2.2 as well.

To extract the DIC in form of CO_2 gas from water, a pH-swing can be used. The induced pH-swing leverages the thermodynamic equilibrium of fractions of DIC at different pH values. The equilibrium ratio of $[CO_2(aq)]+[H_2CO_3]$ over $[HCO_3^-]$ increases 100 folds with a 2 pH-unit change [69], thus providing more CO_2 ready for extraction. However favorable thermodynamically, the kinetics of this

reaction is very slow [70]. To overcome this slow kinetics, using a wider pH range and application of reaction catalysts are suggested [15]. While applicable catalysts are not fully developed, using a wider pH range for effective CO_2 capture is necessary to increase the kinetics of the process in normal operations [15, 71]. However, promising results have been obtained in recent work by Lucas et al. [37], in which by using an asymmetric bipolar membrane (BPM), and addition of Graphene Oxides to the interfacial layer (IL) of the bipolar membrane. The limitations of water transport in the anion exchange layer (AEL) of the membrane is avoided by using the asymmetric properties of the membrane, and using a thin AEL.

2.2 Bipolar membrane electrodialysis for CO_2 capture

Different electrochemical processes can be used to induce the required pH-swing in order to extract CO_2 from water (e.g., electrolysis, bipolar membrane, capacitive deionization and PCET). Sharifian *et al.* [15], Muroyama *et al.* [63], Rahimi *et al.* [26, 50] and Xu *et al.* [72] have recently reviewed these processes. Among the reviewed processes, bipolar membrane electrodialysis is more advanced, easier to scale up, and is less energy intensive while providing the required pH-swing. The BPM is constructed by laminating a cation exchange layer (CEL) and an anion exchange layer (AEL) together. When placed under a reverse bias (i.e., CEL facing the cathode and AEL facing the anode), the junction of the AEL and CEL (called the interfacial layer (IL)) is depleted of ions and H^+ and OH^- ions are produced and transferred across the CEL and AEL respectively, noting that the water dissociation occurs above a certain voltage. This creates a pH gradient across the bipolar membrane [32]. To produce a $\Delta pH = 14$ with BPM, the minimum required thermodynamic voltage required is 0.829 V. This is 2.5 times lower when the same ΔpH is induced by electrolysis, as no gas evolution reaction takes place in BPM [73]. The use of BPM for CO_2 extraction has been studied as early as 1995 [74], in which CO_2 from air was absorbed by an alkaline (KOH) scrubbing liquid. The CO_2 was then extracted by acidification of the scrubbing liquid with an acidic solution (H_2SO_4). The BPM was used to regenerate both the acid and base for the absorber and extraction units. The energy consumption for the acid and base regeneration in the electrodialysis cell was calculated at 2.7 kWh/kg CO_2. Further studies have later investigated different aspects of the same process [75–79], mostly by using flue gas and an alkaline solution absorber, which is later regenerated by BPMED. Sabatino *et al.* [35] have investigated using two configurations of BPM with AEM and CEM for the recovery of CO_2 in a DAC process. Their results show that the performance of a membrane stack with BPM-CEM configuration is comparable to other liquid-scrubbing DAC technologies, at around 6.6 kWh/kg CO_2. The BPM-AEM configuration however suffers from poor selectivity and higher capital costs. It is estimated that a 10-fold increase in the selectivity performance of the AEM is necessary to make this configuration compete with the BPM-CEM setup.

In a recent work by Bui et al. [80], a model has been developed by mimicking a 4-probe BPMED cell. The developed model (validated by experiments) shows that for CO_2 extraction from a rich-bicarbonate solution (0.5 M $KHCO_3$) by BPMED, a minimum energy intensity of 0.63 kWh/kg_{CO2} is necessary. The extraction of CO_2 from rich-bicarbonate solutions (0.5 and 1 M $KHCO_3$) at higher current densities (up to 100 mA/cm^2) is suggested. At higher current densities the coulombic efficiency (fraction of the applied current density that goes toward regenerating CO_2) of the system improves and results in reduced energy intensity. However, bubbling of the CO_2 gas on the surface of the BPM can reduce the available surface of the membrane and therefore decrease efficiency of

the system. To avoid this, the electrodialytic extraction of CO_2 can be performed in pressured membrane stacks. Working at current density of 139 mA/cm^2, at a pressure of 6 atm, reduces the energy consumption up to 29% compared to operation at 1.5 atm [18].

2.2.1 BPMED for CO_2 capture from seawater

Flowrate: Eisaman *et al.* [57], extracted 59% of the DIC in seawater as CO_2 gas by acidification thru BPMED with an energy consumption of 1.53 kWh/kg CO_2. At higher flowrates (from 186 to 360 L/h), more CO_2 could be extracted, as more DIC was available. This was in accordance with a study by Iizuka *et al.* [75], that investigated CO_2 adsorption by BPMED from a carbonate solution. A flowrate between 70 to 216 L/h was tested and higher flowrates resulted in more CO_2 generation and therefore a reduced specific energy consumption. However, when normalized current at different flowrates was calculated, it was understood that flowrate has minimal impact on the produced ΔpH compared to other parameters such as ionic strength and applied voltage [57]. In a study by Vermaas *et al.* [81] which explores ion transport mechanisms through BPM, it was shown that between the cell voltage of 0.4 to 0.7 V, a higher flow velocity (from 0.03 to 1.5 cm/s) increases the current density (up to 2 times). However, at cell voltage of 0.8 V, the current density difference between different flow velocities becomes negligible. The flow orientation in the acidic and basic chambers effect the ΔpH on the surface of the BPM, however the ΔpH in bulk solution over the BPM is not affected and the internal characteristics of the BPM plays a greater role [82].

Applied voltage: The energy consumption of the BPMED process is mostly dependent on the applied voltage (i.e. current density) on the membrane stack to produce the desired ΔpH over the BPM [13]. However, at lower voltages (¡0.7 V/cell), the CO_2 extraction rate is also too low as the required ΔpH is not produced and therefore the DIC is not totally available for extraction [34]. Therefore, a trade-off between the energy consumption and the CO_2 extraction rate exists. A minimum energy consumption of ¡1 kWh/kg CO_2 has been reported by Digdaya *et al.* [19] in which the electrolyte reaction in cathode and anode does not include a water dissociation reaction (WDR) and the corresponding voltage loss in electrodes (due to H_2 and O_2 evolution reactions) is avoided. This is possible by using a reversible redox-couple mixture of 0.1 M $K_3/K_4(Fe(CN)_6)$ solution in electrode compartments (see equation 2.3 and 2.4).

$$\text{Cathode reaction: } [Fe(CN)_6]^{3-} + e^- \longrightarrow [Fe(CN)_6]^{4-} \tag{2.3}$$

$$\text{Anode reaction: } [Fe(CN)_6]^{4-} \longrightarrow [Fe(CN)_6]^{3-} + e^- \tag{2.4}$$

It is worth mentioning that while in a 10 cell membrane stack the cathode/anode (O_2 and H_2 evolution) reaction represent about 20% of the energy consumption, in larger systems (e.g. with 100 to 200 cell pairs) the voltage loss related to these reactions becomes negligible [57]. Unlike rich-bicarbonate solutions (up to 1 M $KHCO_3$ in DAC systems), the coulombic efficiency decreases significantly at higher current densities ($\leq$40% at current densities above 10 mA/cm^2) [80]. This is due to the very low DIC concentration in seawater. The relation between the output pH (and subsequently the transformation rate of HCO_3^- to $H_2CO_3/CO_{2(aq)}$ or CO_3^{2-}) and the applied current density has been investigated in few studies. As expected, production rate of H^+/OH^- increases at higher applied currents [57, 75, 83, 83, 84]. However, above optimal current densities, WDR at the AEM [85] and increased ohmic losses at the BPM [86] increases the energy consumption.

Salinity: While the research on the extraction of CO_2 from seawater is abundant, only in a study

by Eisaman *et al.* [57]the extraction of CO_2 from reverse osmosis (RO) brine (two-time salinity of seawater) is explored. The current density and CO_2 extraction rate over the acid output pH with RO brine was around two times more than the seawater feed. It must be noted that the increased CO_2 rate was due to the doubled concentration of the bicarbonate in the RO compared to seawater. Bipolar membrane processes are sensitive to the salt content of the feed [81]. At high salt concentrations the resistance of the membrane stack is lower and therefore higher current densities can be achieved with the same electric potential. However, conduction of ions through the BPM and AEM increases and causes energy losses. The presence of other anions in water can also decrease the efficiency of the process [81]. This is due to inefficiencies due to the loss of energy associated with transport of other ions (e.g. Cl^-, SO_4^{2-}, OH^-, ...) in AEM and also WDR in BPM [87, 88]. The extraction of the CO_2 from other water resources (surface and sub-surface) that contain DIC, but have lower salinity has not been investigated in literature to the best of our knowledge. While most of the studies have focused on the extraction of gaseous CO_2 from the acidic stream, capture and storage of the DIC in form of solids is also possible through basification of the water. At pH ¿ pK_{a2}, HCO_3^- converts to CO_3^{2-}, and can participate after reacting with dissolved Mg^{2+} and Ca^{2+} in water [33, 89]. Since concentration of Mg^{2+} and Ca^{2+} are much higher than the DIC in water, through this way it is theoretically possible to remove all DIC [90]. However, formation of scaling in the membrane stack and the slow kinetics are the main drawbacks of this method of carbon capture. Sharifian *et al.* [6, 33]have proposed to use the slow kinetics of mineralization as a tool to combat the scaling on the membrane surface. It was possible to extract argonite with a specific energy consumption of 0.88 kWh/kg_{CO2} from the water. Despite the low energy consumption, the fouling and scaling remains the most important challenge this process faces [6]. The scaling and formation of precipitates has also been the case in other electrochemical processes that mineralize the DIC in water [91].

2.3 Research questions

This study tends to address key questions regarding the energy-efficient carbon capture process using BPMED pH swing. It explores the complex interaction of flowrate, voltage, current density, and salinity on energy consumption and DIC removal during carbon capture from water. The experiments are designed to optimize the process, considering alternative electrolytes, and comprehensively understand the influence of feed water characteristics and various operational factors (flow velocity, applied voltage and current density) for carbon capture.

2.4 Materials and methods

2.4.1 Chemicals and solutions

The model seawater was prepared by dilution of a brine solution from Bad Wimpfen, Germany (10%), with equal parts of Karlsruhe tap water and deionized water (45%) and addition of $CaCl_2$ salt (¿99.5% purity, Merck, Germany). The final composition of the model water is presented in Table 2.1. This model water was prepared to have a close ion concentration for sodium, chloride and calcium as North Sea water. A more detailed analysis of the feed water is presented in Table 2.3.

Table 2.1: concentration of ions in the prepared model water and North Sea.

Water	Cl^- (mg/L)	Na^+ (mg/L)	Ca^{2+} (mg/L)	HCO_3^- (mg/L)	EC (mS/cm)	pH
Model water	19,666	13,405	407	182	49 ± 1	7.8 ± 0.2
North Sea	18,980	10,556	400	140	~ 50	7.9–8.4

Table 2.2: Ion-exchange membrane properties (adapted from PCCell Membrane Handling Guide).

Property	PC Acid 60 (AEM)	PC MTE (CEM)	PC bip (BPM)
Resistance ($\Omega \cdot cm^2$)	≈ 2.4 (0.5 N KCl)	≈ 4.5 (0.5 N KCl)	–
IEC (meq g^{-1})	≈ 1.2 (strong basic)	≈ 0.7 (weak basic)	≈ 1.8 (strong basic)
Thickness (μm)	100–110	220	200–350
pH stability	0–11	1–13	0–12
Water-splitting efficiency	–	–	> 0.95
Water-splitting voltage (V)	–	–	0.8–1.0

5 liters of 10 g/L Na_2SO_4 (¿99.5% purity, Merck, Germany) solution was used as the standard electrode rinse solution. 0.1 M solutions of $K_3[Fe(CN)_6]$ (AnalR NORMAPUR, VWR chemicals, Germany) and $K_4[Fe(CN)_6] \cdot 3H_2O$ (AnalR NORMAPUR, VWR chemicals, Germany) were mixed and used as the electrolyte solution in mentioned experiments. 0.1 M HCl was prepared from 37% concentrated hydrochloric acid (AnalaR NORMAPUR, VWR Chemicals, Germany) for the titrimetric determination of DIC in water samples.

2.4.2 Experimental setup

Figure 2.2a shows a schematic diagram of the experimental setup (BED 1-3 Compact measurement, PCCell GmbH, Germany). The system was equipped with online EC (digiLine Ci, Jumo, Germany), pH (tecLine pH, JUMO, Germany) and flowrate meters (type 123, GF Piping Systems, Germany). The pumps and the DC power supply (DPPS-32-15, Voltcraft, Germany) were controlled with the integrated software, which also recorded the data from the sensors. The feed water was prepared in a 100 L tank and was pumped through a filter (0.2 µm) before flowing into the membrane stack. The pH electrodes were calibrated daily.

A 10-cell pair ED cell (PCCell GmbH, Germany) was used (figure 2.2b). A cell pair consisted of a bipolar membrane (PC bip, PCCell) and an anion exchange membrane (PC Acid 60, PCCell), with the effective surface area of 84 cm^2. Membrane properties are summarized in table 2.2. The membranes were separated by 1.5 mm polypropylene spacers. Two end cation exchange membranes (PC MTE, PCCell) were used to separate the cell pairs from the electrolyte solutions. A Pt-Ir and mixed metal oxide coated Ti-stretched mesh was utilized as the anode, while a stainless-steel mesh was used as the cathode (provided by PCCell). The extraction of CO_2 from the acidified stream was carried out using only one membrane contactor (Liqui-Cel EXF-2.5x8, 3M, USA) operating in vacuum mode. The volume of the collected gas was quantified using a milli gas counter (MGC-1 v3.4, Ritter, Germany). To analyze the composition of the extracted and collected gas, a multi gas analyzer (RMS-MOD-IR1, Ritter, Germany) was used.

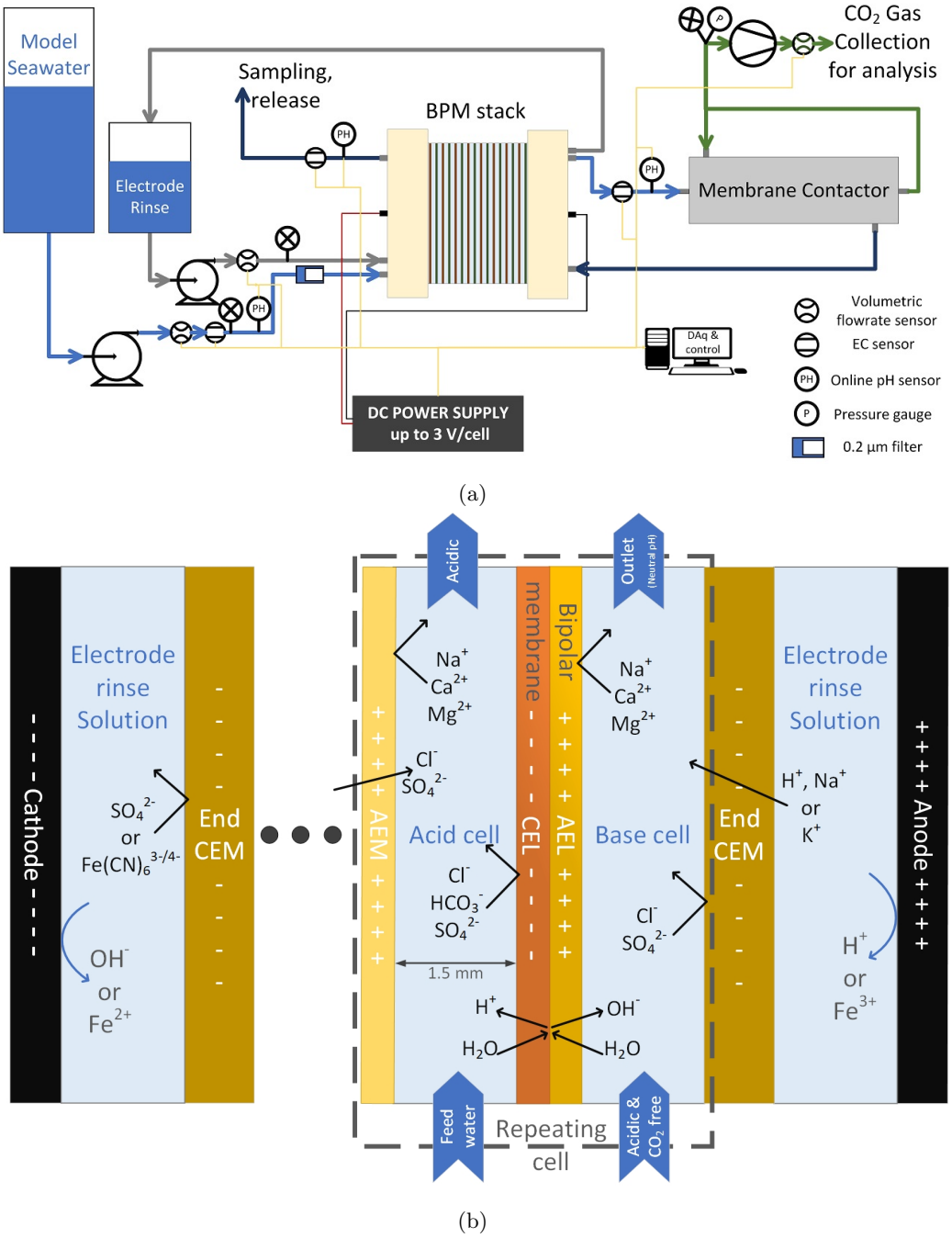

Figure 2.2: (a) Schematic diagram of the electrodialysis and CO_2 gas extraction system. Green lines represent the extracted gas stream, blue lines the model water tubes, grey lines the electrolyte solution tubes, and yellow lines the data transfer wires. Arrows indicate flow directions. (b) Simplified setup of the membrane stack used in the experiments, consisting of ten bipolar membranes (BPM) and nine anion-exchange membranes (AEM). Each repeating cell consists of one AEM and one BPM, except the last, where the AEM is replaced by a cation-exchange membrane (CEM) to prevent electrolyte transfer to the feed water.

A titrator (TitroLine 7000, SI Analytics, Germany) was used to titrate the 200 mL samples from the feed and the outlet of the membrane stack after the CO_2 extraction. A two-point titration was performed with 0.1 M HCl.

2.4.3 Experimental Procedure

While the first sample was taken directly from the feed tank, the second sample was taken from the outlet of the membrane stack after the pump had started and the pH and conductivity in the system had stabilized. Before connection of the DC power supply, the vacuum pump was started and a vacuum of approximately 0.05±0.02 bar was created. After collecting the first sample, the DC power supply was connected to the membrane stack. Every 10 minutes after start-up until 60 minutes, 200 mL samples were collected from the outlet of the membrane stack. The CO_2 content of the extracted gas was stabilized after ca. 7 to 8 minutes, therefore the gas collection in gas bags was started after 10 minutes. This was also done to avoid collection of the remaining atmospheric gases in tubes in the gas bags. All experiments were performed at 21 ± 1 °C.

System cleaning: To prevent scaling from forming and accumulating in the membrane stack, a cleaning procedure was performed after each experiment. The cleaning procedure included (1) rinsing the system with deionized water for 10 minutes, (2) repeating step 1 with an acidic solution of HCl at pH $\leq$ 3 for 5 minutes, (3) rinsing with DI water, (4) rinsing with an acidic solution of citric acid at pH $\leq$ 3 for 5 minutes, leaving the acidic solution in the membrane stack for 10 minutes, and (5) a final rinse with deionized water.

2.4.4 Salinity experiments

To prepare feed water with different salinities (with electrical conductivity of 2 to 50 mS/cm), varying amounts of the Bad Wimpfen brine (1 to 10 %) was mixed with equal parts of Karlsruhe tap water and deionized water. By adding varying amounts of $CaCl_2$, the Na^+: Ca^{2+} ratio was kept constant.

2.4.5 Data analysis

Between the first (pK_a (pH = 6.1) and the second end-point (pH = 4.3) of titration, the remaining 50% of the DIC is turned into dissolved CO_2 and carbonic acid (see Figure 2.1). The amount of total DIC (mol/L) can be therefore calculated from equation 2.5 and the average DIC removal efficiency (R_{DIC}) during the experiment was calculated by equation 2.6.

$$\mathrm{DIC} = \frac{2 \cdot V_{\mathrm{acid}} \cdot c_{\mathrm{acid}}}{V_{\mathrm{sample}}} \tag{2.5}$$

$$R_{\mathrm{DIC}} = \left(1 - \frac{c_{\mathrm{IC,\,waste}}}{c_{\mathrm{IC,\,feed}}}\right) \cdot 100 \tag{2.6}$$

Where V_{acid} is the amount of acid added to the sample between the two end-points (mL), c_{acid} is the concentration of the used acid (mol/L) and V_{sample} is the volume of the sample (mL). In equation

2.6, $c_{IC,\ waste}$ was calculated as the average of the DIC from the samples taken (between 10 – 60 mins) from the outlet of the system, while $c_{IC,\ feed}$ represents the average of the DIC value in the feed tank and the first sample at 0 min.
The specific electrochemical energy consumption of CO_2 extraction was calculated using equation 2.7 by dividing the energy consumption of the membrane stack by the mass of extracted CO_2 gas over the experimental time.

$$El.Energy = \frac{\int U \cdot I \, \mathrm{d}t}{\Delta t \cdot \dot{m}_{\mathrm{CO_2}}} \tag{2.7}$$

where U, I, t, and $\dot{m}_{\mathrm{CO_2}}$ represent the voltage (V), current (A), time of the experiment (s), and mass flow rate of the collected CO_2 gas (kg/s).

2.5 Results and Discussions

In this section, we present the results and discussions of our study focused on the carbon capture from water utilizing bipolar membrane electrodialysis (BPMED). Addressing key research questions and gaps, we examine the influence of feed salinity, flowrate and voltage (i.e. current density) on the energy consumption during the carbon capture process. Additionally, we explore the potential reduction in energy consumption achievable by employing a novel electrolyte solution. Through these experiments, we aim to provide valuable insights into optimizing the efficiency and sustainability of CO_2 capture from water, paving the way for environmentally conscious and economically viable carbon capture technologies.

2.5.1 Feed water/salinity

While CO_2 capture from seawater has been studied extensively, the extraction of CO_2 from other water sources containing bicarbonate (surfaced and subsurface water resources) was, to the best of our knowledge, not considered. In this section the impact of constituent ions and their concentration on the performance of the BPM and CO_2 extraction is investigated and showed in Figure 2.3.

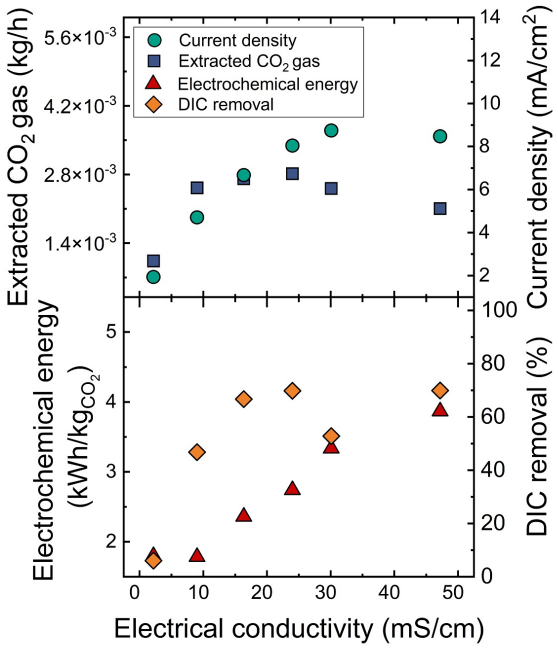

Figure 2.3: Effect of increasing salinity (measured as electrical conductivity) on extracted CO_2 gas, current density, electrochemical energy and DIC removal. Electrolyte: 10 g/L Na_2SO_4, Feed: HCO_3^- 180 mg/L, Flow velocity: 2 cm/s, Electrical potential: 15 V.

It is seen that at 15 V the Current density is not enough to provide the needed ΔpH to convert the available bicarbonate in water to extractable dissolved CO_2 gas (see Figure 2.1) at the lowest salinity (with 2 mS/cm feed an average acidic pH of 6.1 was observed, see Figure 2.9). Therefore extracted CO_2 gas volume was very low compared to higher salinities. Moreover, it has been shown by Bui *et. al.* [80] that at lower current densities (below the requirement for the WDR to start at the BPM), the salt crossover through the BPM is the dominant charge carrier mechanism, and therefore the losses at low current densities are higher, the results in Figure 2.3 and also Figure 2.6 are in agreement with this argument. With increasing salinity (≥9 mS/cm) of the feed water, the extracted CO_2 does not change considerably, however the current density increases. This increase in current density is due to the increasing concentration of ions in the feed solution and lower resistance of the membrane stack and justifies the increase of the electrochemical energy consumption. The results in Figure 2.3 are in line with observations of Eisaman *et al.* [18], where the CO_2 gas rate was increased at lower pH (see Figure 2.9) and higher salinities. Looking at Figure 2.3, the lowest electrochemical energy consumption was observed with 9 mS/cm feed and average acidic pH of 5.3 (See Figure 2.9) at 1.78 kWh/kg CO_2.

2.5.2 Flowrate

Increasing the flowrate diminishes the boundary layer thickness and the retention time of the solution in the membrane stack (and membrane contactor). Note that given the geometry and flow velocities tested with this setup, the system is only in laminar flow. This improves both the water dissociation

reaction in the BPM and the movement of ions through AEM. Moreover, more DIC is available for extraction as CO_2 gas. To enhance comprehension of the mechanisms and patterns tied to the implemented pH swing and its effect on CO_2 capture, experiments were run with various flow rates (ranging from 30 to 70 L/h). The results are shown in Figure 2.4.

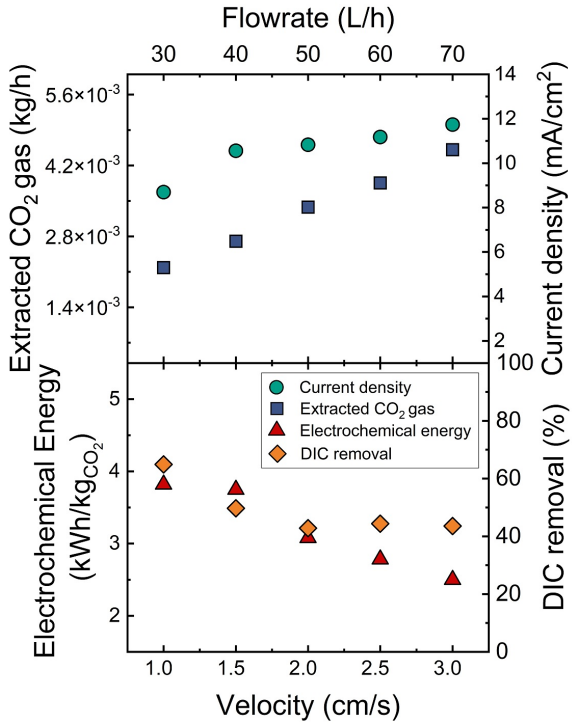

Figure 2.4: Effect of increasing flowrate on extracted CO_2 gas, current density, electrochemical energy and DIC removal. Electrolyte: 10 g/L Na_2SO_4, HCO_3^- 180 mg/L, EC: 50 mS/cm, Electrical potential: 15 V.

As the flowrate and velocity of the feed water increases, the electrical resistance of the stack is reduced and the current density slightly increases (from around 5 to 11 mA/cm^2, see Figure 2.4). This increase of current density provides better conditions for the WDR at the BPM and therefore more CO_2 can be extracted via the membrane contactor (up to 0.005 kg CO_2/h). These results are comparable with results obtained by Iizuka *et al.* [75] where a BPMED stack was used to extract CO_2 from a carbonate solution. The increased CO_2 extraction results in lower energy demand at higher flowrates (from 3.7 to 2.5 kWh/kg CO_2). It is also observed that while the provided ΔpH was greater at low velocities (as less amount of water needed to be acidified, see Figure 2.8), and a higher percentage of the DIC could be removed, the total extracted CO_2 gas was higher at higher flowrates. The higher extracted CO_2 gas resulted in lower electrochemical energy consumption. Figure 2.4 shows that the DIC removal is decreased from more than 60% at 1 cm/s, to 40% at 2.0 – 3.0 cm/s. The slow kinetics of the carbonate-balance shift from bicarbonate to dissolved CO_2 gas and lower retention time of the solution in the membrane contactor at higher velocities are the main reasons for the lower DIC removal at higher flowrates.

2.5.3 Electrolyte/voltage

To avoid the overpotential losses corresponding to WDR at the cathode and anode, a 0.1 M reversible redox-couple solution of $K_3/K_4[Fe(CN)_6]$ was used. Figure 2.5 shows the current density of the membrane stack at different Electric potentials with the two used electrolyte solutions.

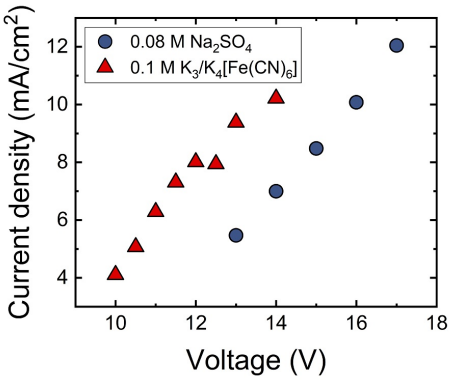

Figure 2.5: Applied voltage on the membrane stack and the corresponding current density, with two different electrolyte solutions. EC: 50 mS/cm, Flow velocity: 2 cm/s.

As expected, an increase of electric potential leads to a linear increase of current in the membrane stack (see Figure 2.5). By using the reversible redox couple solution, it is possible to reduce the needed electric potential by circa 2 volts (meaning a 10-20% reduction in applied voltage). This is also in agreement with previous results obtained by Digdaya *et al.* [19].
Since most of the current is carried by the transfer of the produced H^+ and OH^- at the BPM ($\geq$80% at current densities above 1 mA/cm^2) [19], the reduction of applied electric potential while the current density is constant results in reduced electrochemical energy consumption by the membrane stack. The reduction in applied voltage in Figure 2.5 also shows that by using the 0.1 M $K_3/K_4[Fe(CN)_6]$ electrolyte, it is possible to reduce the over-potentials of the electrodes in BPMED systems.
To understand the extent of the CO_2 extraction at different electrical potentials (and the corresponding current density), experiments were run at different voltages to cover a wide range of current densities (from 4 to 13 mA/cm^2), see Figure 2.6.

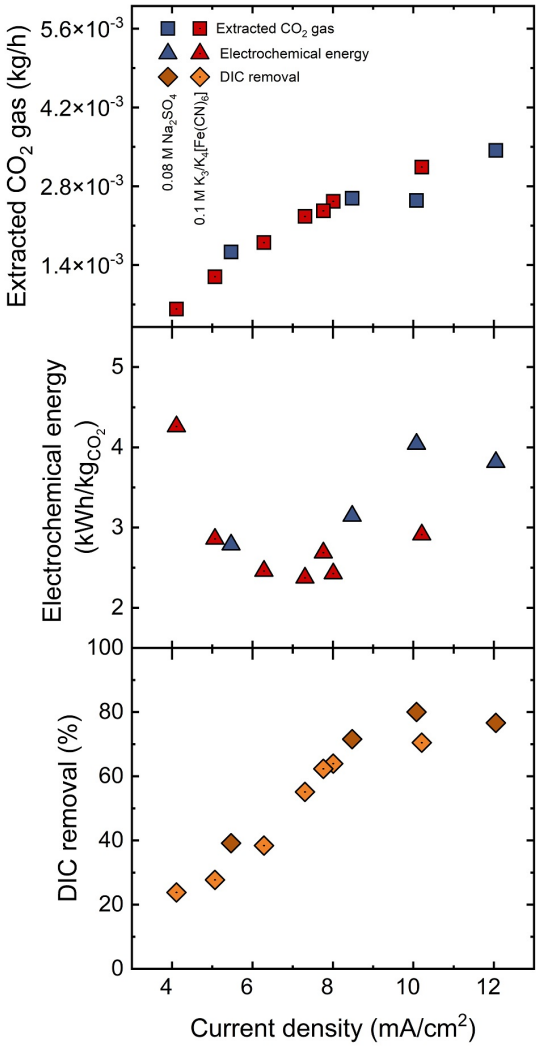

Figure 2.6: Effect of increasing current density on extracted CO_2 gas, electrochemical energy demand and DIC removal. Electrolyte: 10 g/L Na_2SO_4 or 0.1 M $K_3/K_4[Fe(CN)_6]$, Feed: HCO_3^-: 180 mg/L, EC: 50 mS/cm, Flow velocity: 2 cm/s.

As the current density was increased by increasing the applied voltage, the amount of the extracted CO_2 gas was increased with both electrolyte solutions. Figure 2.10 shows that, as expected, the induced pH-swing increases as the production rate of H^+ increases with increasing current density and applied voltage. The increased current density resulted in a significant increased DIC removal from 22% at 4 mA/cm^2 to 80% at 10 mA/cm^2. However, the increase in current density from 10 to 12 mA/cm^2 did not affect the DIC removal and it was slightly lower at around 75% at 12 mA/cm^2. A minimum energy consumption of 2.3 kWh/kg CO_2 is seen at the current density of 7.3 mA/cm^2 (with 0.1 M $K_3/K_4[Fe(CN)_6]$ electrolyte). The energy consumption shows an increase at current densities higher or less than 7.3 mA/cm^2. The same trend is also observed in the study by Eisaman *et al.* [57], where a minimum electrochemical energy demand of ca. 1.6 kWh/kg CO_2 was observed with an acidic pH 5 (see Figure 2.10). It was also observed in the study by Digdaya *et al.* [19] that by

using a reversible electrolyte (0.2 M $K_3/K_4[Fe(CN)_6]$), the energy consumption could be lowered to below 1 kWh/kg CO_2. Figure 2.6 shows comparable results with a 20% reduction in electrochemical energy demand by switching to reversible electrolyte (as mentioned before, close to the losses due to reactions in electrodes in normal operation with Na_2SO_4 electrolyte), several reasons have caused the higher energy consumption in the present study. (i) using only one membrane contactor unlike the other studies where two or three membrane contactors were used for higher gas extraction, (ii) while 10 BPM cell pairs with a total area of 640 cm^2 was used in this study, in the study by Digdaya *et al.* [19] a single stack with area of 64 cm^2 was used. The higher area of BPMs and cell numbers result in higher inefficiencies related to BPM such as ion leakage and selectivity.

2.6 Conclusions

Our study aimed to investigate the potential of BPMED for carbon capture from water sources. The findings provide more insights on the impact of different operative (applied voltage and flowrate) and feed water compositions (salinity and a reversible redox pair) on the extent and electrochemical energy consumption of CO_2 (g) extraction. The study can contribute to industry practitioners by optimizing the BPMED pH swing carbon capture process, offering insights into key factors such as flow rate, voltage, and electrolyte choices. Practical experiments with a pilot-scale BPMED membrane stack demonstrate a 20% reduction in energy consumption through the introduction of a new electrolyte solution, showcasing potential efficiency improvements. The reduction in energy consumption and the optimized bicarbonate extraction demonstrated in this study suggest that BPMED could become a more efficient and cost-effective method for CO_2 capture from water.

A minimum electrochemical energy consumption of 2.3 kWh/kg CO_2 was achieved by using a reversible electrolyte solution (0.1 M $K_3/K_4[Fe(CN)_6]$) at a current density of 7 mA/cm^2. And a maximum 80% of the DIC in water was removed and extracted as CO_2 (g) at 10 mA/cm^2. The low CO_2 (g) extraction due to mass transport limitations because of the low concentration of bicarbonates in water in higher current densities and higher energy losses because of salt crossover in the BPM in current densities less than 7 mA/cm^2 increased the electrochemical energy demand. At higher feed velocities (1 to 3 cm/s) of the solution in the membrane stack, more CO_2 (g) could be extracted while the current density was gradually increased. Subsequently the electrochemical energy demand was lower at higher velocities (2.5 kWh/kg CO_2 at 3 cm/s) while less of the DIC was removed (from 64% at 1 cm/s to 44% at 3 cm/s). Operating the setup at a constant electric potential with different electric conductivities (from 2 to 50 mS/cm), showed that presence of ions is necessary to provide the potential over the BPM for WDR and to induce the ΔpH. While the extracted CO_2 gas did not vary at electrical conductivities above 9 mS/cm, the losses increased, resulting in higher energy demands. An overall minimum electrochemical energy demand of 1.7 kWh/kg CO_2 at the feed conductivity of 9 mS/cm was observed. Apart from reducing the energy costs through process optimization, membrane materials engineering can be leveraged to decrease the system energy demands and therefore increase the total efficiency of the process.

Rigorous cleaning strategies and low concentration of Mg^{2+} in the prepared feed water prevented major scaling of the membrane stack. However, future studies need to be conducted with more similar condition to real seawater before the scale up of the process. Further studies are also needed to study effect of long operation times (days to weeks) and investigate the adverse effects of this long operation on the process efficiency.

2.7 Supporting Information

2.7.1 Feed water composition

The detailed composition of the feed water used in the experiments is shown in Table 2.3. In the first phase of the study, a different feed water composition (with similar concentration of Mg^{2+} and SO_4^{2-} to North Sea water) was used. However, due to extensive scaling and blocking of the membrane stack, the water composition was altered and the experiments were repeated. This shows the importance of further studies to mitigate the scaling and also develop effective cleaning methods. Figure 2.7 shows the extensive scaling and blockage of the membrane stack after the initial experiments.

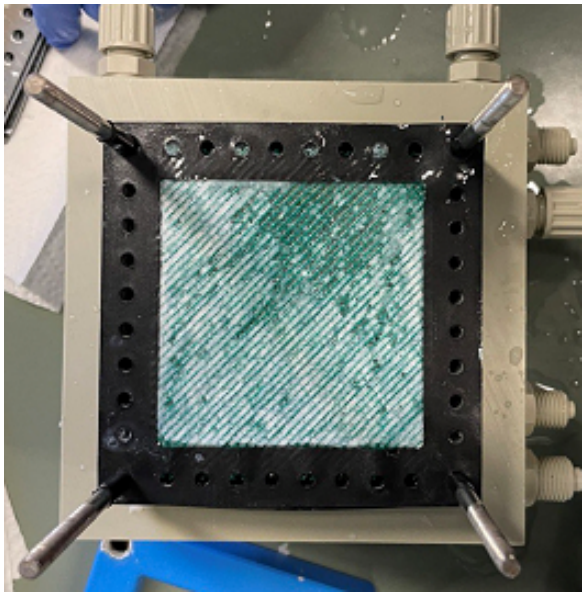

Figure 2.7: Scaling and blockage of the feed spacer in the basic channel of the membrane stack in initial experiments.

Due to the extensive blockage of the basic channels in the membrane stack and ineffective cleaning procedures, authors decided to alter the chemical composition of the feed water by lowering the concentration of the Mg^{2+} and SO_4^{2-}. The membrane stack was checked weekly to make sure there is no formation of scaling after each series of experiments. Further studies are planned to study the scaling in the membrane stack.

2.7.2 pH over time

The extent of acidification in the acidic cell of the membrane stack determines how much of the available bicarbonate and how fast converts to dissolved CO_2 in water. In Figures 2.8 to 2.11, the pH of the acidic and basic cells over time of the experiment are shown.

Table 2.3: Concentration of ions and characteristics of the used model water and North Sea.

	Unit	**Model water**	**North Sea water**
Chloride	g/L	19 ± 0.5	18.98
Sodium	g/L	13.4 ± 0.5	10.55
Sulphate	mg/L	459 ± 50	2649
Magnesium	mg/L	18 ± 4	1272
Calcium	mg/L	407 ± 30	400
Potassium	mg/L	5 ± 2	380
Bicarbonate	mg/L	182 ± 10	140
TDS	g/L	33	32–34.5
DOC	mg/L	–	1.5
EC	mS/cm	49 ± 1	–
pH	–	7.2–8.0	7.9–8.4

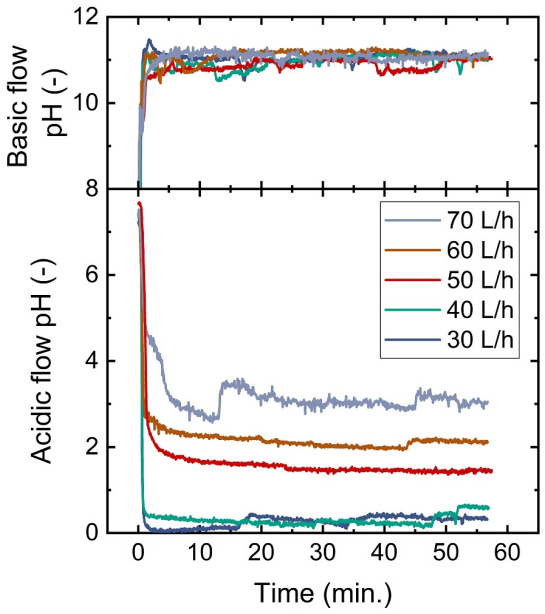

Figure 2.8: pH of the acidic and basic cells over time in variable flowrates (Applied voltage: 15 V, feed: model water, electrolyte: 0.8 M Na_2SO_4).

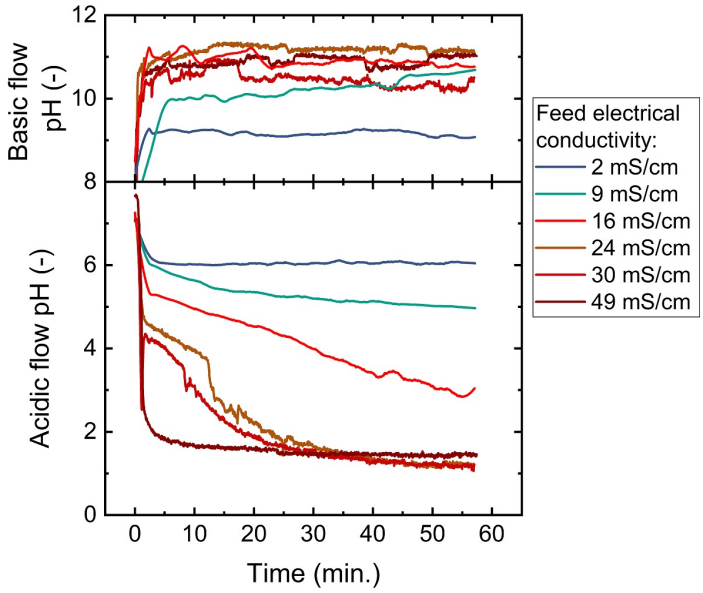

Figure 2.9: pH of the acidic and basic cell over time in variable feed water conductivities (Applied voltage: 15 V, electrolyte: 0.8 M Na_2SO_4).

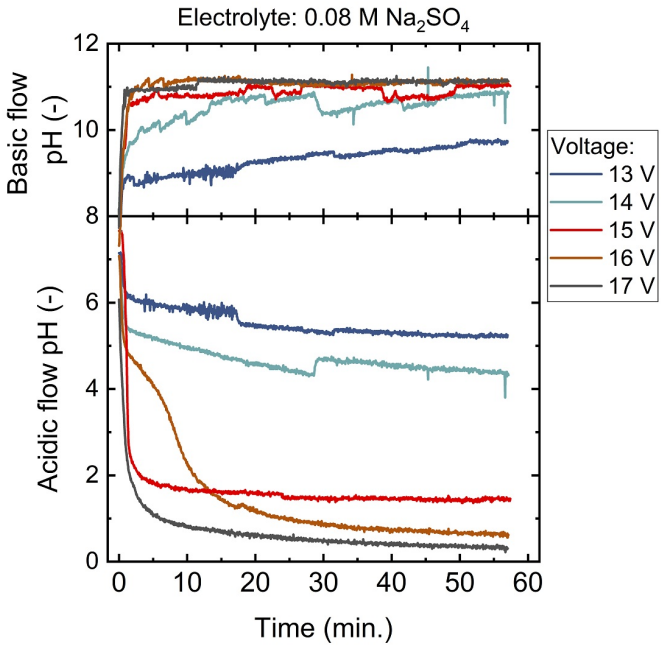

Figure 2.10: pH of the acidic and basic cell over time with 0.08 M Na_2SO_4 electrolyte solutions at different applied voltages (Feed: model water, flow rate: 50 L/h).

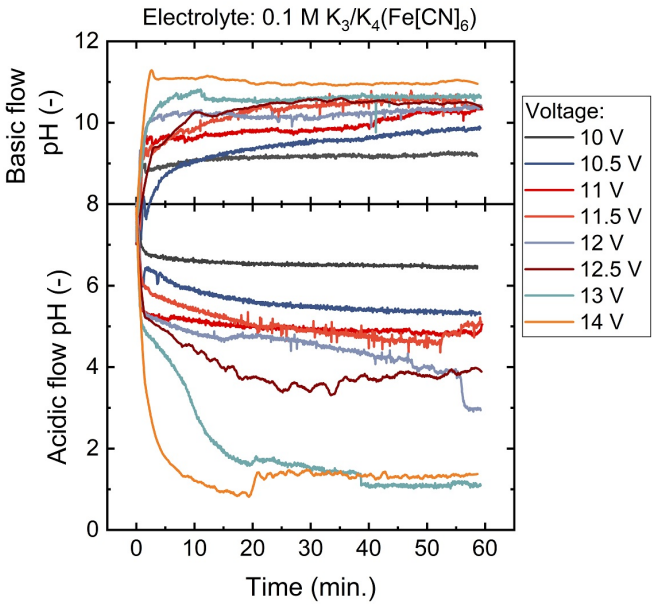

Figure 2.11: pH of the acidic and basic cell over time with 0.1 M $K_3/K_4[Fe(CN)_6]$ electrolyte solution at different applied voltages (Feed: model water, flow rate: 50 L/h).

Chapter 3

Real Time Monitoring Of Scaling Behavior In Bipolar Membrane Electrodialysis

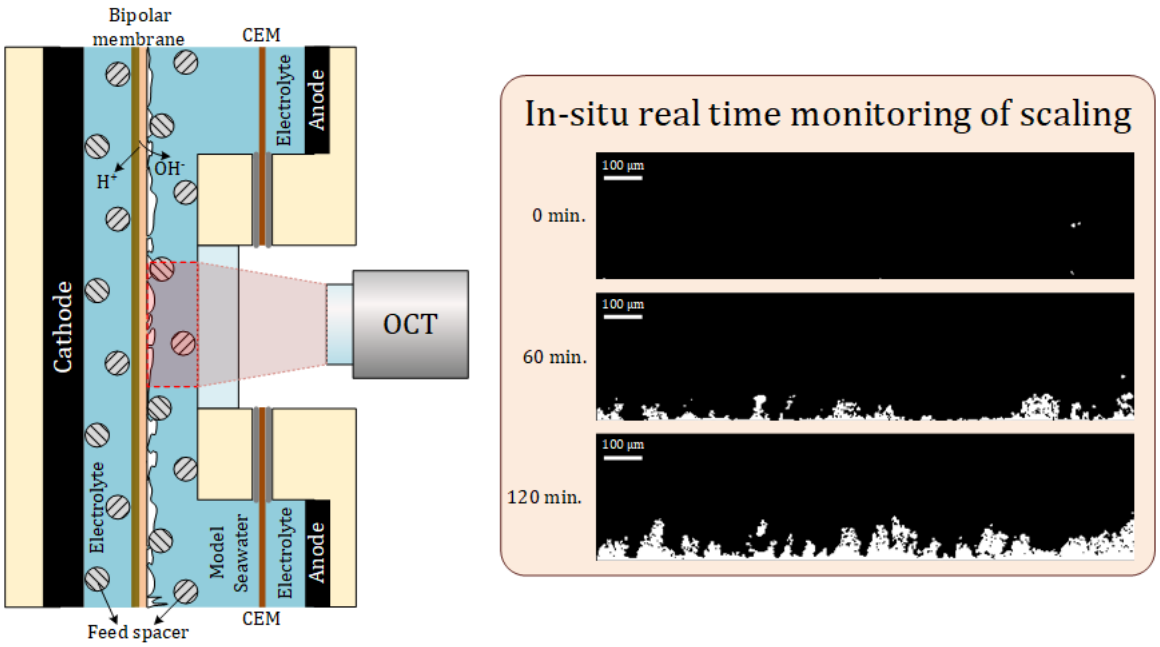

This chapter is published as:
Aliaskari, M., Horn, H., & Saravia, F. (2025). Real time monitoring of scaling behavior in bipolar membrane electrodialysis. *Journal of Membrane Science*, *727*, 124063.
doi: https://doi.org/10.1016/j.memsci.2025.124063

Abstract

In this study, scaling in bipolar membrane electrodialysis (BPMED) was investigated in real time using a custom-made flow cell and Optical Coherence Tomography (OCT). Unlike previous studies that applied OCT in pressure- or thermal-driven membrane processes, this work demonstrates its use in electrodialysis for the first time, enabling in-situ observation and quantification of scaling on the basic side of the bipolar membrane under various operational conditions. The results revealed that higher flow rates and lower applied currents reduced scaling coverage and thickness, attributed to improved hydrodynamics and a lower pH shift. Increasing the system's buffer capacity through higher dissolved inorganic carbon (DIC) concentrations resulted in less scaling, whereas total removal of DIC drastically increased scaling formation due to the loss of buffering capacity, leading to extreme pH shifts. Furthermore, $Mg(OH)_2$ was identified as the dominant scalant under high-pH conditions, confirming its major role in scaling formation in BPMED. Scaling formation was highly non-uniform, emphasizing the strong influence of hydrodynamic conditions and spacer geometry. These findings can be used in the future to develop and test improved fouling mitigation and cleaning strategies, enhancing BPMED performance and its application in CO_2 capture and related processes.

Keywords:

Optical Coherence Tomography; Ion Exchange Membrane; Online Scaling Monitoring; Dissolved Inorganic Carbon; Flow Cell; Carbon Capture

3.1 Introduction

Since the early 2010s, a growing body of research has focused on (indirect) oceanic carbon capture through electrochemical processes [15, 50, 57]. This approach aligns with global efforts to mitigate climate change by controlling and reducing CO_2 emissions [92]. Unlike conventional carbon capture methods (e.g., amine-based absorption or calcium looping), electrochemical processes enable the capture, storage and utilization of the oceanic carbon, with minimal consumption of chemicals and no heat [26].

Among the available electrochemical approaches, bipolar membrane electrodialysis (BPMED) has gained particular attention due to its ability to generate acid and base in situ. Due to its scalability and ability to simultaneously produce acid and base, bipolar membrane (BPM) electrodialysis (ED) is particularly attractive for "pH-swing" carbon capture processes. The BPM consists of an anion exchange and a cation exchange layer laminated together. When subjected to sufficient electrochemical potential (typically ∼0.8 V under ideal conditions [81, 93]), the BPM facilitates the dissociation of water molecules to H^+ and OH^-. The produced acid and base provide the required pH-gradient to transform the dissolved inorganic carbon (DIC) in seawater (ca. 140 mg/L) to either dissolved CO_2 (in the acidic stream) [57], which can be extracted, stored, or utilized, or carbonate crystals (in the alkaline stream) [13] that can be precipitated and potentially used in various applications [6]. While the acidic side of the BPMs has minimal scaling problems, the formation and precipitation of inorganic compounds on the basic side of the membrane (see Figure 3.1) can deteriorate membrane structure, reduce active area and increase the operation costs [94]. This is mainly due to the high

pH of the alkaline stream in the electrochemical stack (pH $\geq$ 9) [33]. Cleaning and membrane replacement costs account for approximately 40–50 % of total in electrochemical processes operational costs [95]. Given its impact on performance and cost, scaling must be better understood to improve BPMED viability.

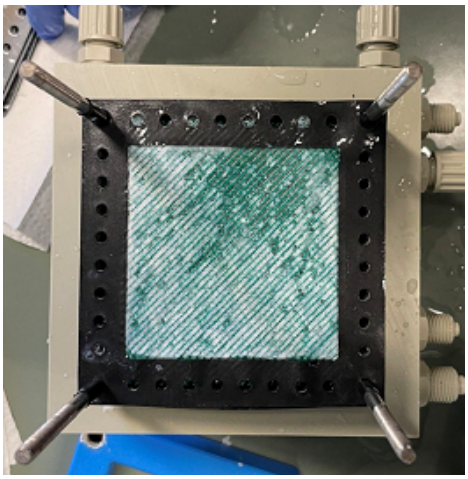

Figure 3.1: Scaling (white) of the feed spacer (green) in the basic channel of the membrane stack, taken from Aliaskari *et al.*[5].

This persistent scaling poses challenges to the development of BPMED-based pH-swing carbon capture systems. Therefore, a better understanding of the scaling mechanisms is needed to develop scaling mitigation and cleaning methods. The goal of this study is to investigate the mechanisms of scaling formation on the alkaline side of BPM, focusing on identifying the contributing factors and evaluating potential mitigation strategies to enhance membrane performance and longevity. While previous studies have relied on ex-situ methods or indirect indicators (e.g., membrane resistance or pressure drop) to investigate scaling, this is the first study to monitor inorganic scaling growth on the surface of bipolar membranes in real time using a proprietary flow cell and optical coherence tomography (OCT) setup.

3.1.1 Scaling in Electrodialysis Membrane Processes

Scaling is one of the fouling forms in membrane systems, caused by the precipitation of salt crystals in water and their deposition and growth on the membrane surface or inside the membrane channels [94]. Variations in salt concentrations above the solubility product and shifts in chemical equilibria (e.g., due to pH deviations) which changes concentration of critical species like carbonate lead to salt precipitation. Andreeva [96] has shown that heterogeneous nucleation (i.e. nucleation on the membrane surface), which occurs due to the strong affinities of counter-ions to the membrane functional groups has a strong influence on scaling in ion exchange membranes. The interaction of operational and water quality parameters affects the kinetics of ion transport and the precipitation of scaling compounds. In the following, key operational factors affecting scaling are summarized.
The **flow rate** impacts the mass transfer of ions and the residence time of the solution within the electrodialysis stack. Higher flow rates enhance mixing, reduce boundary layer thickness and

resistance, and help mitigate scale accumulation on the membrane surface by lowering local supersaturation of salts, which delays the onset of precipitation [97]. Studies have shown that increasing flow rates can alleviate fouling by diluting ion concentration near the membrane surface, thereby reducing the likelihood of crystallization of calcium carbonate and magnesium hydroxide [6, 98]. Conversely, low flow rates allow longer contact time between the solution and membrane, improving DIC conversion efficiency but increasing the risk of localized supersaturation [5]. When the solution becomes highly alkaline (pH ¿ 9), lower flow rates exacerbate scaling, particularly in regions where calcium carbonate and magnesium hydroxide precipitate, due to longer residence times and stronger polarization effects [99].

The **pH** in BPMED systems is determined by the **applied current density**, which drives the water dissociation reaction in the BPM to produce H^+ and OH^- ions. Typically, the acidic side of the membrane exhibits a pH below 4, while the basic side can exceed a pH of 9, depending on the current density and chemical composition of the feed solution. This rise in pH on the basic side is closely tied to scaling, as the solubility of calcium and magnesium salts decreases in alkaline environments, causing the precipitation of compounds such as calcium carbonate and magnesium hydroxide [6, 33]. As current density is increased above 8 mA/cm^2, more rapid pH swings occur, which accelerate the conversion of bicarbonate to CO_2 in the acidic cell and the formation of carbonate minerals in the basic cell [5, 18]. This can also accelerate the onset of scaling by promoting supersaturation of ions such as calcium and magnesium, leading to fouling on the alkaline side of the membrane (see SI Figure 3.11). Rapid ion fluxes caused by elevated current densities can result in local pH shifts near the membrane surface, which, in turn, causes non-uniform scaling and crystal growth in specific areas [100].

Moderate current densities (between 6 and 8 mA/cm^2) allow better control over ion transport without drastically increasing the risk of scaling and fouling [101]. Lower current densities ($\leq$6 mA/cm^2), while reducing scaling, can decrease the CO_2 capture efficiency by slowing down the DIC conversion reaction kinetics [5]. Thus, balancing the current density to achieve efficient DIC transformation while mitigating scaling is crucial. Scaling on the alkaline side of the membrane primarily results from the precipitation of inorganic salts as the solution becomes supersaturated at high pH levels. The scaling composition is often dominated by magnesium hydroxide and calcium carbonate which form as pH rises above 9 [102]. The chemical composition of the feed solution significantly influences the type and extent of scaling, with specific ions like bicarbonate (HCO_3^-), sulfate (SO_4^{2-}), calcium (Ca^{2+}), and magnesium (Mg^{2+}) playing key roles [6, 33, 103].

Bicarbonate ions in the feed solution are one of the most crucial factors for scaling, especially in the context of CO_2 capture. In the alkaline stream, the pH swing causes bicarbonate to convert into carbonate ions, which subsequently precipitate as calcium carbonate when calcium ions are present. This reaction can occur readily when the pH exceeds 9, leading to the deposition of calcium carbonate on the membrane surface and increasing electrical resistance [33, 94].

Sulfate ions contribute to scaling in a different manner. While not as prone to direct precipitation as carbonates, they can interact with bivalent cations like calcium and magnesium to form less soluble compounds such as calcium sulfate. Calcium sulfate tends to precipitate at high salinities and concentrations, particularly in thermal and pressure-driven desalination systems [100]. In BPMED systems, sulfate scaling is generally less prevalent due to the relatively high solubility of sulfate salts in alkaline conditions. For instance, calcium sulfate maintains considerable solubility across a broad pH range, reducing the likelihood of precipitation and scaling. This characteristic contrasts with

salts like calcium carbonate and magnesium hydroxide, which have decreased solubility at higher pH levels, leading to more common scaling issues in BPMED processes [33].

Calcium and magnesium cations have a profound effect on the type and extent of scaling. Calcium is highly prone to precipitating as calcium carbonate and calcium hydroxide when exposed to high pH, making it one of the main contributors to scaling on the alkaline side of the membrane [100]. Magnesium, on the other hand, tends to form magnesium hydroxide, which precipitates at even higher pH levels than calcium compounds (typically above pH 10, see SI Figure 3.11) [94]. Interestingly, the Mg^{2+}/Ca^{2+} ratio can modulate the extent of calcium scaling. Higher magnesium concentrations relative to calcium can inhibit the crystallization of calcium carbonate by occupying sites on the growing crystal surface, leading to amorphous or poorly crystallized precipitates that are less likely to adhere to the membrane. However, when this ratio is low (i.e., calcium dominates), the formation of hard calcium carbonate scales becomes much more prevalent [33, 104]. Additionally, magnesium scaling typically occurs after significant calcium scaling, adding further resistance to the system and complicating cleaning processes [6].

3.1.2 Overview of scaling analysis methods

Scaling in BPM systems can be characterized with a variety of established methods [94]. Scanning Electron Microscopy (SEM) is the most common method for generating high-resolution images of the membrane surface, enabling measurement of scale deposit size and spatial distribution; it provides limited chemical information, with Energy-Dispersive X-ray Spectroscopy (EDX) typically used for elemental surface analysis [103, 105]. X-ray diffraction (XRD) serves as an additional method for the identification of crystalline phases within scaling compounds. However, its application is restricted to ex-situ analysis, thereby failing to facilitate dynamic tracking of the scaling process during operation [79]. While these techniques provide substantial insights, their utilization is restricted to postoperative evaluations and lacks the capacity for real-time monitoring of scaling phenomena. To overcome these limitations, several real-time fouling detection methods can be explored in electrochemical systems. The most relevant are discussed below.

Ultrasonic Time-Domain Reflectometry (UTDR) is another technique used to monitor scaling development in membrane processes [106, 107]. However, UTDR does not provide 2D or 3D characterization of fouling morphology, as it primarily captures single-point or averaged measurements. While UTDR is useful for detecting fouling in commercial systems, its reliance on acoustic contrast and lack of morphological visualization limit its usefulness for detailed characterization in BPMED [108].

In a study by Sharifian *et al.* [33] scaling buildup was measured indirectly through monitoring the increase in the total stack voltage and the pressure drop in the alkaline compartments. While these methods provide an indication of scaling severity, they do not reveal any information on scaling thickness or whereabouts, and cannot distinguish between deposit types. Additionally, scaling may only be detected once it significantly impacts system performance, limiting early detection.

Optical Coherence Tomography (OCT) offers a non-invasive, in-situ imaging technique suitable for monitoring scaling in BPMs in real time. Conventional techniques either lack real-time capabilities or sufficient spatial resolution to track scaling progression. OCT overcomes these limitations by enabling in-situ, high-resolution imaging of scaling growth and distribution, allowing direct observation of how scaling develops under different operating conditions [109]. The real-time imaging helps

track the progression of scaling, offers a clear advantage for optimizing membrane performance and provides mechanistic insights into fouling behavior [108].
OCT has been widely used in biomedical imaging since the early 1990s, establishing its role in high-resolution structural imaging [110, 111]. Over time, it has evolved into a key technique in fields such as material science, biosciences, and water research, where it is utilized to study fouling and scaling in membrane systems [112–115]. Over the past decade, OCT has gained increasing popularity for investigating various foulants in membrane filtration systems, including particulate and colloidal fouling, organic fouling and scaling [108].
Building on this progress, our study presents the first application of OCT for in-situ monitoring of scaling in an electrodialysis system, particularly in BPMED. One drawback of OCT for the analysis of fouling formation in ED is the requirement for optical access to the membrane surface. In ED (including BPMED) the membrane is generally covered, depending on the arrangement, by cation exchange membrane, anion exchange membrane, anode and/or cathode. Therefore, appropriate flow cell design is essential.
BPMED is a promising technology for CO_2 capture and many other processes, but scaling on the alkaline side remains a challenge. This study utilizes a novel flow cell with OCT to monitor scaling in real time, providing new insights into its formation. We investigate how ion concentrations, current density, and flow rate influence scaling mechanisms, aiming to improve understanding of fouling processes. These findings can help optimize BPMED performance and inform scaling mitigation strategies for CO_2 capture and other electrodialysis applications.

3.2 Materials and methods

3.2.1 Flow cell design

A novel flow cell was developed for real-time analysis of scaling formation on the basic side of the BPM using OCT. An exploded view of the flow cell parts is shown in Figure 3.2. The flow cell consisted of three separate parts made from polyoxymethylene (POM). Part 1 had two openings aligned with the designated OCT windows in part 2, and housed the inlet and outlet for the electrolyte solution and the two anodes (Graphite-polymer composite material, Eisenhuth GmbH & Co, Germany), each with an area of 13×3 cm^2. The electrolyte in the Anode compartment was separated from the feed solution by a cation exchange membrane (Fumasep FKL-PK, Fumatech GmbH, Germany) with an active area of 48 cm^2. Part 2 provided the inlet and outlets for the feed water, and included two circular openings that facilitated the OCT imaging through Sapphire windows (Thorlabs GmbH, Germany). The BPM (Fumasep FBM, Fumatech GmbH, Germany) with an active area of 138 cm^2 was placed between parts 2 and 3. Ion-exchange membrane properties are shown in SI Table 3.3. Part 3 provided the inlet and outlet for the electrolyte solution, and also housed the cathode with an area of 13×6 cm^2, equal to the total area of the two anodes. For proper sealing of the flow cell, 1 mm silicon (40±5° Sh.A) gaskets (Schöffler + Wörner GmbH, Germany) were used. The thickness of the gasket dictates the flow channels thickness in the studied region under the OCT windows.
To provide realistic hydrodynamic conditions, spacers (extruded with overlapping filaments, 1 mm thickness with crossing filaments at 90°) was placed above the basic side of the BPM. The feed spacer was positioned at a 45-degree angle relative to the direction of the flow. This orientation is commonly used in membrane processes to optimize flow distribution and minimize pressure drop

across the membrane [116]. This setup enables detailed in-situ monitoring of scaling development on the alkaline side of the membrane.
Both membranes were washed with an acidic solution of HCl (pH $\sim$ 2) for half an hour after each experiment, and kept in 0.5 M NaCl solution in room temperature. The membranes sheets were changed after each set of experiments.

3.2.2 ED system setup with the Flow cell

The ED system was configured with the flow cell integrated as a stack for direct observation of scaling. The system operated at a range of applied current densities (0.3 to 0.8 A) and flow rates (2 to 10 L/h) to simulate realistic conditions found in membrane stacks. In standard conditions a constant feed flow rate of 5 L/h and current density of 0.6 A was used.

3.2.3 Optical coherence tomography

OCT imaging was conducted using the GANYMEDE II spectral domain system (Thorlabs GmbH, Germany), equipped with an LSM04 objective lens (Thorlabs GmbH, Germany). Three-dimensional OCT datasets (C-scans) were captured every 15 minutes during the experiments. The scanned area dimensions were 5 $\times$ 4.5 $\times$ 2 mm^3 (L $\times$ W $\times$ H), with a pixel resolution of 8 m/pixel in the x-y plane. The single-pixel height was 3.16 m, based on a refractive index of 1.31, considering the feed water temperature. Each image had an averaging of 7 scans for improved accuracy. Since the flow cell was placed vertically, images were taken from the upper window, which is downstream in the flow direction. As the solution passes over the bipolar membrane, the induced ΔpH increases, creating higher pH conditions that promote scaling, making the upper window the optimal location for observation. While this study focused on scaling formation, future work could integrate Doppler OCT to simultaneously measure velocity profiles and scaling height, providing deeper insights into flow-scaling interactions. Digital image processing and analysis were carried out using Fiji with the ImageJ2 software [117].

3.2.4 Digital image processing and scaling parameters

The image analysis methodology applied in this study follows the previously developed in-house approach [109, 118], with incremental modifications. First, raw OCT images were converted from 32-bit to 8-bit, and a mean filter was applied to enhance clarity. Figure 3 shows an example of the following image processing steps. The region of interest, specifically the area between spacer filaments, was cropped. A macro was used to detect the region of interest (ROI) in the time 0 image. Pixels outside of the ROI were set to maximum intensity and the ROI pixels were set to 0 (Step A, Figure 3). This edited time 0 image was subtracted from the subsequent images (Step B, Figure 3). The image was then flattened to allow for consistent calculation of structural parameters, regardless of the membranes shape (Step C, Figure 3). Binarization was performed (Step D, Figure 3). Finally, the total volume of the fouling layer was calculated and a height map of the scaling was generated (Step E, Figure 3). The used method provided a detailed structural overview of the scaling layer and a robust analysis of the taken images, building on the methodology originally developed by Bauer *et al.* [109]. Two key parameters were calculated from evaluations to quantify the scaling layer on the membrane, irrespective of its composition. These parameters allow for a uniform assessment. The

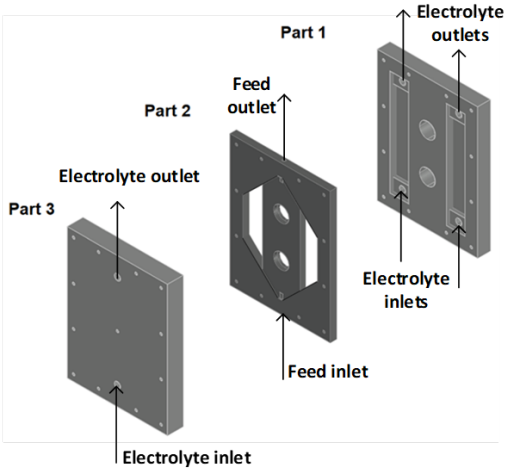

(a)

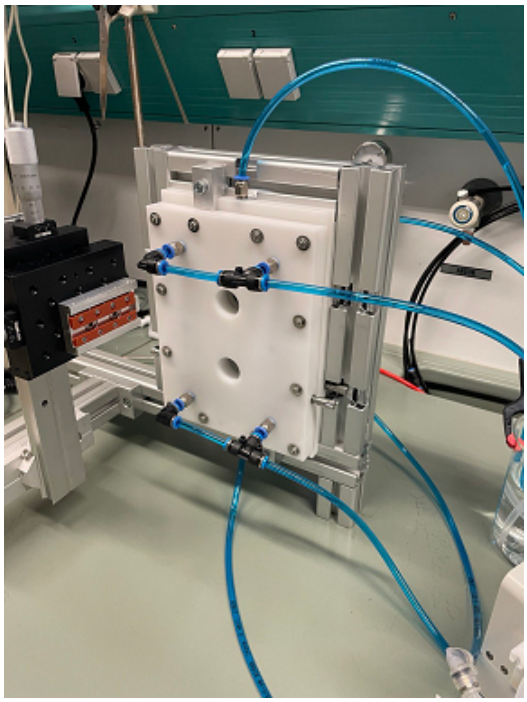

(b)

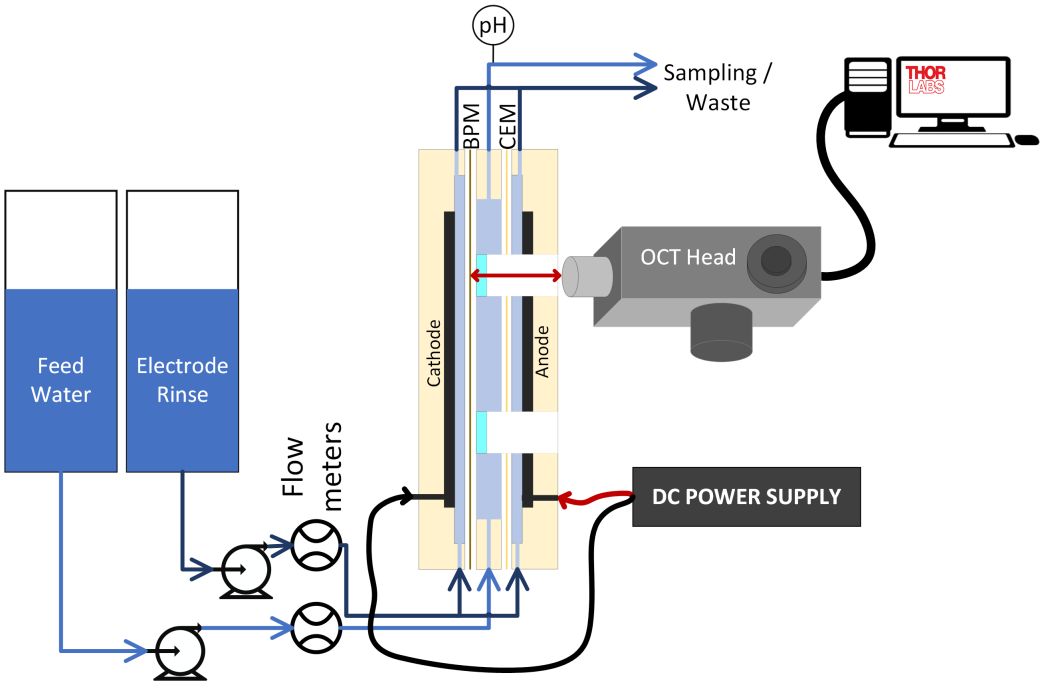

(c)

Figure 3.2: (a) Exploded view of the designed flow cell (total size: 16 × 22 × 5.5 cm^3). (b) The setup with the flow cell. (c) Schematic diagram of flow cell in operation with the OCT imaging system.

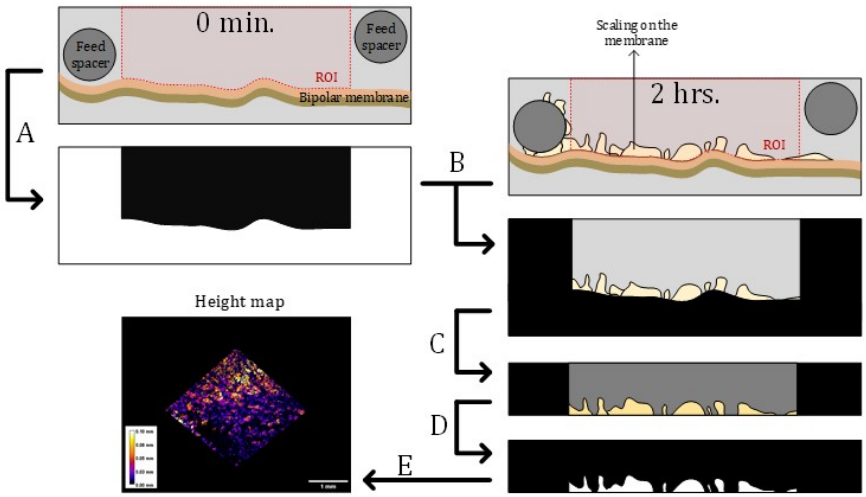

Figure 3.3: Digital image processing steps and height map generation of the scaling layer (A: ROI separation and binarization, B: subtraction of ROI from image A, C: membrane surface flattening, D: binarization, E: height map production).

first parameter, R_S (mean height of scaling), correlates the volume of the scaling layer (V_S [μm^3]) at a specific position on the BPM with the monitored membrane area (A_M [μm^2]) (see equation 3.1). The volume of the Scaling layer (V_S) was determined by counting the number of white voxels in the binary data sets generated from OCT scans. This approach ensures accurate characterization of scaling metrics under varying operational conditions.

$$R_s = \frac{V_s}{A_m} \tag{3.1}$$

The second parameter, ratio of coverage (R_{CO}), quantifies the relationship between the portion of the membrane that is covered by the scaling layer (A_S [μm^2]) and the monitored membrane area (A_M [μm^2]) (see equation 3.2). A macro was used to quantify the covered area of the ROI. The membrane was considered covered if a scaling layer extended at least 30 m above the membrane surface. If R_{CO} is close to 1, most of the membrane is uniformly covered by at least 30 m of scaling. A lower R_{CO} indicates localized, uneven scaling.

$$R_{CO} = \frac{A_s}{A_m} \tag{3.2}$$

3.2.5 Feed water analysis

A titrator (TitroLine 7000, SI Analytics, Germany) was used to titrate 200 mL samples from the feed solution, for calculating the DIC content. A two-point titration was performed with 0.1 M HCl prepared from 37% concentrated hydrochloric acid (AnalaR NORMAPUR, VWR Chemicals, Germany). This analysis was necessary as DIC plays a crucial role in the BPMED process, influencing both CO_2 capture efficiency and scaling behavior on the membrane's basic side.
The scaling layer were washed off the membrane mechanically and with DI water, and dissolved in 0.1 M HCl acid solution, to make sure all precipitates were dissolved. The ion and element concentrations in the feed solution and fouling layer were measured using an inductively coupled

Table 3.1: concentration of ions in the prepared model water and North Sea. [5]

	Cl^- (mg/L)	Na^+ (mg/L)	Mg^{2+} (mg/L)	Ca^{2+} (mg/L)	DIC (mg/L)	SO_4^{2-} (mg/L)	EC (mS/cm)	pH (-)
Model water	19,670	13,405	541 ±10	320 ±5	40 – 50	2,747 ±10	49 ± 1	7.3 ±0.3
North Sea	18,980	10,556	1200	400	140	2650	∼ 50	7.9 – 8.4

plasma optical emission spectrometer (ICP-OES, Agilent Technologies 5110). Anions (including chloride and sulfate) concentrations were determined using a Metrohm ion chromatography system (790 Personal, Metrohm).

3.2.6 Solutions and chemicals

The model seawater, used as a standard solution in all experiments (unless specified otherwise) was prepared by dilution of a brine solution from Bad Wimpfen, Germany (10%), with Karlsruhe tap water (10%) and deionized water (80%) and addition of $CaCl_2$ (>99.5% purity, Merck, Germany) and $MgSO_4$ (>99% purity, Merck, Germany). The final composition of the model water is presented in Table 3.1. The electrolyte solution was a 10 g/L solution of sodium sulfate, prepared from Na_2SO_4 salt (>99.5% purity, Merck, Germany). Various solution compositions were tested to analyze their impact on scaling. The synthetic seawater solutions varied in ion concentration to observe how different levels of DIC and bi-valent ions like magnesium and sulfate influence the scaling behavior. The concentration of DIC in the feed water was adjusted by changing the ratio of added tap water, from 0 to 20 %, resulting in DIC content of 10 to 80 mg/L. Magnesium concentration was adjusted from 3 to 760 mg/L, by using replacement salts of Na_2SO_4 to replace it with Na, or adding extra Mg, by using $MgCl_2$ salt. The sulfate concentration in the feed was adjusted from 400 to 3400 mg/L, by using $MgCl_2$ salt instead of $MgSO_4$ when preparing feeds with lower sulfate concentration. And adding extra Na_2SO_4 to increase its concentration in the feed solution. A detailed analysis of all components of prepared feed solutions is shown in SI Table 3.3.

3.3 Results and Discussions

3.3.1 Flow cell characterization

Current density: As illustrated in Figure 4, flow cell achieved current densities similar to those in the real membrane stack. The flow cell requires a higher voltage to reach the same current densities, primarily due to the type of electrodes used. Despite the voltage differences, the flow cell successfully replicates the essential current density conditions required for accurate simulation of scaling phenomena. **Flow velocity:** The velocity profile in Figure 3.4 was obtained using COMSOL Multiphysics simulations to estimate flow magnitudes within the flow cell. The results of the simulation indicate a velocity of ca. 0.5 cm/s, at the flowrate of 5 L/h. Although slightly lower than in actual membrane stacks (ranging from 1 to several cm/s and yielding Reynolds numbers below 100 [97, 119]), the obtained results remain sufficient for this study. The simulation was conducted without spacers to simplify the model while still capturing key hydrodynamic conditions. Therefore, the presence of feed spacers in the experimental flow cell will induce higher velocities.

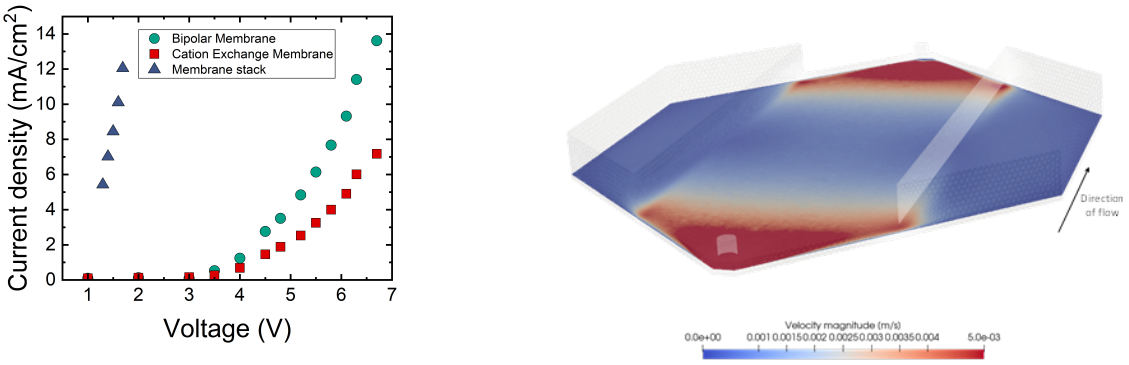

(a) (b)

Figure 3.4: (a) Current density at different voltages in the real membrane stack (shown with triangles and taken from previous study [5]) and flow cell. flow rate: 5 L/h, feed: Model Seawater, electrolyte: 10 g/L Na_2SO_4. (b) Velocity profile in the basic cell in feed flow rate of 5 L/h, without feed spacers.

As such, the results provide a conservative estimate of flow behavior while validating the flow cell's ability to replicate real-world conditions. With the flow cell successfully validated for current density and hydrodynamics, the next step was to investigate how operational parameters influence scaling development in real time.

3.3.2 Effect of current density and flow rate on scaling

To better understand the impact of current density and hydrodynamic conditions influence on scaling formation in the BPMED process, a series of experiments varying the flow rate and applied current over time were conducted.

. In agreement with previous studies [33], scaling volume increased with higher **applied current** (see Figure 3.5). Solutions pH increased as the applied current increased primarily because higher currents create a more alkaline environment on the basic side of the membrane (from pH 9–9.5 at 0.3–0.5 A to pH 10.3 at 0.6 & 0.8 A, see SI Figure 3.13). The higher pH promoted conditions that are more prone to the precipitation of scaling compounds, particularly magnesium hydroxide (see SI Figure 3.13). The higher current leads to a thicker boundary layer on the membrane surface due to enhanced concentration polarization. This enhanced concentration polarization allows a higher local ion concentration near the membrane surface, which promotes supersaturation and scaling formation. The mean height of scaling and membrane coverage was found to be lower at increased **flow rates** (see Figure 3.5). This was attributed to higher turbulence caused by an increase of Reynolds number and reduced ion concentration near the membrane surface, which decreased the local supersaturation of scaling ions and delayed their precipitation. At higher flow rates, ions and precipitates were more effectively flushed from the membrane surface, reducing their accumulation. the stable outlet pH at different flow rates (around pH 10, see SI Figure 3.13) indicated that the flow rate had no significant impact on the overall alkalinity of the solution, and the pH-shift value was driven mainly by the applied current.

In addition to changes in overall scaling volume and height, spatial variations in deposit distribution were also observed, as seen in Figure 3.6. The nonuniform scaling formation is observed in the upper

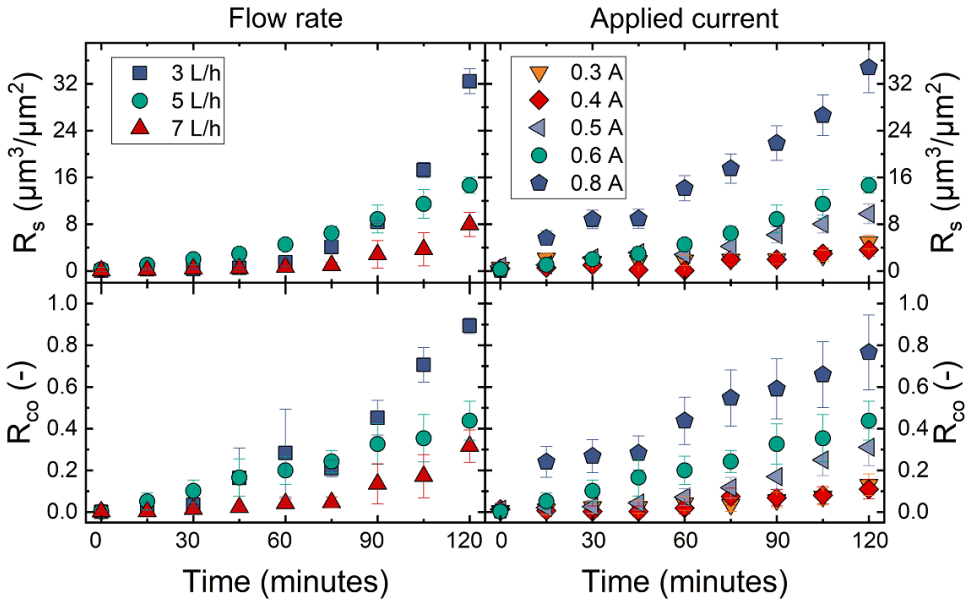

Figure 3.5: Scaling layer characterization under different flow rates and applied currents over time. Model Seawater, DIC ∼ 50 mg/L, applied current: 0.6 A (flow rate experiments), feed flowrate: 5 L/h (applied current experiments), 23±1°C, electrolyte: 10 g/L Na_2SO_4.

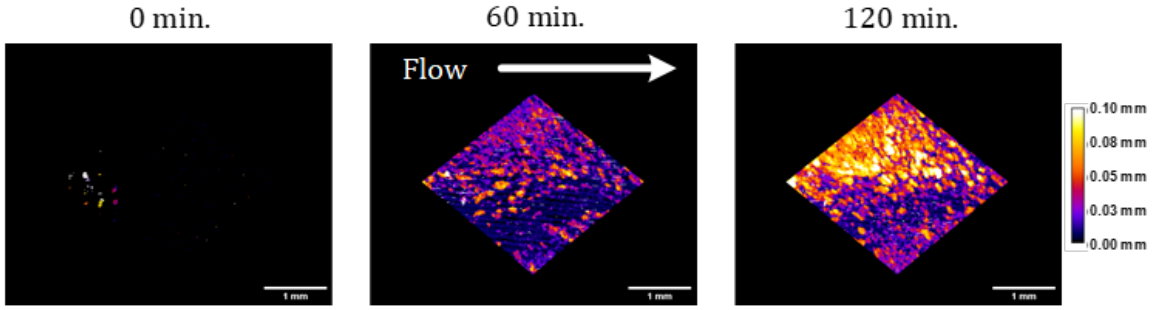

Figure 3.6: Height map of the ROI over time. Applied current of 0.8 A, feed flowrate: 5 L/h, model Seawater, 23±1°C, DIC ∼ 50 mg/L, electrolyte: 10 g/L Na_2SO_4.

half of the ROI (see Figure 3.6). This localized scaling pattern arises due to hydrodynamic effects, particularly the lower velocity of the solution near the membrane surface in the upper part of the rhomboid, downstream of the filament intersection. Variations in flow velocity, influenced by feed spacer geometry, affects local supersaturation conditions and boundary layer thickness, promoting greater ion accumulation and precipitation in certain areas, as shown in previous studies as well [120, 121]. Consequently, regions with lower shear stress experience thicker scaling, contributing to the observed lateral non-uniformity in deposit formation.

3.3.3 Impact of water chemistry on scaling

While flow conditions strongly influence the rate and distribution of scaling, the ionic composition of the feedwater also plays a crucial role. To investigate this, we performed experiments varying magnesium, sulfate, and bicarbonate concentrations. Experiments with different water compositions were conducted to understand how various ions affect scaling in the BPMED process. **Magnesium** plays a key role, as it forms magnesium hydroxide at high pH and can inhibit calcium carbonate crystallization by disrupting crystal growth. To isolate the role of magnesium ions in scaling development, experiments were conducted using solutions with varying Mg^{2+} concentrations. These experiments help explore the Mg/Ca ratio's influence on scaling patterns and membrane fouling. Scaling was found to increase over time when magnesium was present in the feed solution (see Figure 3.7). This can be attributed to magnesium's tendency to form magnesium hydroxide at high pH, which contributes to scaling on the basic side of the membrane. Minimal scaling was observed when magnesium was absent, indicating that magnesium plays a key role in the formation of scaling. Without magnesium, the system relies more heavily on other ions, such as calcium, which are less abundant and lead to reduced scale formation.

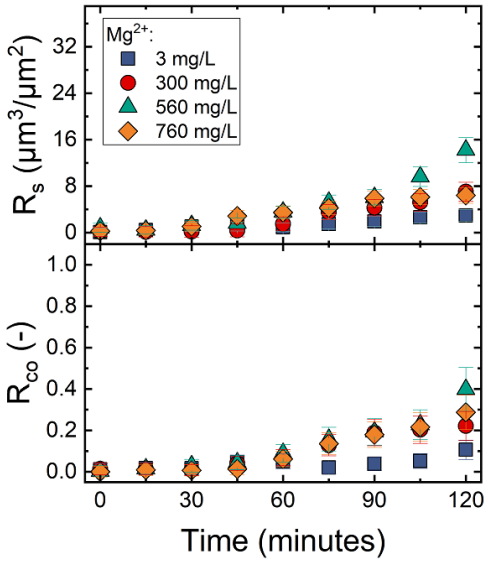

Figure 3.7: Scaling layer characterization at different magnesium concentrations over time. Applied current: 0.6 A, flow rate: 5 L/h, 23±1°C, EC ∼ 50 mS/cm, Ca^{2+}: 320 mg/L, electrolyte: 10 g/L Na_2SO_4.

Interestingly, both the scaling volume and coverage were lower at the highest magnesium concentration (see Figure 3.7). This was attributed to the lowered pH values at increased magnesium levels (from pH ~11 at lowest magnesium concentration to pH ∼ 9.5 at the highest magnesium concentration, due to the formation of magnesium hydroxide which consumed hydroxide ions, see SI Figure 3.15). This lower pH in turn increased the solubility of scaling salts in water, thereby reducing

the scaling volume and coverage. It has been shown that lower magnesium concentrations tend to decrease the solubility of calcite. In contrast, higher concentrations of magnesium can deform the surface crystal structure and disrupt interfacial water, leading to the formation of less stable crystals and higher solubility of magnesium-bearing calcite crystals [122, 123].

Experiments with varying **sulfate** concentrations were conducted to assess its influence on scaling formation. While sulfate is less likely to precipitate directly, it can interact with calcium and magnesium ions to form compounds like calcium sulfate, which can contribute to scaling, especially at higher salinities. Additionally, sulfate can reduce the solubility of other scale-forming ions, indirectly promoting carbonate or hydroxide scaling.

A higher scaling volume was observed as sulfate concentration increased, with a particularly sharp

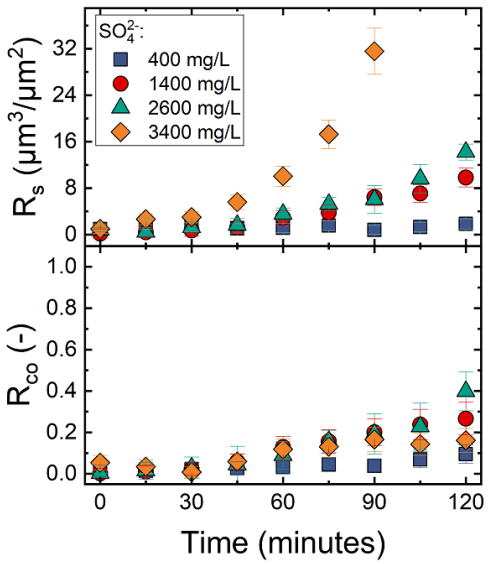

Figure 3.8: Scaling layer characterization at sulfate concentrations over time. Applied current: 0.6 A, flow rate: 5 L/h, 23±1°C, EC ∼ 50 mS/cm, Ca^{2+}: 320 mg/L, electrolyte: 10 g/L Na_2SO_4.

rise at 3,400 mg/L (see Figure 3.8). This is likely due to the formation of calcium sulfate as sulfate interacts with calcium ions in the solution, especially at elevated sulfate concentrations, leading to significant scale formation.

Despite the high scaling volume, a relatively low coverage ratio was observed, indicating that scaling occurred unevenly across the membrane surface (see Figure 3.8) possibly due to localized precipitation and the less soluble nature of calcium sulfate. The relatively narrow range of R_{CO} values (0.1–0.4) observed suggests that scaling was primarily localized rather than uniformly distributed across the membrane surface. The outlet pH remained stable across different sulfate concentrations, consistently around pH 10 (see SI Figure 3.16). This suggests that the sulfate concentration had no significant impact on the alkalinity of the solution.

Bicarbonate plays a crucial role as it converts to carbonate ions at high pH, leading to calcium car-

bonate precipitation. By varying **DIC** concentrations, the study aims to understand how different levels of bicarbonate contribute to scaling. Additionally, these experiments were designed to assess the effect of recirculating CO_2-free water on the basic side of the membrane, which can potentially influence scaling formation in the system. Scaling was observed to increase over time across all

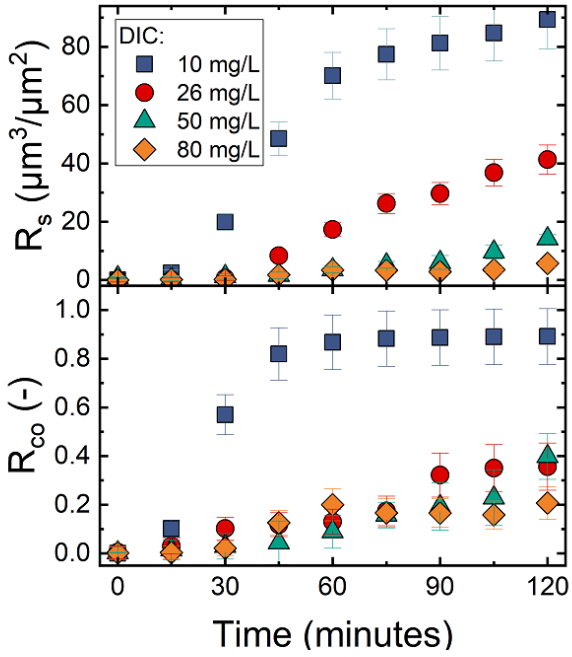

Figure 3.9: Scaling layer characterization at varying DIC contents over time. Applied current: 0.6 A, flow rate: 5 L/h, 23±1°C, EC ∼ 50 mS/cm, Ca^{2+}: 320 mg/L, electrolyte: 10 g/L Na_2SO_4 (*note the different scale in the top graph compared to previous figures.).

DIC concentrations, as expected (see Figure 3.9). Surprisingly, lower DIC concentrations resulted in more scaling. This was explained with the reduced buffer capacity of the solution at lower DIC, that caused a higher pH in lower DIC concentrations (from pH 9 at 80 mg/L DIC to pH ~10 at lower DIC contents, as seen in SI Figure 3.17). The higher pH at lower DIC concentrations promoted faster precipitation, leading to more scale formation even though less bicarbonate ions were initially present.

Membrane coverage increased over time, with the highest coverage observed at the lowest bicarbonate concentration of 10 mg/L (see Figure 3.9). The more uniform scaling at low DIC levels is likely due to the higher pH conditions, which foster more extensive precipitation and a greater surface area covered.

Despite the significant scaling observed in various conditions, no clear impact on the flow cell's resistance was detected (see SI figures 3.13 to 3.17). This lack of correlation between scaling and resistance was likely due to the design and structure of the flow cell used in this study. The flow channels and electrode configuration may have minimized the expected increase in resistance, typically

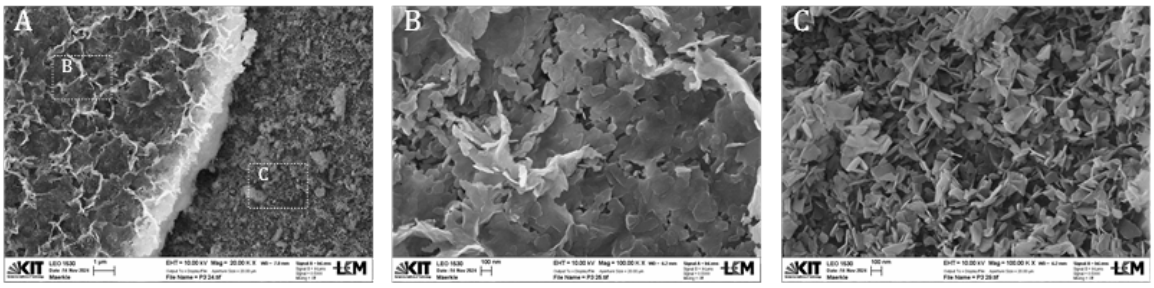

Figure 3.10: SEM images of the basic side of the BPM after one experiment, and rinsing with deionized water at different scales. Applied current: 0.6 A, Flow rate 5 L/h, 23±1°C, EC ∼ 50 mS/cm, Model water, Electrolyte: 10 g/L Na_2SO_4 (*The images illustrate structures and crystals at different magnifications images. Dotted rectangles in image A do not present the exact location).

Table 3.2: Major scaling ions concentrations and their ratio in the feed solution and scaling layer.

	Ca^{2+} (mg/L)	Mg^{2+} (mg/L)	Mg^{2+}/Ca^{2+}	$SO_4{}^{2-}$ (mg/L)
Feed solution	320 ±10	541 ±10	1.7	2,747 ±10
Scaling layer	47 ±10	629 ±10	13.5	222 ±10

seen as scaling accumulates on membranes. Therefore, further studies using a membrane stack closer to real-world operational conditions are necessary to accurately evaluate the relationship between scaling and electrical resistance with the help of results obtained in this study.

3.3.4 SEM and EDX analysis of bipolar membrane

To complement the in-situ OCT results with structural and compositional information, post-experimental SEM and EDX analyses were conducted on the membrane surfaces. SEM and EDX were employed to analyze the surface morphology of the basic side of the BPM. This analysis aims to examine the extent, structure and elemental composition of scaling formed during the experiment at standard condition and also to examine the effectiveness of the cleaning cycles (see SI Figure 3.12). While SEM and EDX provides post-experimental chemical analysis, they complement the OCT results, which capture the in-situ scaling growth over time. A new BPM subjected to one experiment under standard conditions (0.6 A, 5 L/h, model water) and washed only with deionized water to observe the scaling retained on the surface can be seen in Figure 3.10. The membrane samples were collected from the area that was directly beneath the studied imaging window. Figure 3.10 shows SEM images of the basic side of the BPM after one experiment under standard conditions (0.6 A, 5 L/h) and subsequent rinsing with deionized water. As seen in Figure 3.10A, variations in scaling morphology are evident and different layers of scaling can be detected. At the highest magnification (Figure 3.10B and C), flaky plate-like crystals are prominently visible, which are likely formations that contain Mg^{2+} cations [124]. This was also confirmed with EDX results, where magnesium and oxygen elements were abundant in the scaling formations.
Table 3.2 shows that Mg^{2+} cations are prominently present in the crystals formed, at a higher concentration than the feed solution (with lower concentrations of Ca^{2+} and $SO_4{}^{2+}$).

3.4 Conclusions

This study used a novel flow cell and OCT for the first time as a non-destructive/online method to investigate scaling in a "bipolar membrane electrodialysis process" under various operational conditions and water compositions. The results showed that higher applied currents increased the scaling volume and coverage due to the more alkaline environment (up to pH 10.3) on the basic side of the membrane, promoting the precipitation of magnesium hydroxide). Increased flow rates reduced scaling volume and coverage, as improved mixing lowered local supersaturation. At lower flow rates (3 L/h), near-total scaling coverage was observed, demonstrating how slower velocities lead to enhanced scaling.

Magnesium concentration had a dual effect: while scaling increased initially, higher concentrations lowered the outlet pH (from $\tilde{1}1$ to $\tilde{9}.5$), increasing the solubility of scaling salts and resulting in reduced scaling. Higher sulfate concentrations led to increased scaling volume, particularly at 3400 mg/L, though membrane coverage remained low and uneven due to localized precipitation. DIC concentration had a significant impact on scaling. Lower DIC concentrations resulted in more scaling due to lower buffer capacities and therefore higher pH levels, with the highest membrane coverage observed at 10 mg/L DIC. This suggests that recirculating CO_2-free water on the alkaline side, could increase scaling risks by promoting alkalinity and more extensive scale formation.

The SEM images and analysis of the formed scaling layer revealed the significant presence of magnesium cations resulting in formation of flaky, plate-like crystals on the membrane surface, highlighting its dominant role in scaling formation under high-pH conditions. The induced ΔpH (and its effect on the saturation index of the scaling compounds) was considered to be the most important parameter in scaling formation in the BPMED system. However, the magnitude of this ΔpH is not only controlled by the applied current, but also by the buffer capacity of the solution. Thus, lower buffer capacities result in more extreme ΔpH and more scaling. The results highlight the role of current density, flow hydrodynamics, ion composition, and DIC content in scaling formation and distribution. Understanding these interactions is a key step toward developing predictive models and strategies for fouling control and BPMED optimization in real-world applications. The SEM & EDX analysis also confirmed that magnesium hydroxide is the most prevalent form of scaling under high-pH conditions in BPMED. Therefore, future scaling mitigation strategies should prioritize its prevention, and further research should focus on developing targeted mitigation methods to minimize magnesium hydroxide deposition and its impact on membrane performance.

3.5 Supporting Information

3.5.1 Saturation index of possible minerals over pH 7 to 12

The Saturation Index (SI) is a dimensionless parameter that indicates the potential for mineral precipitation or dissolution in a solution. Figure 3.11 shows the saturation index of Mg^{2+} and Ca^{2+} complexes at alkaline pH range.

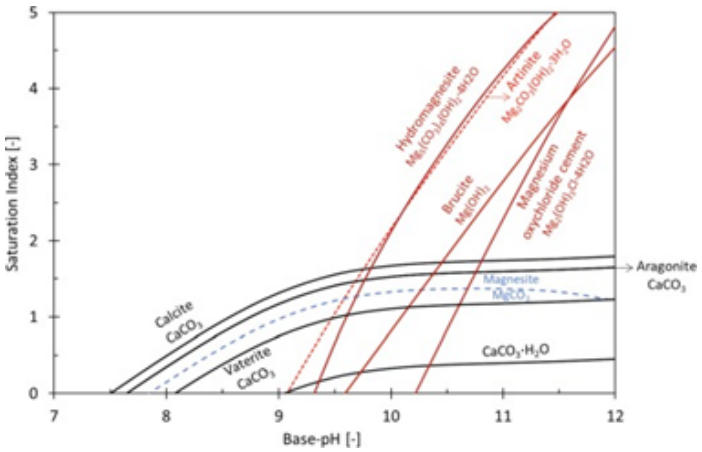

Figure 3.11: The saturation index (SI) of thermodynamically possible minerals in seawater vs. alkaline pH, taken from Sharifian *et al.* [6].

3.5.2 Feed water composition

The composition of the feed solutions, including the adjusted concentrations of dissolved inorganic carbon (DIC), magnesium, and sulfate, is detailed in Table 3.3. These adjustments were made to study the impact of varying ion concentrations on scaling behavior in the BPMED process.

Table 3.3: Composition of the prepared feed solutions with varying concentrations of dissolved inorganic carbon (DIC), magnesium (Mg^{2+}), and sulfate (SO_4^{2-}) for scaling analysis in BPMED.

Mg^{2+} Experiments				
	No added mg/L	**Low Mg^{2+} mg/L**	**Normal Mg^{2+} mg/L**	**High Mg^{2+} mg/L**
Cl^-	18,724	19,601	18,724	19,309
Na^+	12,670	12,670	11,616	11,616
SO_4^{2-}	2,605	2,605	2,605	2,605
Mg^{2+}	<detection limit	305	540	724
Ca^{2+}	344	344	344	344
K^+	26	26	26	26
DIC	50	50	50	50
TDS	34,441	35,618	33,944	34,728
EC (mS/cm)	49.5	51.2	48.8	49.9
SO_4^{2-} Experiments				
	No added mg/L	**Low SO_4^{2-} mg/L**	**Normal SO_4^{2-} mg/L**	**High SO_4^{2-} mg/L**
Cl^-	20,349	19,601	18,724	18,724
Na^+	11,616	11,616	11,616	11,999
SO_4^{2-}	400	1,480	2,880	3,200
Mg^{2+}	559	556	560	560
Ca^{2+}	344	344	344	344
K^+	26	26	26	26
DIC	50	50	50	50
TDS	33,367	33,617	33,944	35,127
EC (mS/cm)	48.0	48.3	48.8	50.5
DIC Experiments				
	No added DIC mg/L	**Low DIC mg/L**	**Normal DIC mg/L**	**High DIC mg/L**
Cl^-	18,722	18,723	18,724	18,727
Na^+	11,615	11,615	11,616	11,617
SO_4^{2-}	2,600	2,603	2,605	2,610
Mg^{2+}	559	559	560	561
Ca^{2+}	333	338	344	355
K^+	25	25	26	26
DIC	10	26	50	80
TDS	33,890	33,917	33,944	33,999
EC (mS/cm)	48.7	48.7	48.8	48.9

3.5.3 Properties of used membranes

3.5.4 SEM analysis of the bipolar membrane and scaling on the membrane surface

SEM Images were captured from the membrane surface to show the effectiveness of cleaning cycles and their impact on the membrane surface. To show this, two samples were prepared: (I) A virgin bipolar membrane soaked in 0.5 M NaCl, representing the initial condition of the membranes before any experiments. (II) A bipolar membrane exposed to multiple experimental cycles and washing

Table 3.4: Membrane Characteristics.

Membrane	FKL-PK-130	FBM
Reinforcement	PEEK woven web	PEEK woven web
Resin Type	Cation	Bipolar Anion/Cation
Thickness / μm	130	150
Resistance / MΩ·cm^2 *	6,5	110
Selectivity / % *	> 98	> 95

*Measured in 1 M NaCl solution

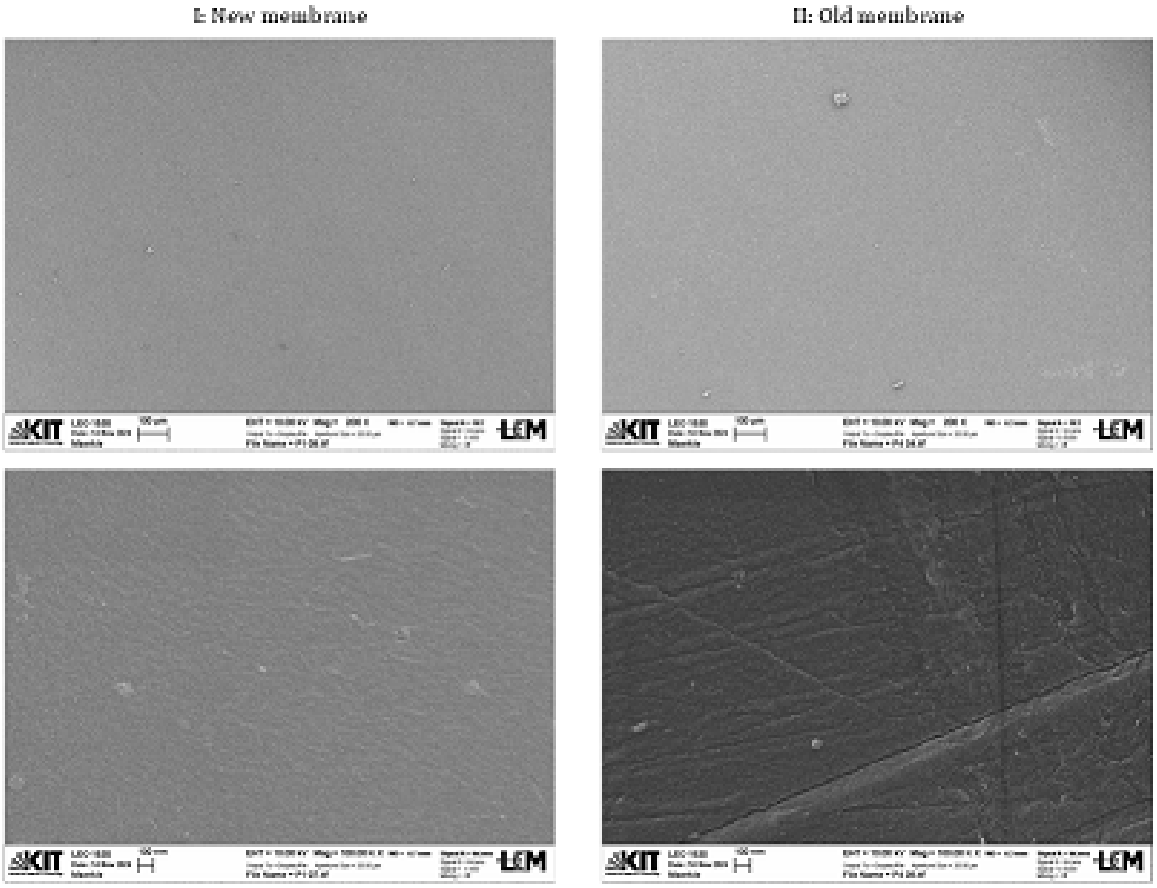

Figure 3.12: SEM images of the basic side of bipolar membranes. (I) A new membrane soaked in 0.5 M NaCl, representing its initial condition. (II) An old membrane subjected to multiple experimental cycles under standard conditions (0.6 A, 5 L/h, model water) and subsequent washing cycles.

steps to assess the cumulative impact of repeated use and cleaning. The comparison highlights minor changes in surface morphology due to repeated usage, however no major damage can be noticed. Only minor scratches can be seen in the old membrane and with higher magnification (Lower images in Figure 3.12).

3.5.5 Operational Parameter Evolution in Flow cell During Bipolar Membrane Electrodialysis

This section provides additional data on the operational parameters of the bipolar membrane electrodialysis (BPMED) system used in this study. The following figures illustrate the evolution of parameters such as current, voltage, resistance of the flow cell, and the pH of the outlet solution on the basic side of the membrane throughout the experiments. These parameters are critical for understanding the behavior of the system under different tested conditions and offer insights into the electrochemical and hydrodynamic conditions that influence scaling formation. By tracking these variables, we gain a clearer picture of the impact that operational changes have on scaling dynamics and membrane performance.

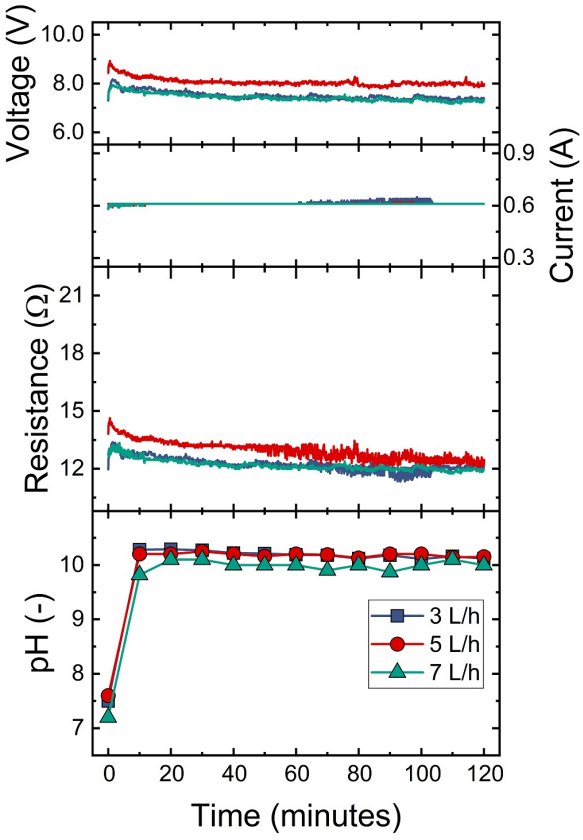

Figure 3.13: Voltage, applied current and the resistance of the flow cell, and pH measurements at outlet of the basic side with various flow rates over time. Model Water, DIC $\sim$ 50 mg/L, Electrolyte 10 g/L Na_2SO_4.

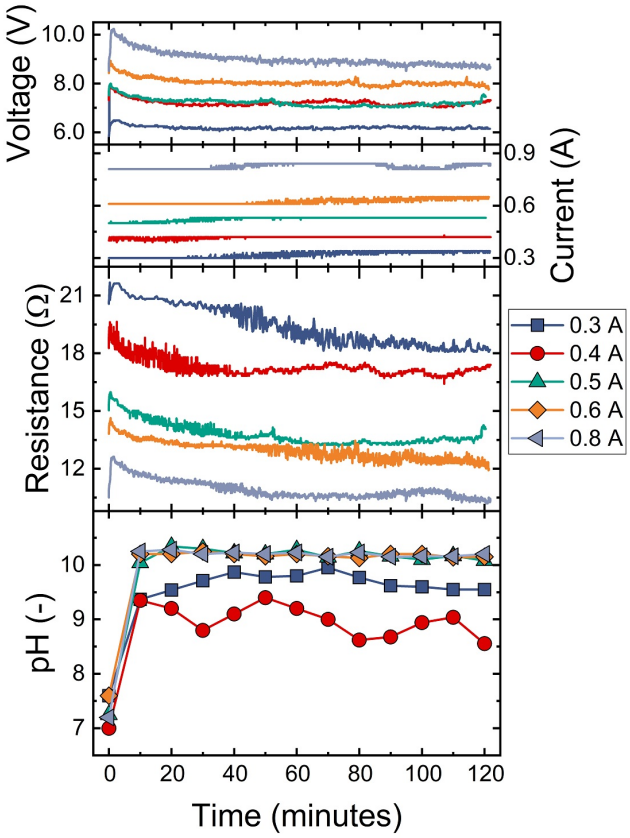

Figure 3.14: Voltage, applied current and the resistance of the flow cell, and pH measurements at outlet of the basic side with various applied currents over time. Model Water, DIC $\sim$ 50 mg/L, Electrolyte 10 g/L Na_2SO_4, 5 L/h.

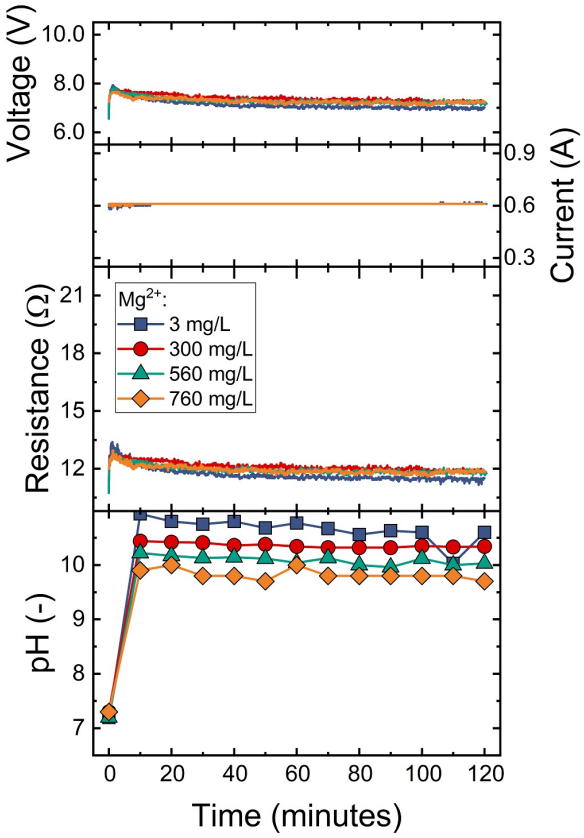

Figure 3.15: Voltage, applied current and the resistance of the flow cell, and pH measurements at outlet of the basic side with various magnesium concentrations over time. DIC $\sim$ 50 mg/L, Electrolyte 10 g/L Na_2SO_4, 5 L/h.

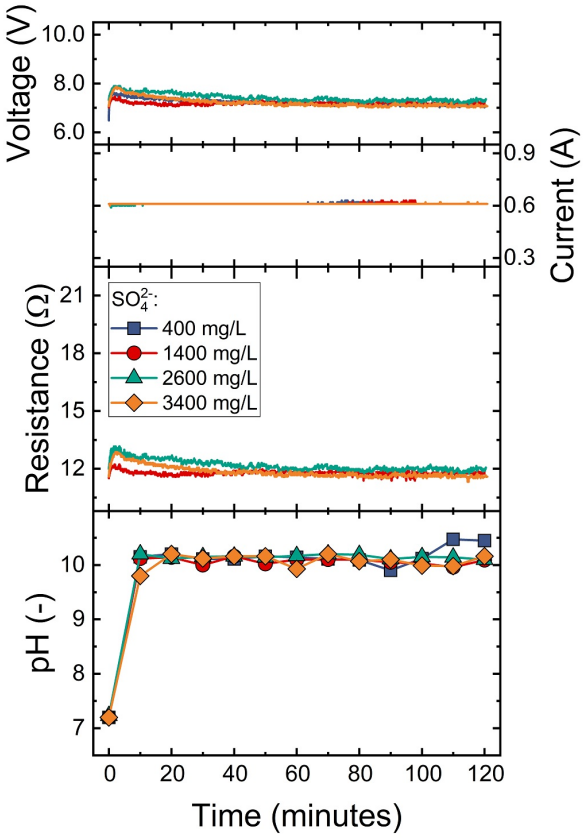

Figure 3.16: Voltage, applied current and the resistance of the flow cell, and pH measurements at outlet of the basic side with various sulfate concentrations over time. DIC $\sim$ 50 mg/L, Electrolyte 10 g/L Na_2SO_4, 5 L/h.

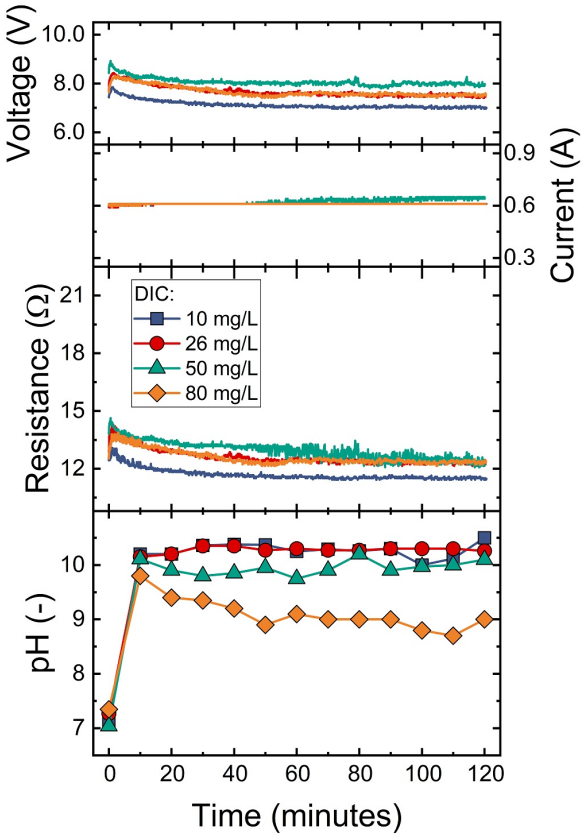

Figure 3.17: Voltage, applied current and the resistance of the flow cell, and pH measurements at outlet of the basic side with various DIC contents over time. Electrolyte 10 g/L Na_2SO_4, 5 L/h.

Chapter 4

Alkaline Closed-Loop Operation of Bipolar Membrane Electrodialysis For Efficient CO_2 Capture From Seawater

Abstract

Bipolar membrane electrodialysis (BPMED) enables electrochemical pH swing for CO_2 capture from seawater, but conventional in-situ operation suffers from scaling and energy losses that limit stability. Here, a closed-loop alkaline BPMED configuration is introduced to continuously regenerate hydroxide while suppressing scaling via recirculation of a softened stream. System performance was evaluated as a function of current density (6–32 mA/cm^2), flow velocity (1–3 cm/s), and salinity (35–100 mS/cm) using model seawater and desalination brines. Optimal operation was achieved at current densities of 8–12 mA/cm^2, extracting over 80 % of the dissolved inorganic carbon with a specific energy consumption (SEC) of 3 kWh/kg CO_2. Increasing flow velocity enhanced mass transport and reduced SEC from 4.5 to less than 3 kWh/kg CO_2, while high salinity caused co-ion leakage and diminished hydroxide selectivity. Under identical conditions, the closed-loop system produced NaOH with SEC values of 1.8–2.2 kWh/kg and current efficiencies of 60-85%. Direct acid/base generation from NaCl brines provided current efficiency benchmarks of up to 90% and SEC as low as 1.8 kWh/kg NaOH, supporting electrochemical consistency. Overall, the closed-loop alkaline BPMED enabled stable, energy-efficient CO_2 capture from seawater while simultaneously generating a NaOH-rich stream.

This chapter is published as:

Aliaskari, M., Horn, H., & Saravia, F. (2026). Alkaline Closed-Loop Operation of Bipolar Membrane Electrodialysis For Efficient CO_2 Capture From Seawater. *Chemical Engineering Journal*, *533*, 174769.
doi: https://doi.org/10.1016/j.cej.2026.174769

4. Alkaline Closed-Loop Operation of Bipolar Membrane Electrodialysis For Efficient CO_2 Capture From Seawater

Keywords:

CO_2 Capture; Ion Exchange Membrane; Dissolved Inorganic Carbon; BPMED; Acid and Base chemistry; pH-swing carbon capture

4.1 Introduction

To mitigate climate change, a global net-zero greenhouse gasses emission is needed, requiring deep decarbonization [125]. Achieving this necessitates carbon removal technologies to offset residual emissions and potentially reach net-negative levels [126]. The surface of the ocean is in constant equilibrium with the atmosphere and with rising CO_2 concentrations, and around 25% of the global CO_2 emissions end up in the ocean as dissolved inorganic carbon (DIC) (mostly as HCO_3^-, in the pH of ∼8.1) [10].
Ocean-based CO_2 capture is a promising solution that leverages the natural sink [15]. It enables negative emissions and provides feedstock for carbon-neutral fuels, supporting hard-to-abate sectors [50] (e.g., the production of carbon-neutral fuels [64, 127]). A promising strategy for capturing CO_2 from seawater is the pH-swing method, which utilizes electrochemical processes to alter the pH of seawater and facilitate the release of DIC as either precipitated $CaCO_{3(s)}$ or gaseous CO_2 [13, 19]. This method is advantageous as it avoids the need for high-temperature or high-pressure conditions.

4.1.1 Bipolar Membrane Electrodialysis for pH-Swing Carbon Capture

Bipolar Membrane Electrodialysis (BPMED) is an electro-membrane process that enables adjustment of pH in solutions by applying an electric field across a stack of ion-exchange membranes (IEMs). The core component is the bipolar membrane (BPM), which consists of an anion-exchange and a cation-exchange layer joined together. When a sufficient voltage is applied (õ0.6 to 0.8 V), water dissociates into protons (H^+) and hydroxide ions (OH^-) in the interfacial layer [81, 93], generating acidic and alkaline streams.
Bipolar membranes can be used in various ways for carbon capture, including both acidic and alkaline pathways (see Figure 4.1). In the acidic pathways, by lowering the pH of the solution, the DIC is transformed into dissolved CO_2 gas and extracted with a membrane contactor [57]. In the alkaline pathway, BPMED is used to precisely elevate the pH of the solution, resulting in precipitation of calcium carbonate ($CaCO_3$) [6]. Another approach to ocean-based carbon capture involves ocean alkalinity enhancement (OAE) by introducing a high-pH stream into the marine environment [128]. This increase in alkalinity shifts the carbonate equilibrium, promoting the absorption of atmospheric CO_2 into the ocean over a time period ranging from several weeks to months [129].
Many electrochemical and membrane-based CO_2 capture systems have been proposed and experimentally demonstrated; a critical performance metric in such systems is the specific energy consumption (SEC) per kilogram of CO_2 captured [130]. For example, Digdaya *et al.* [19] demonstrated a coupled BPMED-based oceanic CO_2 extraction system that achieved energy consumption of less than 1 kWh/kg CO2 under bench-scale conditions. This record low energy demand was achieved by replacing the commonly used water splitting reaction on the electrodes with a reversible redox reaction. A more recent study showed that operating at higher flow velocities (1 → 3 cm/s) can reduce energy demand from 3.7 to 2.5 kWh/kg CO_2 [5].

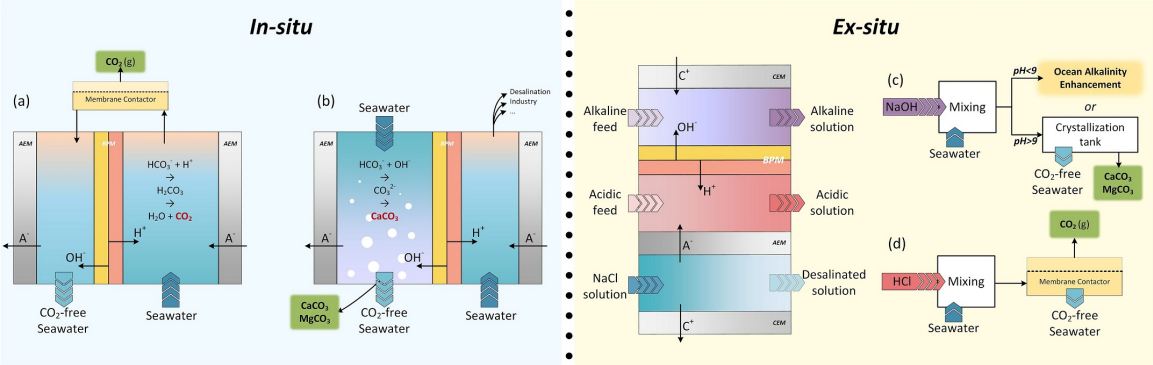

Figure 4.1: Schematic representation of in-situ and ex-situ processes for electrochemical CO_2 capture: a & d show the CO_2 capture via the **acidic route** (adapted from [6]) while b & c illustrate the CO_2 mineralization and ocean alkalinity enhancement via the **basic route**.

4.1.2 The Challenge of Inorganic Scaling in in-situ BPMED

In BPMED operation, high local pH values (on the alkaline side of the membrane) lead to supersaturation and subsequent precipitation of sparingly soluble salts. Scaling accelerates chemical and mechanical degradation of membranes, significantly shortening their lifetime [94]. Additionally, scale formation increases the electrochemical resistance of the membrane stack, resulting in higher energy consumption and operational costs [33]. In a previous study, magnesium hydroxide ($Mg(OH)_2$) has been identified as the primary scaling species in seawater-based BPMED systems [131].

Other scaling agents commonly found in seawater and brines include calcium ions (Ca^{2+}) and sulfate ions (SO_4^{2-}), as well as various mixed carbonate–hydroxide precipitates [33, 50]. These species contribute to membrane fouling under alkaline conditions, with their formation depending on the specific ionic composition and operating parameters of the BPMED system [131]. Digdaya *et al.* [19] proposed softening seawater prior to BPMED to remove Mg^{2+} and Ca^{2+}, which otherwise consume OH^- and cause scaling formation and limit pH rise in the basified stream. However, without these cations, the effluent could reach pH $\geq$ 10, and discharging such alkaline, decarbonized seawater may pose environmental risks, requiring further conditioning before release.

On the other hand, the presence of divalent cations in the alkaline compartment of BPMED promotes salt precipitation, as previously reported [5]. Sharifian *et al.* (2023) [33] evaluated BPMED in the alkalinization mode for CO_2 mineralization, testing different membrane configurations, operating conditions, and cleaning methods. Anion exchange membrane (AEM)-BPM stacks showed about four-fold less scaling than cation exchange membrane (CEM)-BPM. However, scaling occurred under all conditions (just after one hour), and only acid washing, particularly with back-pressure, could fully restore membrane performance. Taken together, these observations imply that, at seawater-like Mg^{2+} and Ca^{2+} levels, sustained in-situ operation would require frequent chemical cleaning and associated downtime, which can dominate operational burden and is not feasible. Repeated exposure to cleaning chemicals may also shorten membrane/spacer lifetime, making divalent-ion removal (softening) a practical prerequisite for stable operation.

4.1.3 Ex-situ BPMED process

In conventional BPMED processes, such as acid and base production from seawater or brine, pretreatment by softening is applied to remove Mg^{2+} and Ca^{2+}. This prevents hydroxide precipitation in the alkaline compartment, reduces the risk of scaling, and helps maintain long-term membrane performance. In contrast to the in-situ approach, ex-situ BPMED processes produce high-purity HCl and NaOH from a pure NaCl feed, which are then mixed with seawater to induce strong acidification (pH $\leq$ 4) for CO_2 capture or alkalinization for mineralization or enhancement of ocean alkalinity (see Figure 4.1C and D).

The ex-situ configuration not only enables stable BPMED operation [132]but also offers an additional benefit, as it reduces the environmental burden of brine disposal while allowing recovery of critical raw materials (e.g., Mg^{2+}) as a valuable resource [133, 134]. The pretreatment prevents hydroxide precipitation in the alkaline compartment of the BPMED, reduces scaling risk, and ensures stable long-term performance [135–137].

Ex-situ BPMED avoids internal scaling since seawater does not directly enter the stack. However, extreme pH swings and the need for purified NaCl solutions require higher thermodynamic voltage and additional processing, increasing energy and operational costs [12, 13, 138]. System performance (including energy efficiency and acid/base production) is primarily governed by feed salinity, applied current density, membrane configuration, and flow rate.

Feed **salinity** has a dual effect on BPMED performance. Low concentrations increase resistance due to reduced ion availability but enhance the interfacial electric field, promoting water dissociation [139]. Conversely, high salinities cause electrostatic screening and co-ion leakage, which diminishes dissociation efficiency. Reig *et al.* [140] showed that increasing NaCl concentration from 50 to 100 g/L reduced SEC to about 1.8 kWh/kg NaOH. However, further increasing salinity to 200 g/L caused SEC to rise again as diffusion and osmotic losses became dominant. Similar behavior was reported by Zhang *et al.* [137], who studied feed conductivities between 30 to 70 g/L NaCl and found that SEC decreased with salinity, achieving 1.5 to 2 kWh/kg NaOH and current efficiency (CE) values around 70 to 80%. Overall, a balance between the solution conductivity and the field strength is needed to achieve efficient water dissociation and low voltage losses [80].

The applied **current density** dictates acid/base production rates, SEC, and CE. At low current densities ($\leq$5 mA/cm^2), water dissociation (WD) dominates charge transport, but a significant fraction of current is also carried by co-ions due to diffusion, lowering selectivity and causing deviations from theoretical voltages [81]. Zhang *et al.* [139]further demonstrated that BPMED efficiency depends on the coupling of interfacial electric field strength and current density. At moderate current densities (roughly 20–100 mA/cm^2), strong local electric fields facilitate efficient WD with minimal overpotential, but at higher densities, ion crowding and electric-field screening reduce field strength and thus WD kinetics. At low to moderate current densities (20–30 mA/cm^2), several studies reported a favorable balance between productivity and energy efficiency: for instance, Cassaro *et al.* [135] observed an SEC of 1.4 kWh/kg NaOH and CE of ca. 80% at 20 mA/cm^2, whereas increasing the current to 40 mA/cm^2 raised the SEC to 1.9 to 2.6 kWh/kg NaOH and reduced CE to 63%. Herrero-Gonzalez *et al.* [141] similarly found that doubling current density from 20 to 40 mA/cm^2 only marginally increased production rate but increased SEC from $\sim$1.05 to 1.5 kWh/kg NaOH. A recent study has proposed integrated approaches that combine selective electrodialysis (SED) and BPMED to simultaneously treat reject brine and capture CO_2 [142]. The SED is used to soften the

reject brine by using selective ion exchange membranes prior to the introduction of the BPMED stack and separating divalent ions, specifically Ca^{2+} and Mg^{2+}.

Virruso *et al.* [143], found that increasing current density from 20 to 50 mA/cm^2 tripled the specific production but raised SEC from 1.9 to 2.7 kWh/kg NaOH. Similarly, Yang *et al.* [144] [35] reported a significantly higher SEC (ca. 7.5 kWh/kg HCl) and lower CE ($\tilde{5}4\%$) at 57 mA/cm^2. Overall, low currents prioritize selectivity and efficiency, while high currents increase throughput at the cost of higher overpotentials and water transport losses.

Higher **solution velocities** reduce the concentration (diffusion) boundary layer thickness at the membrane-solution interface [81, 88], enhancing ionic mass transfer and maintaining near-bulk concentrations at the membrane surface. Conversely, low velocities cause ion depletion, limiting WD and increasing cell voltage and SEC. For instance, Herrero-Gonzalez *et al.* [141] found that tripling the flow rate (2 to 6 L/h) improved current efficiency from 85% to 95% while reducing SEC from 1.2 to 1 kWh/kg NaOH.

The ex-situ BPMED process effectively reduces scaling and membrane fouling but remains limited by process complexity and chemical handling challenges. The separation of acid/base generation and CO_2 absorption requires multiple units and careful control of flow and pH, while handling concentrated acid and base introduces safety and corrosion concerns. These drawbacks motivate the exploration of hybrid approaches that utilize the operational stability of ex-situ systems with the simplicity and integration benefits of in-situ operation.

4.1.4 Opportunities and Knowledge Gaps

Process-level innovations can provide robust solutions for carbon capture from seawater. One promising approach is to take advantage of the simplicity of the in-situ process, while avoiding the fouling issue, using the ex-situ method. The in-situ approach has lower energy requirements for carbon capture and can be directly integrated with seawater. In contrast, the ex-situ approach avoids scaling, but requires harsh pH swings, additional desalination and softening steps and a higher energy input. This work investigates a new concept, named **closed-loop alkaline cell** system. In this configuration, the produced base could be used to precipitate and remove divalent cations externally, creating a softened stream that is fed to the closed-loop alkaline stream.

This work is framed around this novel process and evaluates it by addressing following research questions: (i) whether the hybrid process can mitigate scaling in the alkaline compartment; (ii) how the SEC and current efficiencies in CO_2 capture and NaOH production in closed-loop alkaline cell configuration are affected by current density, flow velocity and alkaline feed salinity; and, (iii) whether under realistic operational constraints, the NaOH production performance metrics are comparable to the ex-situ process.

These questions are investigated experimentally and via process-level benchmarking, by comparing the two products of the closed-loop alkaline cell process (captured CO_2 and NaOH) with the comparable in-situ and ex-situ process.

Table 4.1: concentration of major ions in the North Sea and the prepared model waters[5]

	Cl^- (mg/L)	Na^+ (mg/L)	Mg^{2+} (mg/L)	Ca^{2+} (mg/L)	DIC (mg/L)	SO_4^{2-} (mg/L)	EC (mS/cm)	pH (-)
North Sea	18980	10556	1200	400	120 – 140	2650	∼50	7.9 – 8.4
Model seawater	19800 ±396	11035 ±220	1313 ±26	421 ±8	130 ±15	2775 ±55	53 ±1	8.2 ±0.2
Softened model seawater	20360 ±320	13320 ±200	<20	<50	130 ±15	2775 ±55	54 ±1	8.5 ±0.2
RO-brine (30% recovery)	28280 ±365	15764 ±315	1876 ±37.51	601 ±12	140 ±15	3965 ±80	75 ±1	7.2 ±0.2
RO-brine (50% recovery)	39600 ±300	22070 ±350	2630 ±50	840 ±17	140 ±15	5550 ±110	104 ±1	7.1 ±0.2

4.2 Materials and Methods

4.2.1 Chemicals and Feed Solutions

Model seawater and reverse osmosis (RO) brine solutions were prepared by diluting different rations of a concentrated brine stock (Absolute Ocean, ATI Aquaristik, Germany) with deionized water (electrical conductivity $\leq$4 μS/cm). The concentration of the major ions in the North Sea and the prepared solutions is presented in 4.1. The model seawater and brines were used to ensure controlled and reproducible inorganic composition. The prepared solutions do not fully represent natural seawater components such as natural organic matter, which may contribute to additional fouling or alter membrane performance under long operation times.

In experiments where synthetic seawater was not used, the feed solution was prepared from sodium chloride (NaCl, ≥99.8%, VWR Chemicals) and sodium bicarbonate ($NaHCO_3$, ≥98%, VWR Chemicals) dissolved in deionized water.
5 Liters of a 10 g/L sodium sulfate (Na_2SO_4, ≥99.5%, VWR Chemicals) solution was prepared and used as the electrode rinse in the electrodialysis system. Dilutions of hydrochloric acid (HCl, 37%, VWR Chemicals) and sodium hydroxide (NaOH pellets, VWR Chemicals) were used to prepare acidic and base solutions and neutralization. A 0.1 M solution of HCl was used for DIC measurements, while 1 M solutions of HCl and NaOH were used for acid/base quantification. Unless otherwise stated, 0.05 M HCl and 0.05 M NaOH were used as feed solutions in the respective acid and base compartments of direct acid and base production experiments to reduce cell resistance. 1 M NaOH was also used to soften the model seawater or brines by precipitation and subsequent filtration. Analysis of the samples confirmed the removal of Mg^{2+} and Ca^{2+}, with concentrations below 20 and 50 mg/L, respectively.

4.2.2 Experimental Setups and Procedures

Experiments were conducted using a BED 1–3 Compact electrodialysis system (PCCell GmbH, Germany) equipped with online conductivity sensors (digiLine, Jumo, Germany), pH electrodes (tecLine pH, Jumo, Germany), and flow meters (type 123, GF Piping Systems, Germany). Pumps and the

DC power supply (DPPS-32–15, Voltcraft, Germany) were operated and monitored through the integrated software, which also recorded sensor data. Feedwater was filtered through a 0.2 μm cartridge prior to entering the membrane stack, and pH electrodes were calibrated weekly.
Two experimental configurations were used, as depicted in Figure 4.2. The primary study investigated the closed-loop alkaline configuration for in-situ CO_2 capture, NaOH production and scaling control; for comparison, a second configuration operated in direct acid/base production mode to compare the results with the ex-situ operation.

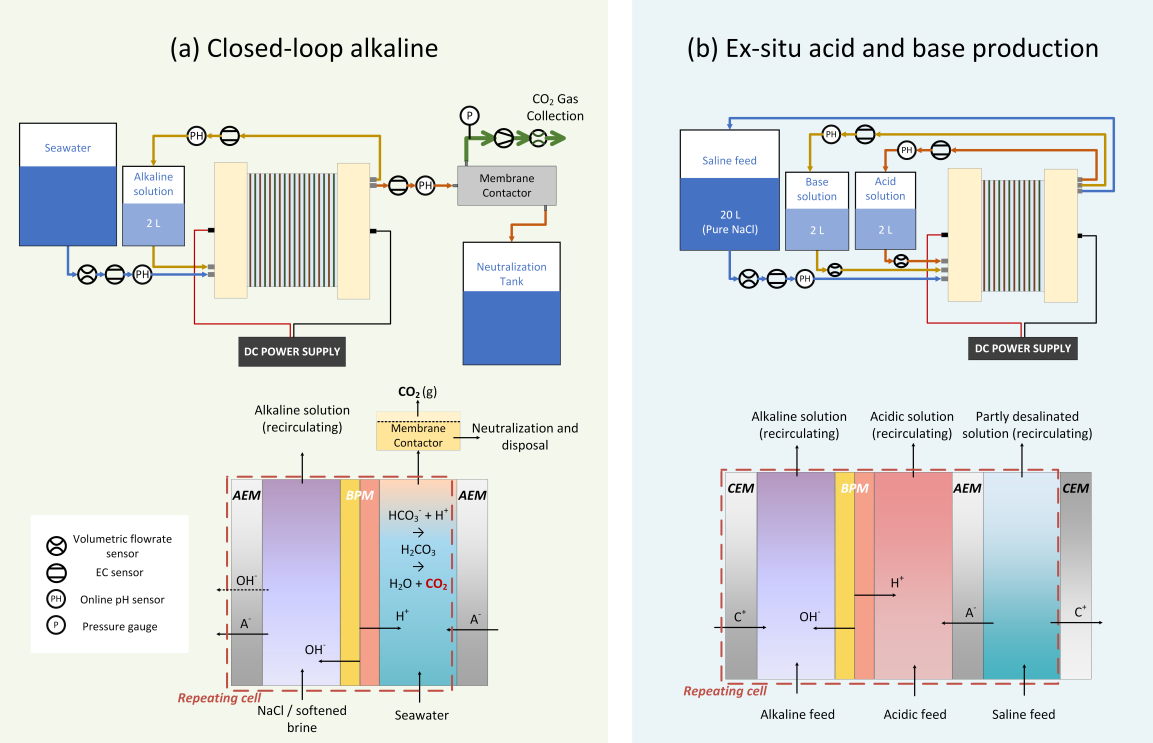

Figure 4.2: Schematic diagrams and the corresponding membrane cell configuration of the experimental setups for (a) closed-loop alkaline BPMED for CO_2 capture and NaOH production and (b) ex-situ acid and base production.

4.2.3 Closed-Loop Alkaline BPMED Experiments with CO_2 Capture

In the closed-loop alkaline tests, the BPMED membrane stack consisted of 10 cell pairs with an effective membrane area of 64 cm^2 per membrane (8 cm × 8 cm). The cell pairs consisted of a bipolar membrane (FBM-PK, Fumatech, Germany) and an anion-exchange membrane (FAB-PK-130, Fumatech, Germany), as seen in Figure 4.2C. Each compartment had a flow channel thickness of 1.5 mm (by polypropylene feed spacers). Two end cation-exchange membranes (PC MTE, PCCell) separated the cell pairs from the electrode rinse compartments. A Pt-Ir and mixed metal oxide coated Ti-stretched mesh was utilized as the anode, while a stainless-steel mesh was used as the cathode (provided by PCCell).
In the closed-loop alkaline loop configuration, the base stream (2 L) was continuously recirculated.

Samples of 15 mL were taken from the alkaline tank at 10 min intervals for titration and measuring the OH^- concentration.
Model seawater was continuously fed through the acidic compartment of the membrane stack. After passing through the acidic cell of the membrane stack (and the subsequent pH reduction), the seawater passed through a single membrane contactor (Liqui-Cel EXF-2.5×8, 3M) for CO_2 extraction. The extracted gas was quantified with a milli gas counter (MGC-1 v3.4, Ritter, Germany) and collected in a gas bag. The composition of the gas was analyzed using a multi-gas analyzer (RMS-MOD-IR1, Ritter, Germany). The CO_2-free seawater was neutralized (with the produced alkaline solution) prior to disposal. A 50 mL sample was taken at the beginning of each run to determine the initial DIC concentration, and additional samples were collected from the outlet at the end of the experiment. Each experiment was conducted for one hour.
Unless otherwise specified, experiments were performed under standard conditions: a flow rate of 50 L/h (corresponding to a solution velocity of ca. 2 cm/s), a current density of 10.9 mA/cm^2, and a temperature of 22 ±2 degrees celsius. Additional experiments were conducted at varied current densities (6 to 32 mA/cm^2) and flow rates (30 to 70 L/h). All experiments were performed under constant current conditions.
To assess the effect of salinity, only the base compartment feed was varied, using pure NaCl solutions (35, 50, and 70 g/L NaCl) or softened seawater with electrical conductivities of 50, 75, and 100 mS/cm. These values corresponded to natural seawater as well as desalination brines at approximately 30% and 50% recovery, respectively. The membrane stack was rinsed with demineralized water after each experiment (for less than 10 minutes). Moreover, it was opened after each set of experiments for visual testing of the bipolar membranes and to make sure no fouling was depositing.

4.2.4 Direct Acid/Base Production Experiments

In the acid and base production tests, the BPMED membrane stack consisted of 5 cell pairs with the same membrane area (64 cm^2). A cell consisted of an AEM (FAB-PK-130, Fumatech, Germany), a BPM (FBM-PK, Fumatech, Germany) and a CEM (FKL-PK-130, Fumatech, Germany), as depicted in Figure 4.2D. The stack was separated from the electrode rinse compartments by end-CEMs (PC MTE, PCCell, Germany), and the same electrode materials as described previously were used.
During operation, the acid and base streams became progressively concentrated, while the saline feed was slightly desalinated. In the acid and base production experiments, 2 L of 0.05 M HCl and 0.05 M NaOH were used as the initial solutions in the acid and base tanks, respectively, to reduce cell resistance. A 20 L NaCl solution with concentrations of 35, 50, or 70 g/L served as the saline feed. The system was operated at a constant flow rate of 50 L/h and a temperature of 22 ± 2 degrees celsius. Each run was performed for three hours, and 12 mL samples were withdrawn from the acid, base, and saline tanks every 30 min for analysis. Experiments were conducted at various current densities (from 10.9 to 29.7 mA/cm^2) to evaluate their influence on performance.
To evaluate the possibility of reducing the demand for pure water, additional tests were performed in which the acid and base tanks were initially filled with 2 L of NaCl solutions (35, 50, or 70 g/L) instead of 0.05 M HCl/NaOH.

Table 4.2: Ion-exchange membrane properties (adapted from membrane data-sheets)

Membrane name	**FKL-PK-130 (CEM)**	**FAB-PK-130 (AEM)**	**PC MTE (End membrane)**	**FBM-PK-130 (BPM)**
Resistance ($\Omega \cdot cm^2$)	<10 (0.5 M NaCl)	<8.5 (0.5 M NaCl)	≈ 4.5 (0.5 N KCl)	–
Thickness (dry - μm)	$120-150$	$110-150$	220	$110-160$
pH stability	$0-14$	$0-14$	$1-13$	$0-14$
Water splitting efficiency	–	–	–	>0.98
Water splitting voltage (V)	–	–	–	<1.2

4.2.5 Analytical Methods

Chloride and sulfate concentrations were determined by ion chromatography (Metrohm 930 Compact IC Flex, Metrosep A Supp 5) while sodium, calcium and magnesium were quantified by inductively coupled plasma–optical emission spectroscopy (ICP-OES, Agilent Technologies 5110).
DIC was measured by two-point titration with 0.1 M HCl (following method in [5]). The concentrations of acid and base samples were determined by titration using 2 M NaOH and 2 M HCl, respectively. All the titrations were performed with an automatic titrator device (TitroLine® 7000, SI Analytics).

4.2.6 Data Analysis

DIC removal was defined as:

$$\text{DIC Removal}\,(\%) = \left(1 - \frac{c_t}{c_0}\right) \times 100 \tag{4.1}$$

Where c_0 represents the initial DIC concentrations in the seawater, and c_t stands for the DIC concentration in the seawater, after acidification, CO_2 extraction and neutralization. The SEC for CO_2 capture or NaOH production was calculated as:

$$\text{SEC} = \frac{\int U\, I\, \mathrm{d}t}{\Delta t\, \dot{m}_i} \tag{4.2}$$

whereis U the cell voltage (V), I is the applied current (A), therefore the numerator represents the total electrical energy input during the experiment. t is the experimental duration (s), and *dotm* is the mass flow rate of the product (kg/s), either extracted CO_2 or produced NaOH. SEC values are reported as kWh/kg of product.
The current efficiency for a given species was calculated as:

$$\text{CE}\,(\%) = \frac{n\, z\, F}{N\, I\, t} \tag{4.3}$$

where n is the number of moles of the target ion or product formed (OH^- or Cl^-), z is its charge number, F is the Faraday constant (96485 C/mol), N is the number of cell pairs in the membrane stack. The denominator represents the total charge passed during the Experiment.

4.3 Results and Discussion

This section presents a comprehensive evaluation of the performance and energy efficiency of BPMED systems for simultaneous NaOH generation and CO_2 capture. The following section investigates the performance and energy efficiency of a closed-loop alkaline BPMED configuration designed for in-situ CO_2 capture in a continuous operation and hydroxide generation.
To contextualize the results and assess the broader efficiency of BPMED-based CO_2 capture, an additional configuration employing direct acid and base generation from saline feed solutions is evaluated. The complementary results serve as a reference for the closed-loop configuration, providing a benchmark for comparison in terms of NaOH productivity, SEC, and CE. Collectively, the comparative results enable identification of the most energy-efficient process configuration and provide insights into optimizing BPMED systems for scalable, electrochemically driven CO_2 capture applications.

4.3.1 Closed-loop Alkaline Cell for Continuous CO_2 Capture and OH^- Production

Current density is the key operational parameter governing the rate of water dissociation in BPMED and, consequently, the production of H^+ and OH^-, driving pH swing and the subsequent CO_2 capture. Increasing the applied current strengthens the interfacial electric field across the bipolar junction, accelerating water splitting and alkalinization in the recirculated base stream. Moreover, the higher pH-swing enhances the conversion of DIC into gaseous CO_2, as reflected by the increasing DIC removal and CO_2 capture efficiency with current density (Figure 4.3a) and shown also in previous study [5]. As expected, the DIC removal values (calculated with titration) uniformly follow the same values and trends of the collected CO_2 gas in all experiments.
The energy consumption followed a non-monotonic trend. A minimum SEC of around 3 kWh/kg CO_2 was observed at 8 mA/cm^2, indicating an optimum balance between water-dissociation (and ΔpH, see Figure 4.8) and ohmic losses. Interestingly, the minimum SEC in the in-situ process was also observed at the same current density (ca. 2.5 kWh/kg CO_2) [5]. Below this threshold, insufficient H^+/OH^- production resulted in incomplete DIC conversion (due to a low ΔpH) and high SEC, whereas further increasing the current density led to rising voltage losses and co-ion transport, both contributing to higher energy demand.

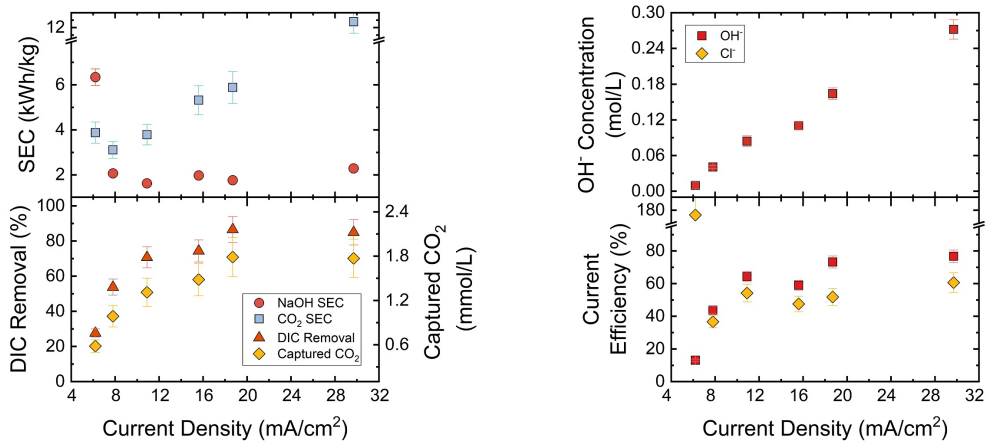

(a) (b)

Figure 4.3: Impact of current density on BPMED closed-loop alkaline operation after 1 hour: (a) SEC for NaOH and CO_2, DIC removal, and captured CO_2; (b) OH^- concentration and current efficiencies of OH^- and Cl^-. Acidic feed: Simulated seawater, DIC: ca. 120 mg/L, 2 cm/s; alkaline feed: 35 g/L NaCl; Electrolyte: 10 g/L Na_2SO_4.

The corresponding current efficiency (Figure 4.3b) show that at low current densities (¡ 7 mA/cm^2) chloride crossover dominates, reaching apparent values up to 180%. Apparent values ¿100% do not violate Faraday's law, but indicate that net chloride transfer is not solely driven by electro-migration and includes non-Faradaic contributions, which are amplified at low current because the total charge passed is small. With increasing current, the fraction of charge carried by hydroxide ions increases as water dissociation reaction dominates, improving selectivity of the BPM and reaching current values of up to 80% for the OH^- current efficiency. These findings are consistent with previous studies reporting strong coupling between field strength and water-dissociation kinetics in BPMs [81, 145]. Overall, moderate current densities between 8 and 12 mA/cm^2 deliver the most favorable trade-off between CO_2 removal, NaOH productivity, and SEC. Mustafa *et al.* [142] reported that the SED-BPMED integrated process achieved a CO_2 capture efficiency of around 50%. The closed-loop alkaline system's ability to exceed 80% DIC removal demonstrates its efficiency.

To investigate the effect of hydrodynamic conditions on CO_2 removal and NaOH production within the BPMED stack, experiments are conducted at various flow velocities. The flow velocity defines the hydrodynamic environment inside the stack and directly affects ion transport, boundary-layer thickness, and mass transfer at the membrane interfaces.

Increasing the solution velocity enhances mass transfer (liquid/membrane) and reduces concentration polarization, thereby stabilizing ionic gradients and maintaining near-bulk electrolyte concentrations at the membrane surface [146]. However, higher velocities also shorten the residence time of the seawater in both the BPMED stack and the downstream membrane contactor, potentially limiting the pH shift and the extent of CO_2 extraction.

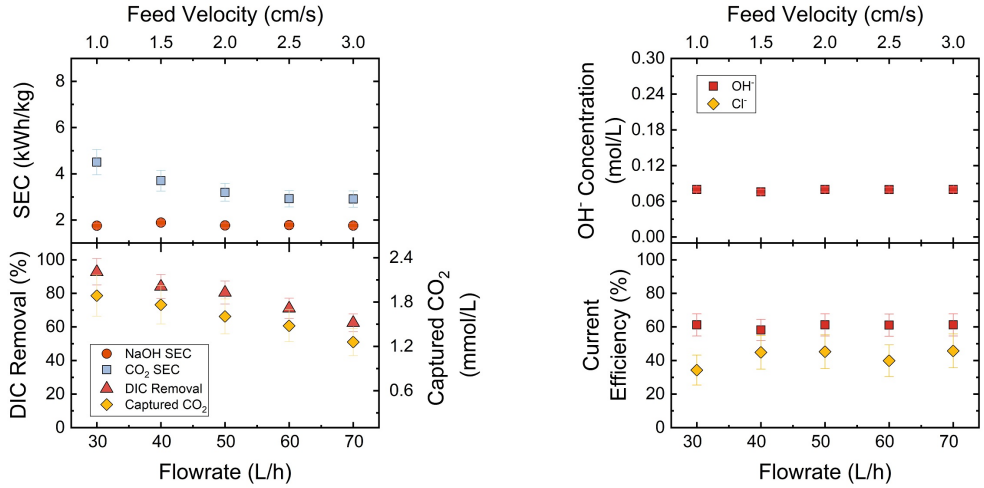

(a) (b)

Figure 4.4: Impact of Flowrate on BPM$^-$ED closed-loop alkaline operation: (a) SEC for NaOH and CO_2, DIC removal, and captured CO_2; (b) OH^- concentration and current efficiencies of OH^- and Cl^- after one hour. Acidic feed: Simulated seawater, DIC: ca. 120 mg/L, 10.9 mA/cm^2; alkaline feed: 35 g/L NaCl; Electrolyte: 10 g/L Na_2SO_4.

Figure 4.4a shows that the NaOH SEC was nearly insensitive to feed velocity in the tested range. Increasing velocity from 1 to 3 cm/s (30–70 L/h) changed the NaOH SEC from ĩ.7–1.9 kWh/kg NaOH (an increase of ¡0.2 kWh/kg, ¡10%). This is consistent with the nearly constant OH^- concentration (0.07–0.08 M) and hydroxide current efficiency (60%) across velocities (Figure 4.4b), indicating that within this hydrodynamic window the NaOH energy demand is governed primarily by cell voltage and charge efficiency rather than external mass-transfer effects. By contrast, the SEC for CO_2 capture decreased as the flow velocity increased from around 4.5 kWh/kg CO_2 at 1 cm/s to approximately 2.9 kWh/kg CO_2at 3 cm/s. This reduction is not related to changes in mass transfer or concentration polarization, but rather results from the higher volumetric seawater throughput through the BPMED system. Figure 4.7 shows that a lower ΔpH was observed as the velocity was increased. And subsequently, as the feed velocity increased from 1 to 3 cm/s, the total amount of extracted CO_2 nearly doubled, from 2.5 to 4.0 mg, while the total electrical energy input to the system remained almost unchanged.

Despite the improved energy performance, increasing the flow velocity reduced the extent of capture: DIC removal decreased from 90% to 50%, shown also with the volume of captured CO_2 per liter: from 1.8 to 1.3 mmol/L. The reduced residence time in the membrane contactor and slightly diminished pH gradient (acidic pH of 3 at 30 L/h to pH 5.5 at 70 L/h) at higher velocities limited the overall conversion of DIC to gaseous CO_2 (see Figure 4.7). As shown in Figure 4.4b, the OH^- concentration and corresponding current efficiency remained nearly constant across the studied range, confirming that ionic transport within the alkaline compartment was not significantly affected under the tested hydrodynamic conditions.

Overall, the results suggest that increasing the flow velocity reduces the CO_2 capture SEC; however, excessive velocities may compromise the pH-driven CO_2 release process by reducing the residence time in the membrane stack and contactor. Using more membrane contactors can be an effective solution to this problem, as long as the required pH-swing is applied. In this setup, a moderate flow velocity of around 2 cm/s strikes a practical balance, maintaining efficient CO_2 capture and SEC for continuous CO_2 capture.

Increasing the feed salinity enhances solution conductivity and lowers ohmic resistance. However, it also promotes the transport of co-ions (Cl^-) and reduces the current efficiency for hydroxide generation. Increasing feed conductivity from 50 to 100 mS/cm decreased the stack voltage from 16 to 13 V at fixed current (around 19%, see Figure 4.9), indicating reduced ohmic losses, but potentially reduced hydroxide selectivity by increasing chloride co-ion leakage and lowering hydroxide current efficiency. It is these competing effects that ultimately define the optimal salinity range for efficient NaOH production and CO_2 capture. Furthermore, depending on the extent of desalination in the other co-located processes, different concentration streams may be available [147]. These can be used directly or blended to achieve the desired ionic strength in the closed-loop alkaline solution. The following experiments therefore investigate how the salinity of the closed-loop alkaline solution affects overall CO_2 capture and NaOH production performance at a constant applied current.

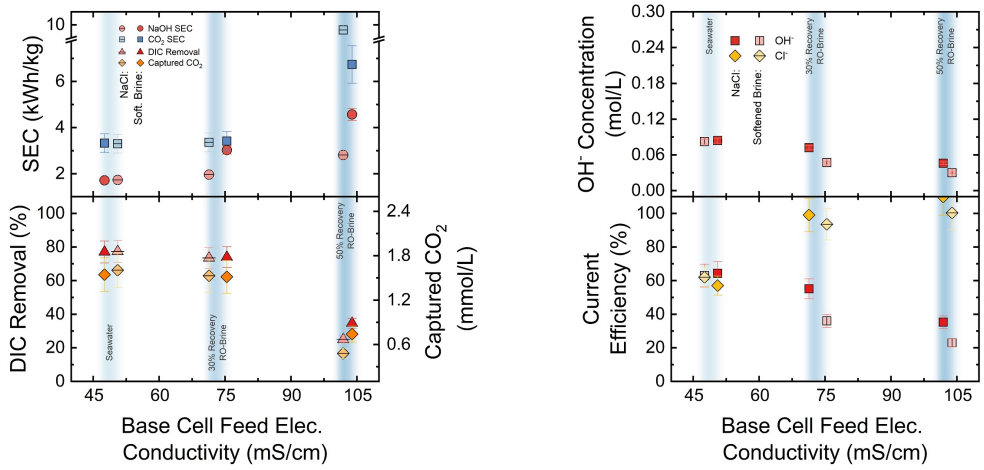

(a) (b)

Figure 4.5: Impact of alkaline cell solution salinity and composition on BPMED closed-loop alkaline operation: (a) SEC for NaOH and CO_2, DIC removal, and captured CO_2; (b) OH^- concentration and current efficiencies of OH^- and Cl^-. Acidic feed: Simulated seawater, DIC: ca. 120 mg/L; 2 cm/s; 10.9 mA/cm^2; Electrolyte: 10 g/L Na_2SO_4.

As shown in Figure 4.5a, the SEC for both NaOH and CO_2 increased with rising feed salinity. At higher ionic strengths, although the stack resistance decreased, co-ion transport and osmotic effects became more pronounced, leading to higher energy losses. This trend was particularly evident at

100 mS/cm, where co-ion leakage and water back-diffusion dominated the charge balance, thereby diminishing process efficiency. The CO_2 capture and DIC removal remained essentially unchanged up to 75 mS/cm (DIC removal $\tilde{7}5$–80%, captured CO_2 $\tilde{1}.5$–1.7 mmol/L), but dropped sharply at the highest salinity (100 mS/cm) to 25–35% DIC removal and $\tilde{0}.6$–0.8 mmol/L captured CO_2. This decline coincided with a marked loss of hydroxide production (Figure 4.5b): OH^- current efficiency decreased and Cl^- current efficiency approached 100%, indicating that an increasing fraction of the applied current was carried by chloride migration rather than water-dissociation products. As a result, the effective pH-swing driving carbonate-to-CO_2 conversion was reduced, thereby limiting CO_2 release in the contactor.

Overall, the results demonstrate that while higher salinity improves bulk conductivity, it deteriorates WD kinetics and increases energy consumption (at similar current densities). When alkaline feed salinity exceeds a certain threshold, electrostatic screening and co-ion leakage significantly limit CO_2 capture efficiency. The findings highlight the need to carefully control ionic strength in BPMED systems designed for seawater and brine-based CO_2 capture applications, especially when operating under closed-loop alkaline conditions.

Across all closed-loop alkaline runs, no macroscopic scaling was observed on membranes, spacers, or channels, and neither the cell voltage (at fixed current) nor the outlet-pH drifted with time (Figures 4.7 to 4.9). However, confirming long-term stability will require extended continuous operation with real seawater (multi-hour to multi-day) combined with more detailed post-mortem characterization (e.g., deposit mass/coverage and compositional analysis) and also investigating the extent and impact of organic foulants in the system as well; these assessments are beyond the scope of the present study and will be addressed in future work. Having established how current density, flow velocity, and ionic strength govern CO_2 extraction and NaOH production in the closed-loop configuration, the next section investigates the production of acid (HCl) and base (NaOH) from seawater and brines by BPMED. This benchmark isolates the basic electrochemical performance (concentration, SEC and CE) under comparable salinity, flow velocity, and applied current conditions, providing a consistent basis on which to validate trends and trade-offs in the subsequent process comparison.

4.3.2 Direct Use of Seawater/RO-Brine in BPMED for Acid/Base Generation

Building on the closed-loop analysis, this section evaluates BPMED operated directly on seawater and brine for acid/base generation. Direct acid and base generation from NaCl solutions represents a practical alternative operation mode of BPMED, enabling the direct electrochemical conversion of saline solutions into chemical reagents such as HCl and NaOH. In this configuration, water dissociation at the bipolar junction supplies H^+ and OH^- ions that are selectively transported into the respective acid and base compartments. Higher current densities are expected to enhance the rate of water dissociation and thus increase acid and base concentrations.

Furthermore, substituting pre-dosed acid and base feeds with brine solutions provides a more resource-efficient approach that reduces the need for deionized water; however, this modification is anticipated to increase the SEC due to osmotic effects, and higher co-ion leakage. The primary purpose of these experiments was to establish a performance benchmark (particularly for base production, SEC and CE) against which the closed-loop BPMED configuration could be evaluated,

allowing a direct comparison of their energy demands and electrochemical performance under comparable operating conditions. The process provides an opportunity to simultaneously valorize saline wastes and supply reagents for downstream CO_2 capture or pH-swing applications, which is actively used by companies in pilot scale [148].

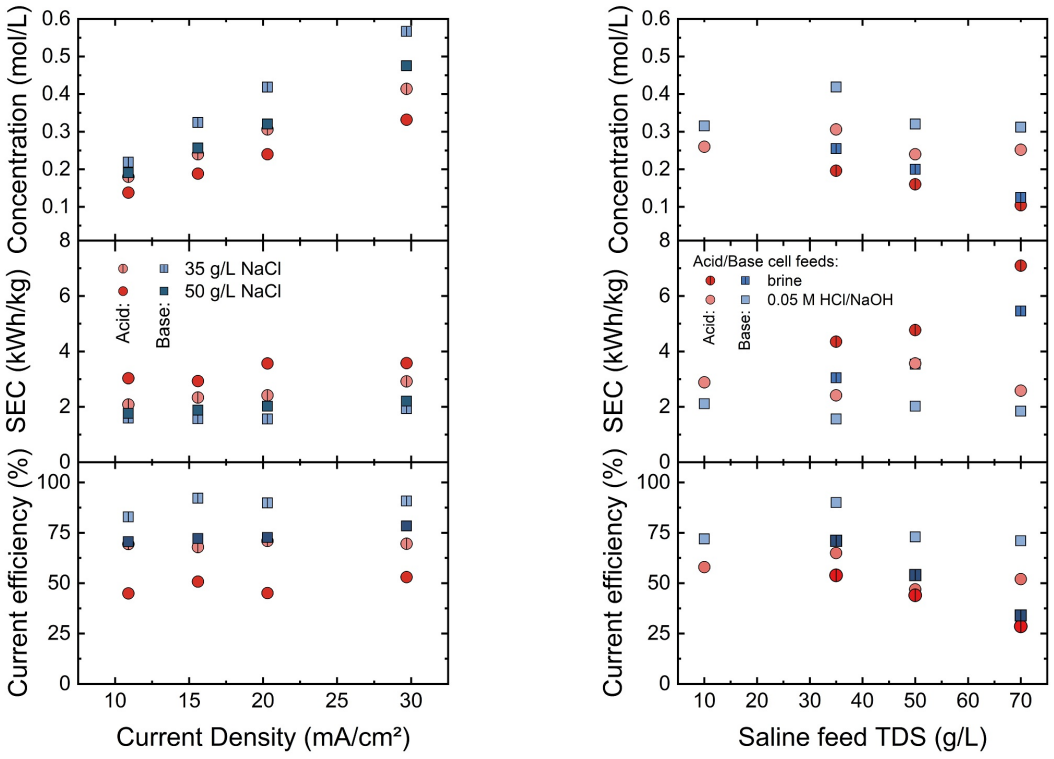

(a) (b)

Figure 4.6: Impact of (a) current density (acid feed: 0.05 M HCl, base feed: 0.05 M NaOH, saline feed: 35 or 50 g/L NaCl) and (b) feed composition (saline, acid and base feed: brine with mentioned salinity of NaCl, current density: 20.3 mA/cm^2) on the concentration and SEC of the produced acid and base. Electrolyte: 10 g/L Na_2SO_4, 2 cm/s.

The effect of current density and feed composition on the performance of direct BPMED acid and base generation is shown in Figure 4.6. As shown, increasing current density significantly enhanced acid and base production, consistent with the higher water dissociation at higher interfacial electric fields. The concentrations of both products increase nearly linearly, 0.4 and 0.6 mol/L at 30 mA/cm^2 while using 35 g/L saline feed. Throughout all the experiments, the concentration of NaOH exceeds that of HCl. This has also been observed in other studies and is primarily due to the higher mobility of protons. Resulting in dominant acid diffusion across the membranes, causing a decrease in H^+ concentration in the acid solution. The NaOH SEC increases slightly with higher current densities, rising from around 1.8 kWh/kg NaOH at 10 mA/cm^2 to over 2.2 kWh/kg NaOH at 30 mA/cm^2. This limited variation suggests that ohmic and overpotential losses remain relatively

stable within the tested range, indicating efficient ionic transport.

The current efficiency for hydroxide generation remains within a narrow range of across different current densities (Figure 4.6a), indicating that co-ion leakage and back-diffusion are largely unaffected by current density under these conditions. The results in Figure 4.6b highlight the impact of feed composition. When pre-dosed 0.05 M HCl/NaOH feeds are replaced by saline solutions, both product concentrations and current efficiencies decrease by roughly 20%. Consequently, the SEC also increases when saline solutions replace acid and base feeds. This behavior is attributed to enhanced co-ion leakage and osmotic water transport at higher ionic strengths, which dilute the generated acid and base and reduce effective charge utilization, as also observed in a previous study by [149].

When a constant current density of 20.3 mA/cm^2 was applied and the salinity of the saline solution increased (0.05 M HCl/NaOH in acid and base cells, see Figure 4.6b), the maximum base concentration and current efficiency with the lowest SEC was observed at 35 g/L NaCl. This can be attributed to the competing effects of ionic conductivity and co-ion transport. At low salinities, the limited availability of charge carriers increases solution and membrane resistance, resulting in higher voltage losses and, consequently, higher SEC. Conversely, at high salinities, although the solution resistance decreases, the stronger electrostatic screening of the bipolar interface and enhanced co-ion migration (Na^+ and Cl^-) reduce water dissociation efficiency and charge selectivity, thereby lowering the current efficiency. Using saline solutions in the acid and base compartments (Figure 4.6b) reduces efficiency and increases energy consumption due to interference from Na^+ and Cl^- ions. These ions impede the selective transport of H^+ and OH^- across the bipolar membrane, thereby reducing the water dissociation rate and current efficiency. Additionally, higher salt concentrations increase the salt-limiting current, thereby increasing the energy required for acid and base production, particularly when saline solutions are used in all compartments.

Overall, the direct acid/base generation mode reached a minimum NaOH SEC of 1.8 kWh/kg and achieved hydroxide current efficiencies of 70–90%. In the closed-loop alkaline configuration, NaOH was produced with similarly low SEC (1.8–2.2 kWh/kg NaOH) but with lower hydroxide current efficiency (typically 60%, up to 85% depending on conditions). Importantly, the closed-loop alkaline process delivers this NaOH production while simultaneously enabling CO_2 capture (CO_2 SEC down to $\leq$3 kWh/kg CO_2 at optimal current density and $\geq$80% DIC removal), whereas the direct mode only benchmarks the electrochemical acid/base generation step. Because the CO_2-capture water stream is decoupled from the high-pH regeneration loop, no upstream softening is required for the CO_2-capture stream, in contrast to conventional in-situ operation, where exposure to high pH drives precipitation. This reduction in upstream conditioning is relevant for scale-up because large-scale ocean-capture assessments often identify water intake/pumping and pretreatment as one of the major contributors to overall energy/cost. Overall, these results indicate that the closed-loop alkaline process preserves near-benchmark NaOH energy efficiency while offering a more integrated and pretreatment-lean pathway for continuous seawater CO_2 capture.

At scale, seawater handling becomes a major constraint, and published techno-economic analyses show that water intake/pumping and pretreatment can account for roughly half of the total energy demand and a major fraction of total costs in ocean-capture systems [150]. The treated seawater from electrochemical ocean capture can be described as being primarily modified by DIC removal (with pH managed by process recombination/neutralization), but recent discussions emphasize that low-DIC and/or high-pH discharge could still impact marine organisms near the outfall, especially

at high removal and low dilution, and that technology-specific environmental evidence remains limited [3, 151]. Therefore, responsible scale-up should proceed through staged pilot deployments that quantify local mixing and carbonate chemistry changes with monitoring and modeling to support permitting and environmental safety.

4.4 Conslusions

A closed-loop alkaline bipolar membrane electrodialysis (BPMED) configuration was successfully demonstrated for continuous CO_2 capture from seawater, achieving stable operation without any performance decay (e.g., voltage drop) or visible deposits on membranes or feed spacers. The CO_2 capture and hydroxide generation rates increased with current density, reaching more than 80 % dissolved inorganic carbon (DIC) removal at 32 mA/cm^2. Optimal energy performance was obtained at 8–12 mA/cm^2, with a minimum SEC of less than 3 kWh/kg CO_2. In this process, NaOH solutions with a concentration of up to 0.1 M and an SEC of less than 2 kWh/kg NaOH were produced.
Increasing flow velocity (1 to 3 cm/s) improved CO_2 capture SEC from 4.5 to 2.9 kWh/kg CO_2, while hydroxide current efficiency remained nearly constant at around 60%. The generated NaOH can be repurposed within the process to soften a portion of the feed stream by precipitating divalent cations and to neutralize the acidified seawater effluent before release to ocean. Feed salinity strongly affected selectivity: higher ionic strength (ca. 100 mS/cm) increased co-ion leakage and SEC, reducing hydroxide current efficiency by up to 25 %. Moderate salinities (50–70 mS/cm) offered the best balance between conductivity and selectivity at the tested current density. Direct acid/base generation from NaCl brine achieved benchmark values of 1.8–2.2 kWh/kg NaOH and up to 90 % current efficiency, which is comparable to the NaOH SEC in the closed loop process and shows the electrochemical consistency of the BPMED process across configurations.
Overall, the closed-loop BPMED operation enables energy-efficient CO_2 capture coupled with stable NaOH regeneration. This approach provides a scalable and sustainable way to capture CO_2 from seawater and utilise resources in a circular way.

4.5 Supporting information

4.5.1 Operational Parameter Evolution during Closed-loop alkaline experiments for CO_2 capture

This section presents supplementary data on the operational parameters of the bipolar membrane electrodialysis (BPMED) system utilized in this study. The Figures 4.7 to 4.9 depict the progression of key variables (including current, voltage, and the pH of the acidic outlet solution) throughout the experimental runs. These parameters are essential for characterizing system behavior under varying test conditions and provide valuable insights into the electrochemical factors that govern performance of the system.

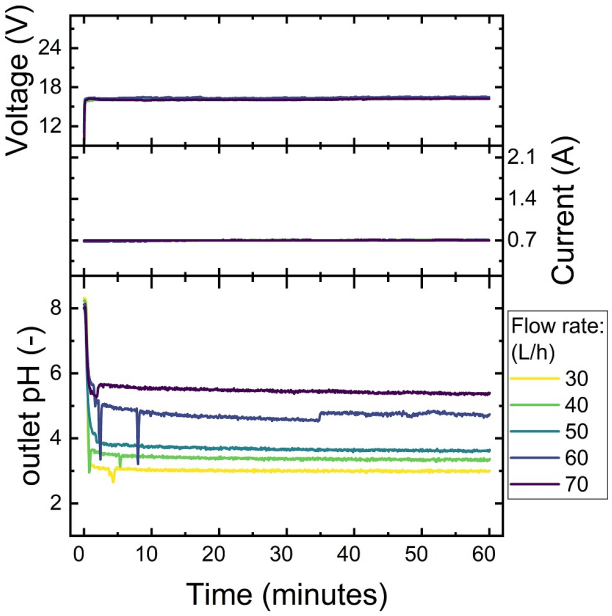

Figure 4.7: Voltage, current and the pH measurements at outlet of the acidic side with various flow rates over time. Model Water, Electrolyte 10 g/L Na_2SO_4.

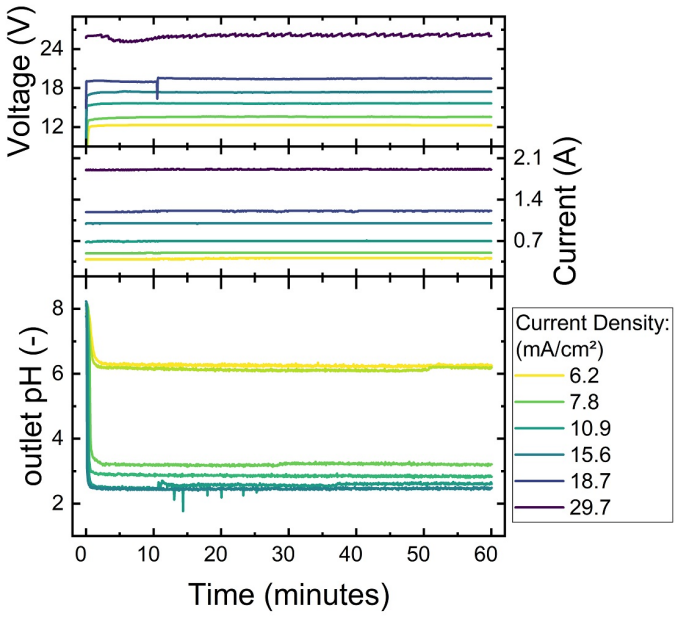

Figure 4.8: Voltage, current and the pH measurements at outlet of the acidic side with different applied current densities over time. Model Water, Electrolyte 10 g/L Na_2SO_4, 50 L/h.

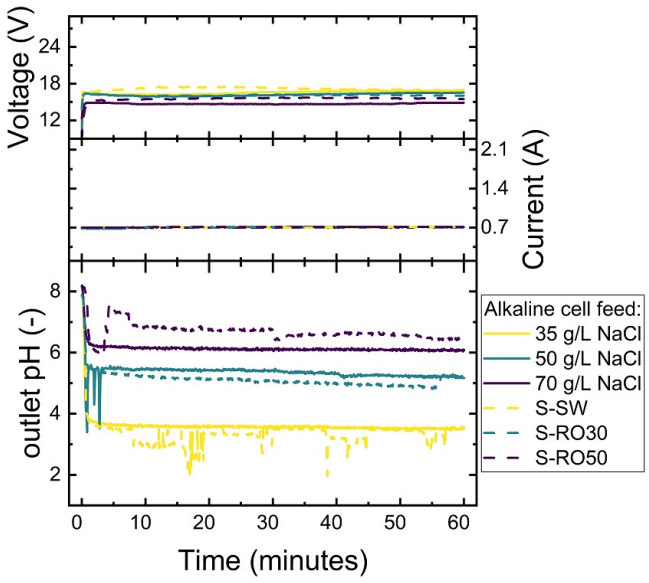

Figure 4.9: Voltage, current and the pH measurements at outlet of the acidic side with different feed solutions in the closed-loop alkaline cell. Electrolyte 10 g/L Na_2SO_4, 50 L/h. (S-SW: softened sea water; S-RO30: softened reverse osmosis brine at 30% recovery; S-RO50: softened reverse osmosis brine at 50% recovery).

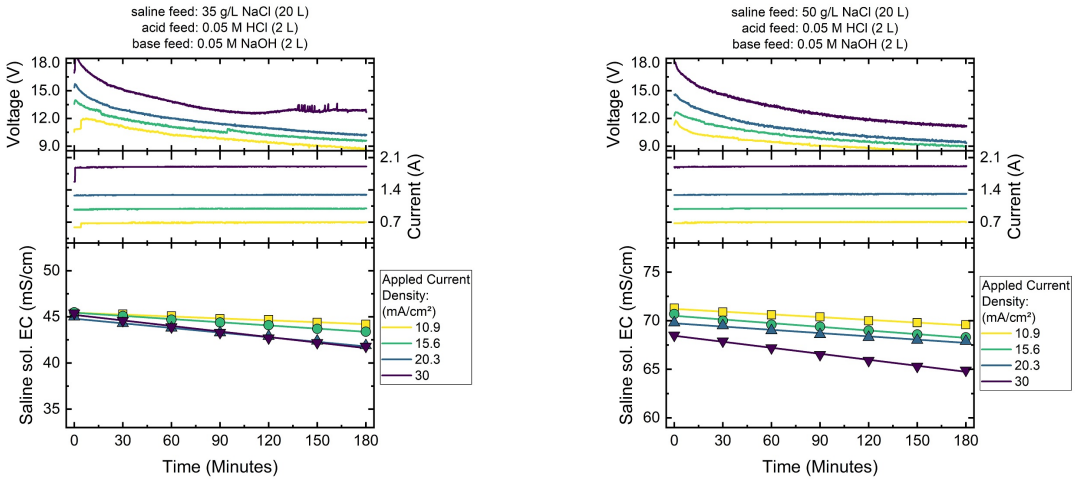

Figure 4.10: Voltage and current of the membrane stack and the electrical conductivity measurements of the saline cell tank during acid and base production experiments. Electrolyte 10 g/L Na_2SO_4, 50 L/h.

4.5.2 Operational Parameter Evolution during direct acid and base production experiments

This section outlines the operational parameters of the BPMED system used for producing acid and base from saline solutions. Figures 4.10 and 4.11 illustrate the evolution of key variables (i.e. current, voltage, and the electrical conductivity of the saline feed) over the course of the experimental runs. Operation at higher current levels (Figure 4.10) was found to enhance the degree of desalination of the saline solution, indicating more intensive ion removal. However, since the system processed a relatively large volume (20 L) of solution, the overall reduction in salinity was not substantial.
The reduction in applied voltage over time is explained by the increase of the electrical conductivity (and the subsequent reduction of membrane stack resistance). The reason for this low conductivity is using demineralized water (with 0.05 M HCl or NaOH) as feed for acid and base solutions. Over time and with production of acid and base (and increase of conductivity), the overall membrane stack resistance is reduced and therefore lower voltages can be applied. It is also seen that when a saline solution of NaCl is used in the acid and base cells (Figure 4.11b), the voltage is started at a lower value, and is more stable during the time of the experiment.

4.5.3 Voltage, current and resistance of the membrane stack

To further illustrate the operational stability differences between the two configurations, Figure 4.12 compares stack voltage, current, and apparent stack resistance during the 60 min run. While both cases operated at similar stack voltages ($\tilde{1}5$V), the in-situ configuration shows a gradual current decay accompanied by a stepwise increase in stack resistance ($\tilde{2}2 \rightarrow 27\ \Omega$). In contrast, the closed-loop alkaline process maintains nearly constant voltage, current and resistance ($\tilde{2}2\ \Omega$) over the same time. Post-run photos (Figure 4.15) confirm this trend: the in-situ membrane/spacer assembly

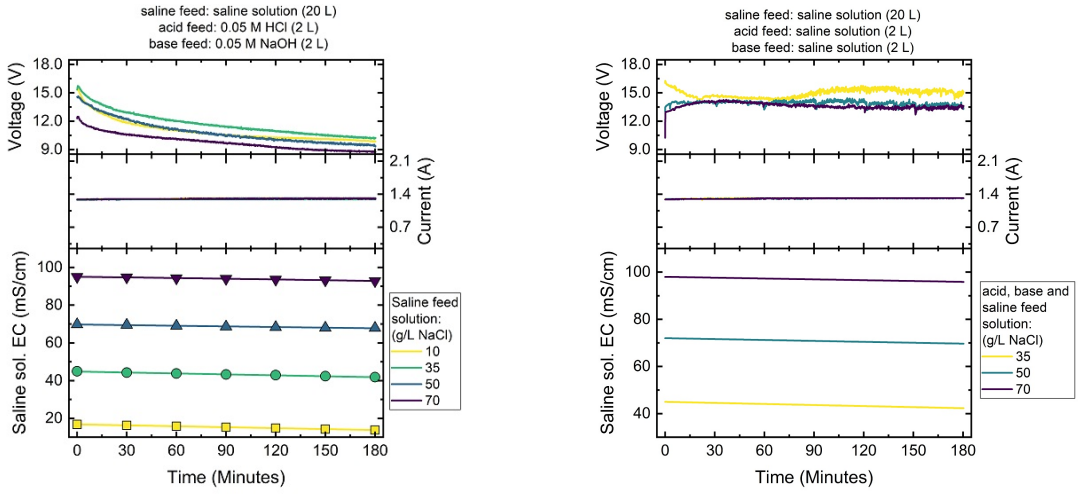

(a) (b)

Figure 4.11: Voltage and current of the membrane stack and the electrical conductivity measurements of the saline cell tank during acid and base production experiments. Electrolyte 10 g/L Na_2SO_4, 50 L/h, current density 20.3 mA/cm^2.

exhibits clearly visible deposits, whereas no visible deposits are in the closed-loop alkaline process. This figure therefore provides complementary evidence to the stable parameter trends reported for the closed-loop alkaline experiments.

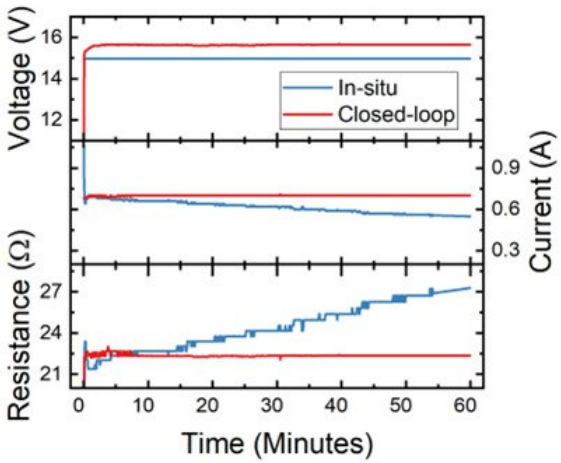

Figure 4.12: Voltage, current and resistance of the membrane stack over time in in-situ and closed-loop alkaline CO_2 capture system. 10 cell pairs, 50 L/h, electrolyte: 10 g/L Na2SO4, In-situ feed: seawater (both acidic and alkaline streams), Closed-loop feed: seawater (acidic stream), softened seawater (alkaline loop).

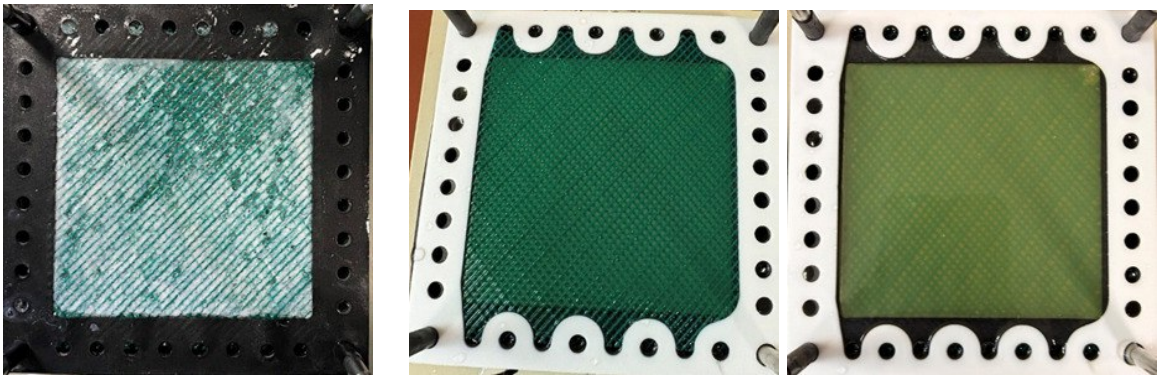

(a) (b) (c)

Figure 4.13: Corresponding post-run photos of the membrane/spacer surfaces (in-situ photo taken from [5].

4.5.4 Application of anti-scalants*

Antiscalants are dosed to suppress/delay precipitation of sparingly soluble salts as concentration (RO) and/or temperature (thermal) increase, reducing scaling-related performance loss and downtime. Since BPMED can be applied to desalination brines/RO concentrate, which may already contain residual antiscalant from upstream pretreatment, we tested whether such formulations remain effective under BPMED's extreme alkaline boundary-layer conditions. Because $Mg(OH)_2$ and mixed carbonate scales remain the dominant limitation for BPMED operation (see Chapter 3). Therefore, a separate, preliminary evaluation of commercial antiscalants that are commonly used in RO and thermal desalination plants was performed. Commercial products fall into three broad classes[152]:

- **Carboxylate-based polymers**, e.g. poly(acrylic acid) (PAA) and poly(maleic acid) (PMA).
- **Phosphorus-based polymers**, e.g. polyphosphates, phosphonates, and phosphate esters.
- **Sulfonate-based polymers**, e.g. poly(sulfonic acid) and poly(ethylene sulfonic acid).

Their proposed working mechanisms include adsorption on active crystal growth sites, distortion of the crystal lattice, chelation of divalent cations, and dispersion of fine precipitates. In practice, all products are used at low concentrations, so their effectiveness is strongly dose-limited. Furthermore, it is not obvious whether these formulations remain stable and effective at the very high pH and local supersaturation conditions present on the basic side of a BPM operating for CO_2 capture. The following tests were therefore designed as a quick check, not as a full optimization study; the results are negative and should be interpreted as such[153, 154]. Moreover, Poly(maleic acid) (PMA), a carboxylate-based polymer showing promise in desalination plants, to mitigate and inhibit $Mg(OH)_2$ precipitation under relevant conditions, was tested as well [155].

Beaker turbidity tests with simulated RO brine Beaker tests were first conducted to evaluate whether the chosen products could suppress bulk precipitation in a high-salinity and pH matrix representative of seawater or RO brine in the alkaline cell of the BPMED. The tested solutions were RO concentrate corresponding to roughly 30 % recovery from North Sea seawater (see Table 4.1). For each test, 500 mL of saline solution were dosed with a given antiscalant at the supplier's

*This section is not part of the submitted manuscript

maximum recommended concentration. NaOH was then added to reach three different alkalinity levels (2.5, 5.0 and 7.5 mmol/L NaOH, corresponding to bulk pH values of approximately 9.9, 10.1 and 10.3, respectively). Turbidity, pH and electrical conductivity were measured over 5 h, and the results were compared to a blank without antiscalant.

The following product antiscalants were tested:

- P-free formulations: PMA, FF-8II, RPI-2800.
- Low-P formulation: FF-5115.
- P-based formulations: FF-2a, RPI-4900 and selected mixtures with PMA.

*FF: Free-Flow products from Dr. Nähring company [156].
*RPI: RPI Antiscalants supplied from Ropur company [157].
*PMA solution prepared from stock solution (50% w/w solution, VWR, Germany), following the recipe from [155], with a concentration of 10 mg/L in solution.

As seen in figure 4.14, the blank solutions exhibited an increase in turbidity at all NaOH doses, reaching several hundred NTU within 2–4 h, consistent with extensive $Mg(OH)_2/CaCO_3$ precipitation. P-free carboxylate polymers only delayed the onset of turbidity and slightly reduced the final turbidity at moderate NaOH dosage; at the highest dose of NaOH they were essentially unable to prevent bulk precipitation. The low-P formulation FF-5115 showed improved delay and lower turbidity at intermediate pH, but again lost effectiveness as the NaOH dose increased.

Phosphorus-based products (FF-2a and especially RPI-4900, alone or combined with PMA) showed the strongest inhibition in the beaker tests. Turbidity was used as a rapid proxy for precipitation; relative to the blank, a longer induction time before turbidity onset and a lower initial turbidity rise indicate delayed nucleation and/or reduced formation of suspended precipitates. At 2.5 and 5 mmol/L NaOH, FF-2a and RPI-4900 both delayed the onset of turbidity and reduced its rise compared to the blank, whereas the other formulations had negligible effect under these conditions. Based on this ranking criterion, RPI-4900 and the RPI-4900+PMA mixture were selected as the most promising candidates for validation in the BPMED system.

This entire screening is still weak from a process point of view: it is short-term, purely bulk turbidity-based and carried out in a well-mixed beaker with homogeneous pH, which is very different from the conditions at the BPM surface. To test the antiscalants, the best performers were used in a BPMED carbon capture process.

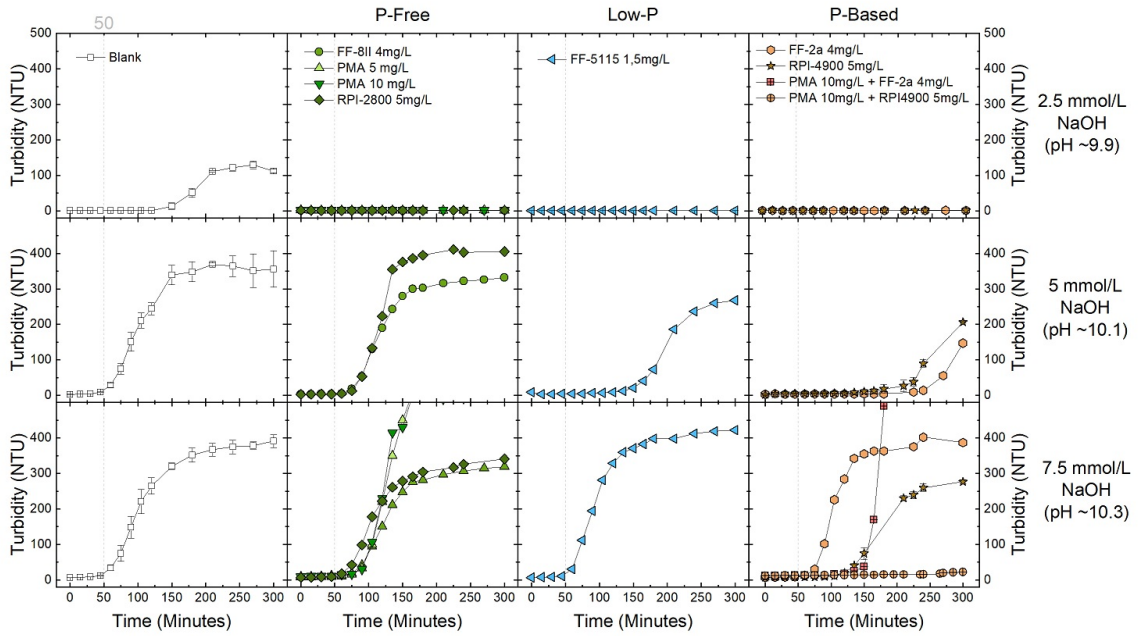

Figure 4.14: Turbidity over time, with different antiscalants added to the simulated RO brine (30% recovery)

Application in the in-situ configuration

The two most promising formulations (RPI-4900 and RPI-4900+PMA) were then tested directly in the BPMED setup following the protocol used in Chapter 2. In these experiments, 60 L of RO brine dosed with the antiscalant (at the supplier's recommended maximum dose) was fed first to the acidic cell. after CO_2 extraction with a membrane contactor, the solution was fed to the alkaline cell. The test was performed at relatively low current densities (6 mA/cm^2) and 50 L/h (corresponding to a velocity of 2 cm/s) and CO_2 capture was performed with 30–50% DIC removal achieved.

Despite the encouraging beaker results, the outcome in the real cell was clearly negative: Severe precipitation was observed on the basic side of the BPM, particularly even at low current densities where local ΔpH are lowest. Visual inspection of the membranes and spacers, as well as OCT images of the membranes, showed thick, heterogeneous deposits that are fully consistent with the $Mg(OH)_2$-dominated scaling characterized in Chapter 3.

Commercial RO antiscalants, despite showing some performance in laboratory bulk tests, proved ineffective at mitigating scaling under the realistic, high-pH conditions of the BPMED process for CO_2 capture. It is assumed that this is due to the high interfacial pH and localized supersaturation on the surface of the bipolar membrane, that are outside the antiscalants design scope, which is optimized for $CaCO_3$ at moderate pH. Consequently, the research on antiscalant use was abandoned, with a focus on the process-level innovations to avoid the scaling problem inside the membrane stack by using products of the process. All data and conclusions in the main part of chapter 4 are therefore based on operation without antiscalants.

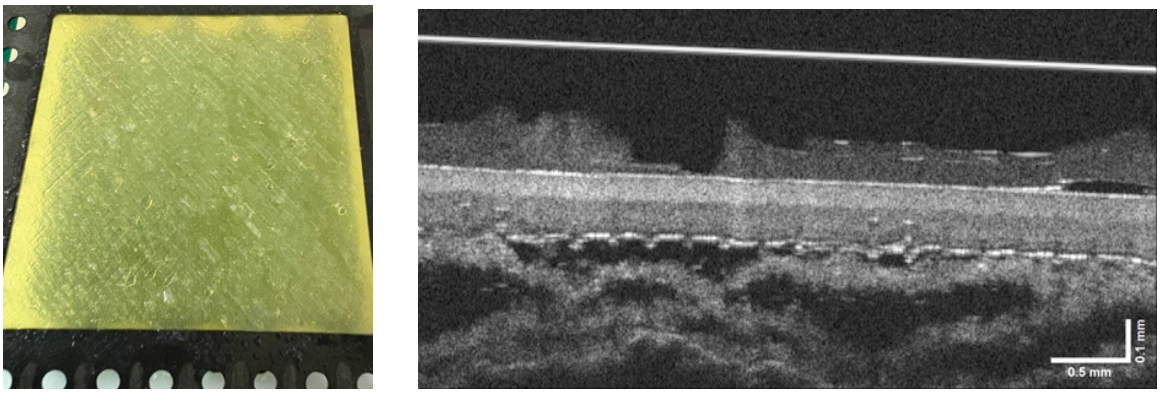

(a) (b)

Figure 4.15: (a) Visible precipitation of salts on the alkaline side of the bipolar membrane, (b) a homogenious scaling layer has been formed with the presence of antiscalant RPI-4900 + PMA.

Chapter 5

Conclusions and Outlook

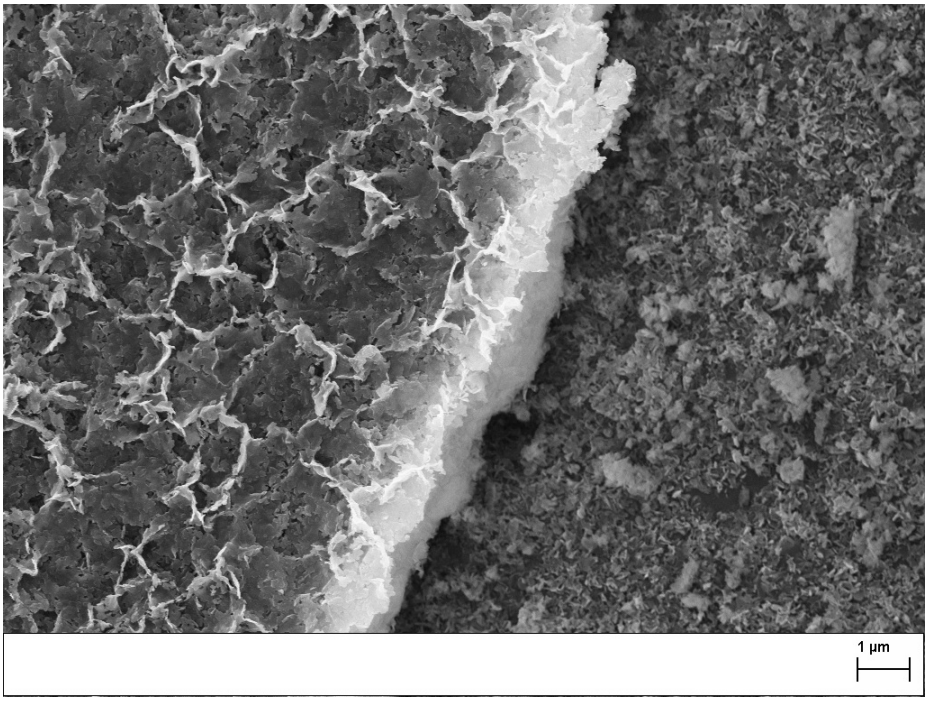

Carbon capture from atmosphere has a **limited, yet vital role** in the race towards the net zero emission targets. In this regard, bipolar membrane electrodialysis (BPMED) promises a fully electrified way for CO_2 capture from seawater and desalination brines through pH-swing. However its practical use has been constrained by high specific energy consumption (SEC) and severe inorganic scaling on the alkaline side of the bipolar membrane (BPM). This thesis addresses these constraints by (i) mapping the operating window of BPMED for CO_2 capture from seawater (DIC $\approx$ 120 mg/L), (ii) elucidating the working mechanisms of inorganic scaling at the alkaline BPM surface using an in-house developed in-situ Optical Coherence Tomography (OCT) flowcell, and (iii) designing and validating a closed-loop alkaline BPMED configuration that couples seawater CO_2 capture with NaOH co-production while avoiding scaling. Across these three components, BPMED is shown to

Image: SEM picture of the scaling layer formed on basic side of the bipolar membrane.

capture CO_2 at specific electrochemical energy consumptions of roughly 1.7–2.8 kWh/kg CO_2 and to produce NaOH at 1.8–2.2 kWh/kg NaOH up to 90% current efficiency, provided that current density, flow velocity, salinity and configuration lie within defined ranges.

5.1 Main Findings

The global aim of the thesis was to investigate how BPMED can be designed and operated to achieve energy-efficient, scalable CO_2 capture from seawater. The results show that this is only possible when electrochemical driving force (6–32 mA/cm^2), hydrodynamics (1–3 cm/s), feed solutions conductivity (5–80 mS/cm) and process architecture (in-situ vs. closed-loop alkaline) are treated as a coupled design space, not optimised independently.

RQ1 quantifies how feed salinity, hydrodynamics (flow rate), current density, and electrolyte composition jointly govern single-pass DIC removal and the specific electrical energy consumption (SEC) of BPMED-based CO_2 capture from seawater (Chapter 2). Across the tested conditions, an intermediate current-density window of ∼7-10 mA/cm^2 minimized SEC, reaching ≈2.3 kWh/kg CO_2 for seawater and as low as 1.7 kWh/kg CO_2 with redox-free electrolyte, while achieving ∼60% single-pass DIC removal. Increasing overall DIC conversion (e.g., by enhancing downstream gas–liquid transfer such as additional membrane-contactor area) can increase the captured CO_2 and lower SEC per kg CO_2 on an electrical basis, although any auxiliary energy demand must be accounted for at the system level. Increasing the linear velocity from 1 to 3 cm/s reduced SEC from ∼3.7 to ∼2.5 kWh/kg CO_2, but decreased single-pass DIC removal from ∼65% to ∼40%, highlighting a clear trade-off between capture fraction and energy intensity.

To answer **RQ2** (Chapter 3) and elucidate inorganic scaling on the alkaline side of bipolar membranes, we developed a dedicated flow cell that enables real-time observation through an optical window combined with OCT. This setup provides in-situ, spatially resolved information on when and where deposits form during operation. Across seawater-like conditions, scaling was dominated by $Mg(OH)_2$ and formed heterogeneously: deposits preferentially nucleated and grew in low-shear regions between spacer filaments. At current densities above 10 mA/cm^2 and a linear velocity of 1 cm/s, the mean deposit thickness increased rapidly to the order of tens of micrometres and the membrane area coverage reached ≥60%; in contrast, at lower current densities and 3 cm/s only thin, patchy layers developed. Importantly, increasing DIC within the seawater range mitigated scaling by buffering the local pH rise, whereas complete DIC removal intensified scaling even in the absence of carbonate species. Overall, the results show that spacer-induced hydrodynamics and DIC buffering jointly control the spatial structure and severity of $Mg(OH)_2$ scaling, which cannot be inferred reliably from bulk voltage trends or feed composition alone.

To answer **RQ3** (Chapter 4), we evaluated a closed-loop alkaline BPMED configuration integrated with a membrane contactor to enable simultaneous CO_2 capture from seawater and NaOH co-production while limiting scaling. In the tested process, a softened solution is recirculated in the alkaline loop while a fraction of the produced NaOH can be used externally to precipitate Mg^{2+} and Ca^{2+}, thereby regenerating a fresh, softened alkaline feed for recirculation; in addition, the alkaline product stream can be applied for neutralization of the acidified, CO_2-depleted seawater prior to discharge. Under current densities of 8–12 mA/cm^2 and alkaline-loop conductivities of 35–70 mS/cm, the system achieved up to 80% DIC removal at an SEC of ≈2.8 kWh/kg CO_2, while producing NaOH up to ≈0.1 mol/L with an SEC of ≈1.8 kWh/kg NaOH and a current efficiency of ≈70% within 1

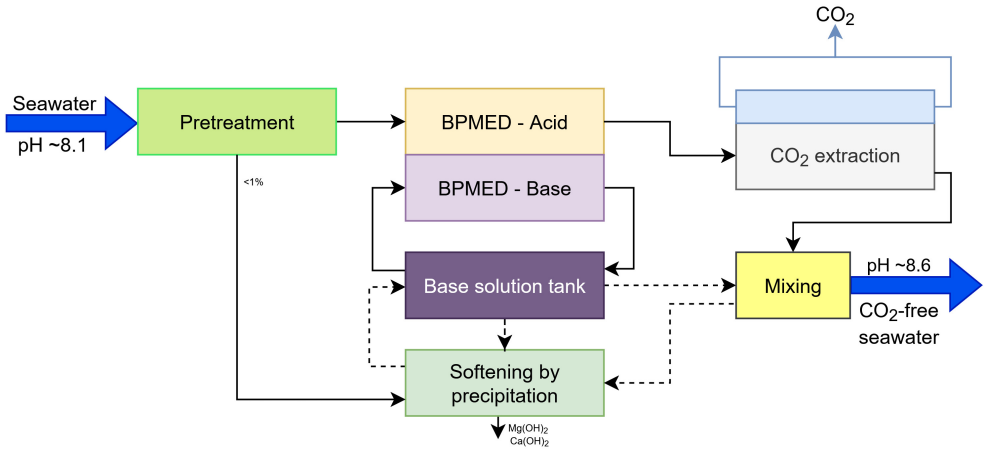

Figure 5.1: schematic diagram of the proposed CO_2 capture system

h. Over the investigated operation time and over the course of the experiments, no visible scaling was observed in the closed-loop stack, in contrast to in-situ operation under comparable currents and flows (Chapters 2–3), indicating that decoupling the pH swing from direct BPM exposure to divalent cations effectively mitigates the dominant scaling constraint of conventional in-situ concepts. To benchmark NaOH production performance, additional acid/base operation tests (used for ex-situ CO_2 capture configuration) with NaCl and softened reverse-osmosis brine reached NaOH current efficiencies approaching ∼75% at an SEC of ∼1.8 kWh/kg NaOH, comparable to the closed-loop case, while enabling higher NaOH concentrations (up to 0.5 mol/L after 3 h). In principle, it has been shown that the performance of BPMED for ocean-based CO_2 capture is governed by a narrow but controllable electrochemical window. By identifying an energy-optimal regime of around 7–10 mA/cm^2 and quantifying the trade-off between SEC and CO_2 capture as the flow rate increases, the operating windows of previous proof-of-concept BPMED studies can be defined quantitatively. Mechanistically, OCT imaging and SEM-EDX analysis shows that $Mg(OH)_2$-dominated scaling is locally structured by spacer-induced hydrodynamics and that DIC acts as a strong buffer that can be used to control scaling (precise pH-control); the common recommendation to remove carbonate is therefore incomplete without considering its role in buffering and pH shifts. Moreover, the work showed that a hybrid configuration, in which in-situ BPMED operation (direct seawater feed to the stack for CO_2 capture) is combined with an ex-situ configuration (softening a smaller side stream of seawater to produce NaOH), can exploit the respective strengths of both process concepts (see Figure 5.1).

5.2 Limitations and Future Directions

The conclusions from this thesis are bounded by: (i) lab- and pilot-scale cells and stacks (membrane areas of maximum 100 cm^2 with $\leq$ 10 cell pairs) operated over one to three hours; (ii) model seawater and synthetic RO brines with controlled inorganic composition and negligible organic or biological fouling; (iii) current densities mostly in the range 6–32 mA/cm^2, velocities 1–3 cm/s; (iv) structural but not mineral-specific OCT diagnostics; and (v) the absence of a full techno-economic, life-cycle

and environmental assessments. On this basis, the most relevant next steps are:

- Scale-up to stacks with $\gg 10$ cell pairs and higher throughputs, validating the identified operation window (7–12 mA/cm^2, 2–3 cm/s) and monitoring current distribution, voltage drop and pressure drop over time.
- Development and calibration of multiphysics models coupling ion transport, water transport and water dissociation, and precipitation kinetics, validated against SEC/current-efficiency data and OCT-derived scaling from this work.
- Dedicated investigation on bipolar membrane design and interfaces is required to further lower the voltage (overpotential) associated with the water dissociation reaction and thereby reduce the overall energy demand of the BPMED process.
- Long-duration tests ($\gg 10^2$ h) in real seawater and plant brines, including organic and biological fouling, combined with techno-economic assessments of closed-loop alkaline BPMED integrated into operational desalination plants.
- Quantitative assessment of the environmental impact and carbon-removal efficacy of oceanic CO_2 capture methods, including (i) monitoring the chemistry of the discharged (alkalinised and/or decarbonised) seawater in the receiving environment (pH, alkalinity, DIC, major ions) and (ii) continuous, high-resolution measurements of air–sea CO_2 fluxes to rigorously verify that the modified seawater column re-equilibrates with the atmosphere and takes up CO_2 at rates consistent with modelled removal claims.

Bibliography

[1] Net Zero by 2050 – Analysis, May 2021.

[2] NASA Salinity, .

[3] R. A Marquez, A. C Nielander, J Resasco, T. F Jaramillo, and C. B Mullins. Electrochemical Ocean-Based Carbon Capture: Roadblocks to Scale-Up. *ACS Energy Letters*, January 2026. doi: 10.1021/acsenergylett.5c04249. Publisher: American Chemical Society.

[4] International Energy Agency. *Direct Air Capture: A key technology for net zero*. OECD, April 2022. doi: 10.1787/bbd20707-en.

[5] M Aliaskari, J Wezstein, F Saravia, and H Horn. A systematic analysis of operating parameters for CO_2 capture from seawater by Bipolar Membrane Electrodialysis (BPMED). *Separation and purification technology*, page 126679, 2024. doi: 10.1016/j.seppur.2024.126679.

[6] R Sharifian, L Boer, R. M Wagterveld, and D. A Vermaas. Oceanic carbon capture through electrochemically induced in situ carbonate mineralization using bipolar membrane. *Chemical Engineering Journal*, page 135326, 2022. doi: 10.1016/j.cej.2022.135326.

[7] G Shirah. NASA Scientific Visualization Studio | Ocean Surface CO_2 Flux with Surface Winds, November 2020.

[8] Paris Agreement, 2015.

[9] World Energy Outlook 2024 – Analysis. Technical report, IEA, October 2024.

[10] P Friedlingstein, M O'Sullivan, M. W Jones, R. M Andrew, J Hauck, P Landschützer, C Le Quéré, H Li, I. T Luijkx, A Olsen, G. P Peters, W Peters, J Pongratz, C Schwingshackl, S Sitch, J. G Canadell, P Ciais, R. B Jackson, S. R Alin, A Arneth, V Arora, N. R Bates, M Becker, N Bellouin, C. F Berghoff, H. C Bittig, L Bopp, P Cadule, K Campbell, M. A Chamberlain, N Chandra, F Chevallier, L. P Chini, T Colligan, J Decayeux, L. M Djeutchouang, X Dou, C Duran Rojas, K Enyo, W Evans, A. R Fay, R. A Feely, D. J Ford, A Foster, T Gasser, M Gehlen, T Gkritzalis, G Grassi, L Gregor, N Gruber, Gürses, I Harris, M Hefner, J Heinke, G. C Hurtt, Y Iida, T Ilyina, A. R Jacobson, A. K Jain, T Jarníková, A Jersild, F Jiang, Z Jin, E Kato, R. F Keeling, K Klein Goldewijk, J Knauer, J. I Korsbakken, X Lan, S. K Lauvset, N Lefèvre, Z Liu, J Liu, L Ma, S Maksyutov, G Marland, N Mayot, P. C McGuire, N Metzl, N. M Monacci, E. J Morgan, S.-I Nakaoka, C Neill, Y Niwa, T Nützel, L Olivier, T Ono, P. I Palmer, D Pierrot, Z Qin, L Resplandy, A Roobaert, T. M

Rosan, C Rödenbeck, J Schwinger, T. L Smallman, S. M Smith, R Sospedra-Alfonso, T Steinhoff, Q Sun, A. J Sutton, R Séférian, S Takao, H Tatebe, H Tian, B Tilbrook, O Torres, E Tourigny, H Tsujino, F Tubiello, G van der Werf, R Wanninkhof, X Wang, D Yang, X Yang, Z Yu, W Yuan, X Yue, S Zaehle, N Zeng, and J Zeng. Global Carbon Budget 2024. *Earth System Science Data*, 17(3):965–1039, March 2025. doi: 10.5194/essd-17-965-2025.

[11] N. R Bates, Y. M Astor, M. J Church, K Currie, J. E Dore, M González-Dávila, L Lorenzoni, F Muller-Karger, J Olafsson, and J. M Santana-Casiano. A Time-Series View of Changing Surface Ocean Chemistry Due to Ocean Uptake of Anthropogenic CO and Ocean Acidification. *Oceanography*, 27(1):126–141, 2014. doi: 10.5670/oceanog.2014.16.

[12] M. D Eisaman, J. L Rivest, S. D Karnitz, C.-F de Lannoy, A Jose, R. W DeVaul, and K Hannun. Indirect ocean capture of atmospheric CO_2: Part II. Understanding the cost of negative emissions. *International Journal of Greenhouse Gas Control*, 70:254–261, 2018. doi: 10.1016/j.ijggc.2018.02.020.

[13] C.-F de Lannoy, M. D Eisaman, A Jose, S. D Karnitz, R. W DeVaul, K Hannun, and J. L Rivest. Indirect ocean capture of atmospheric CO_2: Part I. Prototype of a negative emissions technology. *International Journal of Greenhouse Gas Control*, 70:243–253, 2018. doi: 10.1016/j.ijggc.2017.10.007.

[14] M. D Eisaman, S Geilert, P Renforth, L Bastianini, J Campbell, A. W Dale, S Foteinis, P Grasse, O Hawrot, and C. R Löscher. Assessing the technical aspects of ocean-alkalinity-enhancement approaches. *State Planet: SP*, 2(Chapter 3):1–29, 2023. doi: 10.5194/sp-2-oae2023-3-2023.

[15] R Sharifian, R. M Wagterveld, I. A Digdaya, C Xiang, and D. A Vermaas. Electrochemical carbon dioxide capture to close the carbon cycle. *Energy & Environmental Science*, 14(2):781–814, 2021. doi: 10.1039/d0ee03382k.

[16] T Liu, Y Wang, Y Wu, W Jiang, Y Deng, Q Li, C Lan, Z Zhao, L Zhu, D Yang, T Noël, and H Xie. Continuous decoupled redox electrochemical CO_2 capture. *Nature Communications*, 15(1):10920, December 2024. doi: 10.1038/s41467-024-55334-3.

[17] S Kim, M. P Nitzsche, S. B Rufer, J. R Lake, K. K Varanasi, and T. A Hatton. Asymmetric chloride-mediated electrochemical process for CO_2 removal from oceanwater. *Energy & Environmental Science*, 16(5):2030–2044, 2023. doi: 10.1039/D2EE03804H.

[18] M. D Eisaman, L Alvarado, D Larner, P Wang, and K. A Littau. CO_2 desorption using high-pressure bipolar membrane electrodialysis. *Energy & Environmental Science*, 4(10):4031–4037, 2011. doi: 10.1039/C1EE01336J.

[19] I. A Digdaya, I Sullivan, M Lin, L Han, W.-H Cheng, H. A Atwater, and C Xiang. A direct coupled electrochemical system for capture and conversion of CO_2 from oceanwater. *Nature communications*, 11(1):1–10, 2020. doi: 10.1038/s41467-020-18232-y.

[20] S Voskian and T. A Hatton. Faradaic electro-swing reactive adsorption for CO_2 capture. *Energy & Environmental Science*, 12(12):3530–3547, December 2019. doi: 10.1039/C9EE02412C.

[21] M Abdinejad, M Massen-Hane, H Seo, and T. A Hatton. Oxygen-Stable Electrochemical CO_2 Capture using Redox-Active Heterocyclic Benzodithiophene Quinone. *Angewandte Chemie (International Ed. in English)*, 63(52):e202412229, December 2024. doi: 10.1002/anie.202412229.

[22] J Fortunato, Y. K Shin, M. A Spencer, A. C. T van Duin, and V Augustyn. Choice of Electrolyte Impacts the Selectivity of Proton-Coupled Electrochemical Reactions on Hydrogen Titanate. *The Journal of Physical Chemistry C*, 127(25):11810–11821, June 2023. doi: 10.1021/acs.jpcc.3c01057.

[23] M. H Youn, K. T Park, Y. H Lee, S.-P Kang, S. M Lee, S. S Kim, Y. E Kim, Y. N Ko, S. K Jeong, and W Lee. Carbon dioxide sequestration process for the cement industry. *Journal of CO_2 Utilization*, 34:325–334, 2019. doi: 10.1016/j.jcou.2019.07.023.

[24] Pau Farràs, Peter Strasser, and Alexander J. Cowan. Water electrolysis: Direct from the sea or not to be? *Joule*, 5(8):1921–1923, August 2021. doi: 10.1016/j.joule.2021.07.014.

[25] H Strathmann. Electrodialysis, a mature technology with a multitude of new applications. *Desalination*, 264(3):268–288, 2010. doi: 10.1016/j.desal.2010.04.069.

[26] M Rahimi, A Khurram, T. A Hatton, and B Gallant. Electrochemical carbon capture processes for mitigation of CO 2 emissions. *Chemical Society Reviews*, 2022. doi: 10.1039/D2CS00443G.

[27] L Legrand, O Schaetzle, R. C. F de Kler, and H. V. M Hamelers. Solvent-Free CO_2 Capture Using Membrane Capacitive Deionization. *Environmental Science & Technology*, 52(16):9478–9485, August 2018. doi: 10.1021/acs.est.8b00980.

[28] E Yeo, H Shin, T Kim, S Kim, and J. S Kang. Electrochemically driven capacitive CO_2 capture technologies. *Journal of Environmental Chemical Engineering*, 13(2):116092, April 2025. doi: 10.1016/j.jece.2025.116092.

[29] A Hassan, M Afshari, and M Rahimi. A Membraneless Electrochemically Mediated Amine Regeneration for Carbon Capture. *Nature Communications*, 16(1):6333, July 2025. doi: 10.1038/s41467-025-61525-3.

[30] *A Research Strategy for Ocean-based Carbon Dioxide Removal and Sequestration*. National Academies Press, Washington, D.C., April 2022. doi: 10.17226/26278.

[31] Direct Ocean Capture and Storage v1.0 — Isometric, .

[32] R Pärnamäe, S Mareev, V Nikonenko, S Melnikov, N Sheldeshov, V Zabolotskii, H. V. M Hamelers, and M Tedesco. Bipolar membranes: A review on principles, latest developments, and applications. *Journal of Membrane Science*, 617:118538, 2021. doi: 10.1016/j.memsci.2020.118538.

[33] R Sharifian, H. C Van der Wal, M Wagterveld, and D. A Vermaas. Fouling Management in Oceanic Carbon Capture Via In-Situ Electrochemical Bipolar Membrane Electrodialysis. *Chemical Engineering Journal*, 2022. doi: 10.1016/j.cej.2023.141407.

[34] F Sabatino, M Mehta, A Grimm, M Gazzani, F Gallucci, G. J Kramer, and M van Sint Annaland. Evaluation of a direct air capture process combining wet scrubbing and bipolar membrane electrodialysis. *Industrial & Engineering Chemistry Research*, 59(15):7007–7020, 2020.

[35] F Sabatino, M Gazzani, F Gallucci, and M van Sint Annaland. Modeling, Optimization, and Techno-Economic Analysis of Bipolar Membrane Electrodialysis for Direct Air Capture Processes. *Industrial & Engineering Chemistry Research*, 61(34):12668–12679, 2022. doi: 10.1021/acs.iecr.2c00889.

[36] S. Z Oener, M. J Foster, and S. W Boettcher. Accelerating water dissociation in bipolar membranes and for electrocatalysis. *Science*, 369(6507):1099–1103, August 2020. doi: 10.1126/science.aaz1487.

[37] Lucas, J Bui, M Hwang, K Wang, A Bell, A Weber, S Ardo, H Atwater, and C Xiang. Asymmetric Bipolar Membrane for High Current Density Electrodialysis Operation with Exceptional Stability. 2023. doi: 10.26434/chemrxiv-2023-n4c6x.

[38] R Klaassen, P Feron, and A Jansen. Membrane contactor applications. *Desalination*, 224 (1-3):81–87, 2008. doi: 10.1016/j.desal.2007.02.083.

[39] C Hepburn, E Adlen, J Beddington, E. A Carter, S Fuss, N Mac Dowell, J. C Minx, P Smith, and C. K Williams. The technological and economic prospects for CO_2 utilization and removal. *Nature*, 575(7781):87–97, November 2019. doi: 10.1038/s41586-019-1681-6.

[40] M Hofmann and H. J Schellnhuber. Ocean acidification: a millennial challenge. *Energy & Environmental Science*, 3(12):1883–1896, 2010. doi: 10.1039/C000820F.

[41] M Meinshausen, J Lewis, C McGlade, J Gütschow, Z Nicholls, R Burdon, L Cozzi, and B Hackmann. Realization of Paris Agreement pledges may limit warming just below 2 C. *Nature*, 604(7905):304–309, 2022.

[42] S. E Tanzer and A Ramírez. When are negative emissions negative emissions? *Energy & Environmental Science*, 12(4):1210–1218, 2019. doi: 10.1039/C8EE03338B.

[43] L Chen, G Msigwa, M Yang, A. I Osman, S Fawzy, D. W Rooney, and P.-S Yap. Strategies to achieve a carbon neutral society: a review. *Environmental Chemistry Letters*, 20(4):2277–2310, 2022. doi: 10.1007/s10311-022-01435-8.

[44] N Thonemann and M Pizzol. Consequential life cycle assessment of carbon capture and utilization technologies within the chemical industry. *Energy & Environmental Science*, 12(7): 2253–2263, 2019. doi: 10.1039/C9EE00914K.

[45] J Artz, T. E Müller, K Thenert, J Kleinekorte, R Meys, A Sternberg, A Bardow, and W Leitner. Sustainable conversion of carbon dioxide: an integrated review of catalysis and life cycle assessment. *Chemical reviews*, 118(2):434–504, 2018. doi: 10.1021/acs.chemrev.7b00435.

[46] D. W Keith, G Holmes, D. S Angelo, and K Heidel. A process for capturing CO_2 from the atmosphere. *Joule*, 2(8):1573–1594, 2018. doi: 10.1016/j.joule.2018.05.006.

[47] O Gutierrez-Sanchez, B De Mot, N Daems, M Bulut, J Vaes, D Pant, and T Breugelmans. Electrochemical Conversion of CO_2 from Direct Air Capture Solutions. *Energy & fuels*, 36 (21):13115–13123, 2022. doi: 10.1021/acs.energyfuels.2c02623.

[48] X Shi, H Xiao, H Azarabadi, J Song, X Wu, X Chen, and K. S Lackner. Sorbents for the direct capture of CO_2 from ambient air. *Angewandte Chemie International Edition*, 59(18): 6984–7006, 2020. doi: 10.1002/anie.201906756.

[49] H. D Willauer, F DiMascio, D. R Hardy, M. K Lewis, and F. W Williams. Development of an electrochemical acidification cell for the recovery of CO_2 and H_2 from seawater. *Industrial & Engineering Chemistry Research*, 50(17):9876–9882, 2011. doi: 10.1021/ie2008136.

[50] P Aleta, A Refaie, M Afshari, A Hassan, and M. M Rahimi. Direct Ocean Capture: The Emergence of Electrochemical Processes for Oceanic Carbon Removal. *Energy & Environmental Science*, 2023. doi: 10.1039/d3ee01471a.

[51] R Chauvy and L Dubois. Life cycle and techno-economic assessments of direct air capture processes: An integrated review. *International Journal of Energy Research*, 46(8):10320–10344, 2022. doi: 10.1002/er.7884.

[52] O Gutiérrez-Sánchez, B Bohlen, N Daems, M Bulut, D Pant, and T Breugelmans. A State-of-the-Art Update on Integrated CO_2 Capture and Electrochemical Conversion Systems. *ChemElectroChem*, 9(5):e202101540, 2022. doi: 10.1002/celc.202101540.

[53] X Wu, R Krishnamoorti, and P Bollini. Technological options for direct air capture: a comparative process engineering review. *Annual Review of Chemical and Biomolecular Engineering*, 13:279–300, 2022. doi: 10.1146/annurev-chembioeng-102121-065047.

[54] M Erans, E. S Sanz-Pérez, D. P Hanak, Z Clulow, D. M Reiner, and G. A Mutch. Direct air capture: process technology, techno-economic and socio-political challenges. *Energy & Environmental Science*, 15(4):1360–1405, 2022. doi: 10.1039/D1EE03523A.

[55] R. E Zeebe and D Wolf-Gladrow. *CO_2 in seawater: equilibrium, kinetics, isotopes*. Number 65. Gulf Professional Publishing, 2001.

[56] H. D Willauer, D. R Hardy, M. K Lewis, E. C Ndubizu, and F. W Williams. Extraction of CO_2 from seawater and aqueous bicarbonate systems by ion-exchange resin processes. *Energy & fuels*, 24(12):6682–6688, 2010. doi: 10.1021/ef101212e.

[57] M. D Eisaman, K Parajuly, A Tuganov, C Eldershaw, N Chang, and K. A Littau. CO_2 extraction from seawater using bipolar membrane electrodialysis. *Energy & Environmental Science*, 5(6):7346–7352, 2012. doi: 10.1039/c2ee03393c.

[58] K Lackner, H.-J Ziock, and P Grimes. Carbon dioxide extraction from air: is it an option? Technical report, Los Alamos National Lab.(LANL), Los Alamos, NM (United States), 1999.

[59] N McQueen, K. V Gomes, C McCormick, K Blumanthal, M Pisciotta, and J Wilcox. A review of direct air capture (DAC): scaling up commercial technologies and innovating for the future. *Progress in Energy*, 3(3):032001, 2021. doi: 10.1088/2516-1083/abf1ce.

[60] R Custelcean. Direct air capture of CO_2 using solvents. *Annual Review of Chemical and Biomolecular Engineering*, 13:217–234, 2022. doi: 10.1146/annurev-chembioeng-092120-023936.

[61] A Sodiq, Y Abdullatif, B Aissa, A Ostovar, N Nassar, M El-Naas, and A Amhamed. A review on progress made in direct air capture of CO_2. *Environmental Technology & Innovation*, page 102991, 2022. doi: 10.1016/j.eti.2022.102991.

[62] C Beuttler, L Charles, and J Wurzbacher. The role of direct air capture in mitigation of anthropogenic greenhouse gas emissions. *Frontiers in Climate*, 1:10, 2019. doi: 10.3389/fclim.2019.00010.

[63] A Muroyama, A Patru, and L Gubler. CO_2 separation and transport via electrochemical methods. *Journal of the Electrochemical Society*, 2020. doi: 10.1149/1945-7111/abbbb9.

[64] B. D Patterson, F Mo, A Borgschulte, M Hillestad, F Joos, T Kristiansen, S Sunde, and J. A Van Bokhoven. Renewable CO_2 recycling and synthetic fuel production in a marine environment. *Proceedings of the National Academy of Sciences*, 116(25):12212–12219, 2019. doi: 10.1073/pnas.1902335116.

[65] S Chatterjee and K.-W Huang. Unrealistic energy and materials requirement for direct air capture in deep mitigation pathways. *Nature communications*, 11(1):3287, 2020. doi: 10.1038/s41467-020-17203-7.

[66] S. C Doney, V. J Fabry, R. A Feely, and J. A Kleypas. Ocean acidification: the other CO_2 problem. *Annual review of marine science*, 1:169–192, 2009. doi: 10.1146/annurev.marine.010908.163834.

[67] R Weiss. Carbon dioxide in water and seawater: the solubility of a non-ideal gas. *Marine chemistry*, 2(3):203–215, 1974. doi: 10.1016/0304-4203(74)90015-2.

[68] A Oschlies, L Bach, R Rickaby, T Satterfield, R. M Webb, and J.-P Gattuso. Climate targets, carbon dioxide removal and the potential role of Ocean Alkalinity Enhancement. *State of the Planet Discussions*, 2023:1–11, 2023. doi: 10.5194/sp-2-oae2023-1-2023.

[69] S Datta, M. P Henry, Y. J Lin, A. T Fracaro, C. S Millard, S. W Snyder, R. L Stiles, J Shah, J Yuan, and L Wesoloski. Electrochemical CO_2 capture using resin-wafer electrodeionization. *Industrial & Engineering Chemistry Research*, 52(43):15177–15186, 2013. doi: 10.1021/ie402538d.

[70] Y Pocker and D. W Bjorkquist. Stopped-flow studies of carbon dioxide hydration and bicarbonate dehydration in water and water-d2. Acid-base and metal ion catalysis. *Journal of the American Chemical Society*, 99(20):6537–6543, 1977. doi: 10.1021/ja00462a012.

[71] T León, J López, R Torres, J Grau, L Jofre, and J.-L Cortina. Describing ion transport and water splitting in an electrodialysis stack with bipolar membranes by a 2-D model: Experimental validation. *Journal of Membrane Science*, 660:120835, 2022. doi: 10.1016/j.memsci.2022.120835.

[72] J Xu, G Zhong, M Li, D Zhao, Y Sun, X Hu, J Sun, X Li, W Zhu, and M Li. Review on electrochemical carbon dioxide capture and transformation with bipolar membranes. *Chinese Chemical Letters*, 34(8):108075, 2023. doi: 10.1016/j.cclet.2022.108075.

[73] H Strathmann, J. J Krol, H.-J Rapp, and G Eigenberger. Limiting current density and water dissociation in bipolar membranes. *Journal of Membrane Science*, 125(1):123–142, 1997. doi: 10.1016/S0376-7388(96)00185-8.

[74] A Bandi, M Specht, T Weimer, and K Schaber. CO_2 recycling for hydrogen storage and transportation—electrochemical CO_2 removal and fixation. *Energy Conversion and Management*, 36(6-9):899–902, 1995. doi: 10.1016/0196-8904(95)00148-7.

[75] A Iizuka, K Hashimoto, H Nagasawa, K Kumagai, Y Yanagisawa, and A Yamasaki. Carbon dioxide recovery from carbonate solutions using bipolar membrane electrodialysis. *Separation and purification technology*, 101:49–59, 2012. doi: 10.1016/j.seppur.2012.09.016.

[76] H Nagasawa, A Yamasaki, A Iizuka, K Kumagai, and Y Yanagisawa. A new recovery process of carbon dioxide from alkaline carbonate solution via electrodialysis. *AIChE journal*, 55(12): 3286–3293, 2009. doi: 10.1002/aic.11907.

[77] I Taniguchi, D Ioh, S Fujikawa, T Watanabe, Y Matsukuma, and M Minemoto. An alternative carbon dioxide capture by electrochemical method. *Chemistry Letters*, 43(10):1601–1603, 2014. doi: 10.1246/cl.140508.

[78] T Chen, Y Zhao, Y Zhao, Y Xie, Z Ji, X Guo, Y Zhao, and J Yuan. Competitive Ion Migration and Process Optimization of Carbon Sequestration and Seawater Decalcification in a Bipolar Electrodialysis Process. *ACS Sustainable Chemistry & Engineering*, 2021. doi: 10.1021/acssuschemeng.0c09232.

[79] Y Zhao, J Wang, Z Ji, J Liu, X Guo, and J Yuan. A novel technology of carbon dioxide adsorption and mineralization via seawater decalcification by bipolar membrane electrodialysis system with a crystallizer. *Chemical Engineering Journal*, 381:122542, 2020.

[80] J Bui, E Lucas, E. W Lees, A. K Liu, H. A Atwater Jr, C Xiang, A. T Bell, and A. Z Weber. Analysis of bipolar membranes for electrochemical CO_2 capture from air and oceanwater. *Energy & Environmental Science*, 2023. doi: 10.1039/d3ee01606d.

[81] D. A Vermaas, S Wiegman, T Nagaki, and W. A Smith. Ion transport mechanisms in bipolar membranes for (photo) electrochemical water splitting. *Sustainable Energy & Fuels*, 2(9): 2006–2015, 2018. doi: 10.1039/c8se00118a.

[82] R Sharifian, M. A Blommaert, M Bremer, R. M Wagterveld, and D. A Vermaas. Intrinsic bipolar membrane characteristics dominate the effects of flow orientation and external pH-profile on the membrane voltage. *Journal of Membrane Science*, 638:119686, 2021. doi: 10.1016/j.memsci.2021.119686.

[83] Y Zhao, L Wang, Z Ji, J Liu, X Guo, F Li, S Wang, and J Yuan. Collaborative disposal of problematic calcium ions in seawater and carbon and sulfur pollutants in flue gas by bipolar membrane electrodialysis. *Desalination*, 494:114654, 2020. doi: 10.1016/j.desal.2020.114654.

[84] H. D Willauer, F DiMascio, D. R Hardy, and F. W Williams. Feasibility of CO_2 extraction from seawater and simultaneous hydrogen gas generation using a novel and robust electrolytic cation exchange module based on continuous electrodeionization technology. *Industrial & Engineering Chemistry Research*, 53(31):12192–12200, 2014. doi: 10.1021/ie502128x.

[85] F Maletzki, H.-W Rösler, and E Staude. Ion transfer across electrodialysis membranes in the overlimiting current range: stationary voltage current characteristics and current noise power spectra under different conditions of free convection. *Journal of Membrane Science*, 71(1-2): 105–116, 1992. doi: 10.1016/0376-7388(92)85010-G.

[86] F. G Wilhelm, N. F. A Van der Vegt, M Wessling, and H Strathmann. Chronopotentiometry for the advanced current–voltage characterisation of bipolar membranes. *Journal of Electroanalytical Chemistry*, 502(1-2):152–166, 2001. doi: 10.1016/S0022-0728(01)00348-5.

[87] Y Tanaka. Water dissociation reaction generated in an ion exchange membrane. *Journal of Membrane Science*, 350(1-2):347–360, 2010. doi: 10.1016/j.memsci.2010.01.010.

[88] Y Tanaka. Acceleration of water dissociation generated in an ion exchange membrane. *Journal of Membrane Science*, 303(1-2):234–243, 2007. doi: 10.1016/j.memsci.2007.07.020.

[89] M. J Mitchell, O. E Jensen, K. A Cliffe, and M. M Maroto-Valer. A model of carbon dioxide dissolution and mineral carbonation kinetics. *Proceedings of the Royal Society A: Mathematical, Physical and Engineering Sciences*, 466(2117):1265–1290, 2010. doi: 10.1098/rspa.2009.0349.

[90] W Wang, M Hu, Y Zheng, P Wang, and C Ma. CO_2 fixation in Ca^{2+}-/Mg^{2+}-rich aqueous solutions through enhanced carbonate precipitation. *Industrial & Engineering Chemistry Research*, 50(13):8333–8339, 2011. doi: 10.1021/ie1025419.

[91] E. C La Plante, X Chen, S Bustillos, A Bouissonnie, T Traynor, D Jassby, L Corsini, D. A Simonetti, and G. N Sant. Electrolytic Seawater Mineralization and the Mass Balances That Demonstrate Carbon Dioxide Removal. *ACS ES&T Engineering*, 2023. doi: 10.1021/acsestengg.3c00004.

[92] Report of the Conference of the Parties to the United Nations Framework Convention on Climate Change (21st Session), 2015.

[93] J. C Bui, I Digdaya, C Xiang, A. T Bell, and A. Z Weber. Understanding multi-ion transport mechanisms in bipolar membranes. *ACS applied materials & interfaces*, 12(47):52509–52526, 2020. doi: 10.1021/acsami.0c12686.

[94] S Mikhaylin and L Bazinet. Fouling on ion-exchange membranes: Classification, characterization and strategies of prevention and control. *Advances in Colloid and Interface Science*, 229: 34–56, 2016. doi: 10.1016/j.cis.2015.12.006.

[95] V. D Grebenyuk, R. D Chebotareva, S Peters, and V Linkov. Surface modification of anion-exchange electrodialysis membranes to enhance anti-fouling characteristics. *Desalination*, 115 (3):313–329, 1998. doi: 10.1016/S0011-9164(98)00051-4.

[96] M Andreeva. *Impact of surface properties of cation-exchange membranes on the formation of Ca^{2+} and Mg^{2+} containing scales during electrodialysis of their aqueous solutions*. PhD thesis, Université Paris-Est; Kuban State agrarian university, 2017.

[97] S. K. A Al-Amshawee and M. Y. B. M Yunus. Electrodialysis desalination: The impact of solution flowrate (or Reynolds number) on fluid dynamics throughout membrane spacers. *Environmental Research*, page 115115, 2022. doi: 10.1016/j.envres.2022.115115.

[98] P Długołcki, A Gambier, K Nijmeijer, and M Wessling. Practical potential of reverse electrodialysis as process for sustainable energy generation. *Environmental science & technology*, 43 (17):6888–6894, 2009. doi: 10.1021/es9009635.

[99] L Gurreri, A Tamburini, A Cipollina, G Micale, and M Ciofalo. CFD prediction of concentration polarization phenomena in spacer-filled channels for reverse electrodialysis. *Journal of Membrane Science*, 468:133–148, 2014. doi: 10.1016/j.memsci.2014.05.058.

[100] M Lisitsin-Shmulevsky, X Li, D Hasson, H Shemer, and R Semiat. Solubility limits of CaSO4 polymorphs in seawater solutions. *Desalination*, 475:114200, 2020. doi: 10.1016/j.desal.2019.114200.

[101] F. L. T Shee, J Arul, S Brunet, and L Bazinet. Chitosan solubilization by bipolar membrane electroacidification: Reduction of membrane fouling. *Journal of Membrane Science*, 290(1-2): 29–35, 2007. doi: 10.1016/j.memsci.2006.12.023.

[102] H Liu and Q She. Scaling-Enhanced Scaling during Electrodialysis Desalination. *ACS ES&T Engineering*, 4(5):1063–1072, 2024. doi: 10.1021/acsestengg.3c00549.

[103] H Ren, Q Wang, X Zhang, R Kang, S Shi, and W Cong. Membrane fouling caused by amino acid and calcium during bipolar membrane electrodialysis. *Journal of Chemical Technology & Biotechnology: International Research in Process, Environmental & Clean Technology*, 83(11): 1551–1557, 2008. doi: 10.1002/jctb.1969.

[104] C Casademont, G Pourcelly, and L Bazinet. Effect of magnesium/calcium ratios in solutions treated by electrodialysis: Morphological characterization and identification of anion-exchange membrane fouling. *Journal of colloid and interface science*, 322(1):215–223, 2008. doi: 10.1016/j.jcis.2008.02.068.

[105] A. T Tran, N Jullok, B Meesschaert, L Pinoy, and B Van der Bruggen. Pellet reactor pretreatment: A feasible method to reduce scaling in bipolar membrane electrodialysis. *Journal of colloid and interface science*, 401:107–115, 2013. doi: 10.1016/j.jcis.2013.03.036.

[106] A. P Mairal, A. R Greenberg, W. B Krantz, and L. J Bond. Real-time measurement of inorganic fouling of RO desalination membranes using ultrasonic time-domain reflectometry. *Journal of Membrane Science*, 159(1-2):185–196, 1999. doi: 10.1016/S0376-7388(99)00058-7.

[107] G.-Y Chai, A. R Greenberg, and W. B Krantz. Ultrasound, gravimetric, and SEM studies of inorganic fouling in spiral-wound membrane modules. *Desalination*, 208(1-3):277–293, 2007. doi: 10.1016/j.desal.2006.06.018.

[108] K. T Huisman, B Blankert, H Horn, M Wagner, J. S Vrouwenvelder, S Bucs, and L Fortunato. Noninvasive monitoring of fouling in membrane processes by optical coherence tomography: A review. *Journal of Membrane Science*, page 122291, 2023. doi: 10.1016/j.memsci.2023.122291.

[109] A Bauer, M Wagner, F Saravia, S Bartl, V Hilgenfeldt, and H Horn. In-situ monitoring and quantification of fouling development in membrane distillation by means of optical coherence tomography. *Journal of Membrane Science*, 577:145–152, 2019. doi: 10.1016/j.memsci.2019.02.006.

[110] W Drexler, U Morgner, F. X Kärtner, C Pitris, S. A Boppart, X. D Li, E. P Ippen, and J. G Fujimoto. In vivo ultrahigh-resolution optical coherence tomography. *Optics letters*, 24(17):1221–1223, 1999. doi: 10.1364/OL.24.001221.

[111] D Huang, E. A Swanson, C. P Lin, J. S Schuman, W. G Stinson, W Chang, M. R Hee, T Flotte, K Gregory, and C. A Puliafito. Optical coherence tomography. *science*, 254(5035):1178–1181, 1991. doi: 10.1126/science.1957169.

[112] M. R Wang. *Optical Coherence Tomography and Its Non-medical Applications*. IntechOpen, 2020.

[113] W Drexler and J. G Fujimoto. *Optical coherence tomography: technology and applications*. Springer Science & Business Media, 2008.

[114] Y Gao, S Haavisto, W Li, C. Y Tang, J Salmela, and A. G Fane. Novel approach to characterizing the growth of a fouling layer during membrane filtration via optical coherence tomography. *Environmental science & technology*, 48(24):14273–14281, 2014. doi: 10.1021/es503326y.

[115] Y Gao, S Haavisto, C. Y Tang, J Salmela, and W Li. Characterization of fluid dynamics in spacer-filled channels for membrane filtration using Doppler optical coherence tomography. *Journal of Membrane Science*, 448:198–208, 2013. doi: 10.1016/j.memsci.2013.08.011.

[116] S. K. A Al-Amshawee and M. Y. B. M Yunus. Electrodialysis membrane desalination with diagonal membrane spacers: a review. *Environmental Science and Pollution Research*, pages 1–25, 2023. doi: 10.1007/s11356-023-28727-y.

[117] J Schindelin, I Arganda-Carreras, E Frise, V Kaynig, M Longair, T Pietzsch, S Preibisch, C Rueden, S Saalfeld, and B Schmid. Fiji: an open-source platform for biological-image analysis. *Nature methods*, 9(7):676–682, 2012. doi: 10.1038/nmeth.2019.

[118] A Bauer. Einsatz der optischen Kohärenztomographie zur kontinuierlichen Überwachung von Scaling bei der Membrandestillation. 2020.

[119] M Ciofalo, M Di Liberto, M La Cerva, and A Tamburini. Turbulent heat transfer in spacer-filled channels: experimental and computational study and selection of turbulence models. *International Journal of Thermal Sciences*, 145:106040, 2019. doi: 10.1016/j.ijthermalsci.2019.106040.

[120] C Picioreanu, J. S Vrouwenvelder, and M. C. M Van Loosdrecht. Three-dimensional modeling of biofouling and fluid dynamics in feed spacer channels of membrane devices. *Journal of Membrane Science*, 345(1-2):340–354, 2009. doi: 10.1016/j.memsci.2009.09.024.

[121] A Qamar, S Bucs, C Picioreanu, J Vrouwenvelder, and N Ghaffour. Hydrodynamic flow transition dynamics in a spacer filled filtration channel using direct numerical simulation. *Journal of Membrane Science*, 590:117264, 2019. doi: 10.1016/j.memsci.2019.117264.

[122] J. A Koskamp, S. E Ruiz Hernandez, N. H De Leeuw, and M Wolthers. First steps towards understanding the non-linear impact of Mg on calcite solubility: a molecular dynamics study. *Minerals*, 11(4):407, 2021. doi: 10.3390/min11040407.

[123] A. V Subhas, N. E Rollins, W. M Berelson, J Erez, P Ziveri, G Langer, and J. F Adkins. The dissolution behavior of biogenic calcites in seawater and a possible role for magnesium and organic carbon. *Marine chemistry*, 205:100–112, 2018. doi: 10.1016/j.marchem.2018.08.001.

[124] C. L Wetteland, J de Jesus Sanchez, C. A Silken, N.-Y. T Nguyen, O Mahmood, and H Liu. Dissociation of magnesium oxide and magnesium hydroxide nanoparticles in physiologically relevant fluids. *Journal of Nanoparticle Research*, 20:1–17, 2018. doi: 10.1007/s11051-018-4314-3.

[125] H Adun, J. D Ampah, O Bamisile, Y Hu, I Staffell, and H. R Gilani. Near-term carbon dioxide removal deployment can minimize disruptive pace of decarbonization and economic risks towards United States' net-zero goal. *Communications Earth & Environment*, 5(1):770, December 2024. doi: 10.1038/s43247-024-01916-4.

[126] Mitigation Pathways Compatible with 1.5°C in the Context of Sustainable Development. In Intergovernmental Panel on Climate Change (IPCC), editor, *Global Warming of 1.5°C: IPCC Special Report on Impacts of Global Warming of 1.5°C above Pre-industrial Levels in Context of Strengthening Response to Climate Change, Sustainable Development, and Efforts to Eradicate Poverty*, pages 93–174. Cambridge University Press, Cambridge, 2022. doi: 10.1017/9781009157940.004.

[127] D Dhamo, J Kühn, S Lüttin, M Rubin, and R Dittmeyer. Coupling the high-temperature Fischer–Tropsch synthesis and the skeletal isomerization reaction at optimal operation conditions in the Power-to-Fuels process route for the production of sustainable aviation gasoline. *Sustainable Energy & Fuels*, 8(9):2094–2103, 2024. doi: 10.1039/D3SE01351K.

[128] T Khangaonkar, B. R Carter, L Premathilake, S. K Yun, W Ni, M. M Stoll, N. D Ward, L. G Hemery, C Torres Sanchez, C. V Subban, M. C Ringham, M. D Eisaman, T Pelman, K Tallam, and R. A Feely. Mixing and dilution controls on marine CO_2 removal using alkalinity enhancement. *Environmental Research Letters*, 19(10):104039, September 2024. doi: 10.1088/1748-9326/ad7521.

[129] M. C Ringham, N Hirtle, C Shaw, X Lu, J Herndon, B. R Carter, and M. D Eisaman. An assessment of ocean alkalinity enhancement using aqueous hydroxides: kinetics, efficiency, and precipitation thresholds. *Biogeosciences*, 21(15):3551–3570, August 2024. doi: 10.5194/bg-21-3551-2024.

[130] K Khoiruddin, I. G Wenten, and U. W. R Siagian. Advancements in Bipolar Membrane Electrodialysis Techniques for Carbon Capture. *Langmuir*, 40(18):9362–9384, May 2024. doi: 10.1021/acs.langmuir.3c03873.

[131] M Aliaskari, H Horn, and F Saravia. Real time monitoring of scaling behavior in bipolar membrane electrodialysis. *Journal of Membrane Science*, 727:124063, June 2025. doi: 10.1016/j.memsci.2025.124063.

[132] M Reig, S Casas, O Gibert, C Valderrama, and J. L Cortina. Integration of nanofiltration and bipolar electrodialysis for valorization of seawater desalination brines: Production of drinking and waste water treatment chemicals. *Desalination*, 382:13–20, 2016. doi: 10.1016/j.desal.2015.12.013.

[133] G Battaglia, L Ventimiglia, F Vicari, A Tamburini, A Cipollina, and G Micale. Characterization of Mg(OH)2 powders produced from real saltworks bitterns at a pilot scale. *Powder Technology*, 443:119918, 2024. doi: 10.1016/j.powtec.2024.119918.

[134] J Lopez, A Filingeri, A Culcasi, M. F de Labastida, A Tamburini, J. L Cortina, G Micale, and A Cipollina. Electrodialysis with Bipolar Membranes to valorise saline waste streams: Analysing the fate of valuable minor elements. *Science of The Total Environment*, 958:177934, 2025. doi: 10.1016/j.scitotenv.2024.177934.

[135] C Cassaro, G Virruso, A Culcasi, A Cipollina, A Tamburini, and G Micale. Electrodialysis with bipolar membranes for the sustainable production of chemicals from seawater brines at pilot plant scale. *ACS Sustainable Chemistry & Engineering*, 11(7):2989–3000, 2023. doi: 10.1021/acssuschemeng.2c06636.

[136] R Ibáñez, A Pérez-González, P Gómez, A. M Urtiaga, and I Ortiz. Acid and base recovery from softened reverse osmosis (RO) brines. Experimental assessment using model concentrates. *Desalination*, 309:165–170, 2013. doi: 10.1016/j.desal.2012.10.006.

[137] W Zhang, M Miao, J Pan, A Sotto, J Shen, C Gao, and B Van der Bruggen. Process economic evaluation of resource valorization of seawater concentrate by membrane technology. *ACS Sustainable Chemistry & Engineering*, 5(7):5820–5830, 2017. doi: 10.1021/acssuschemeng.7b00555.

[138] R Sharifian. *Electrochemical Oceanic Carbon Capture*. PhD thesis, TU Delft, 2022.

[139] H Zhang, D Cheng, C Xiang, and M Lin. Tuning the Interfacial Electrical Field of Bipolar Membranes with Temperature and Electrolyte Concentration for Enhanced Water Dissociation. *ACS Sustainable Chemistry & Engineering*, 11(21):8044–8054, May 2023. doi: 10.1021/acssuschemeng.3c00142.

[140] M Reig, S Casas, C Valderrama, O Gibert, and J. L Cortina. Integration of monopolar and bipolar electrodialysis for valorization of seawater reverse osmosis desalination brines: Production of strong acid and base. *Desalination*, 398:87–97, 2016. doi: 10.1016/j.desal.2016.07.024.

[141] M Herrero-Gonzalez, J López, G Virruso, C Cassaro, A Tamburini, A Cipollina, J. L Cortina, R Ibañez, and G Micale. Analysis of operational parameters in acid and base production using an electrodialysis with bipolar membranes pilot plant. *Membranes*, 13(2):200, 2023. doi: 10.3390/membranes13020200.

[142] J Mustafa, N Ghasem, M. H El-Naas, B Van der Bruggen, and A. H Al-Marzouqi. Synergistic approach for carbon dioxide capture and reject brine treatment: Integrating selective electrodialysis and bipolar membrane electrodialysis. *Journal of Cleaner Production*, 438:140578, 2024. doi: 10.1016/j.jclepro.2024.140578.

[143] G Virruso, C Cassaro, A Tamburini, A Cipollina, and G Micale. Performance Evaluation of an Electrodialysis with Bipolar Membranes Pilot Plant Operated in Feed & Bleed Mode. *Chemical Engineering Transactions*, 105:73–78, 2023. doi: 10.3303/cet23105013.

[144] Y Yang, X Gao, A Fan, L Fu, and C Gao. An innovative beneficial reuse of seawater concentrate using bipolar membrane electrodialysis. *Journal of Membrane Science*, 449:119–126, 2014. doi: 10.1016/j.memsci.2013.07.066.

[145] J. C Bui, K. R. M Corpus, A. T Bell, and A. Z Weber. On the nature of field-enhanced water dissociation in bipolar membranes. *The Journal of Physical Chemistry C*, 125(45): 24974–24987, 2021. doi: 10.1021/acs.jpcc.1c08276.

[146] S Pawlowski, J. G Crespo, and S Velizarov. Profiled Ion Exchange Membranes: A Comprehensible Review. *International Journal of Molecular Sciences*, 20(1):165, January 2019. doi: 10.3390/ijms20010165.

[147] Y Morales, P Samanta, F Tantish, H Horn, and F Saravia. Water management for Power-to-X offshore platforms: an underestimated item. *Scientific Reports*, 13(1):12286, July 2023. doi: 10.1038/s41598-023-38933-w.

[148] Captura: Technology.

[149] A Filingeri, M Herrero-Gonzalez, J O'Sullivan, J. L Rodriguez, A Culcasi, A Tamburini, A Cipollina, R Ibañez, M. C Ferrari, and J. L Cortina. Acid/Base Production via Bipolar Membrane Electrodialysis: Brine Feed Streams to Reduce Fresh Water Consumption. *Industrial & Engineering Chemistry Research*, 2024. doi: 10.1021/acs.iecr.3c03553.

[150] Techno-economic analysis of electrochemical carbon capture from oceanwater integrated with hydrates-based sequestration. *Applied Energy*, 392:125960, August 2025. doi: 10.1016/j.apenergy.2025.125960.

[151] G Hooper, H. S Findlay, T. G Bell, R. W Wilson, and P. R Halloran. Removal of dissolved inorganic carbon from seawater for climate mitigation: potential marine ecosystem impacts. *Frontiers in Climate*, 7, July 2025. doi: 10.3389/fclim.2025.1528951. Publisher: Frontiers.

[152] A. A Al-Hamzah, E. J Smith, and C. M Fellows. Inhibition of Homogeneous Formation of Magnesium Hydroxide by Low-Molar-Mass Poly(acrylic acid) with Different End-Groups. *Industrial & Engineering Chemistry Research*, 54(7):2201–2207, February 2015. doi: 10.1021/ie504869e.

[153] W Yu, D Song, W Chen, and H Yang. Antiscalants in RO membrane scaling control. *Water research*, 183:115985, 2020. doi: 10.1016/j.watres.2020.115985.

[154] L. A Melnik, D. D Kucheruk, and G. N Pshinko. Antiscalants in the Process of Reverse Osmosis: Antiscaling Mechanism and Modern Problems of Application. *Journal of Water Chemistry and Technology*, 42(6):450–464, November 2020. doi: 10.3103/S1063455X20060077.

[155] Z Amjad and P. G Koutsoukos. Evaluation of maleic acid based polymers as scale inhibitors and dispersants for industrial water applications. *Desalination*, 335(1):55–63, February 2014. doi: 10.1016/j.desal.2013.12.012.

[156] Dr. Nähring - beste Produkte für die Wasseraufbereitung 2023, .

[157] Antiscalants – ROPUR | Toray Membrane Europe, April 2017.